MODELING OF NO_x FORMATION IN CIRCLUAR LAMINAR JET FLAMES

A Thesis

by

VIVEK SIWATCH

Submitted to the Office of Graduate Studies of
Texas A&M University
in partial fulfillment of the requirements for the degree of

MASTER OF SCIENCE

December 2005

Major Subject: Mechanical Engineering

MODELING OF NO_x FORMATION IN CIRCULAR LAMINAR JET FLAMES

A Thesis

by

VIVEK SIWATCH

Submitted to the Office of Graduate Studies of
Texas A&M University
in partial fulfillment of the requirements for the degree of

MASTER OF SCIENCE

Approved by:

Chair of Committee,	Kalyan Annamalai
Committee Members,	Je Han
	Sharath Girimaji
Head of Department	Dennis O' Neal

December 2005

Major Subject: Mechanical Engineering

ABSTRACT

Modeling of NO_x Formation in Circular Laminar Jet Flames. (December 2005)
Vivek Siwatch, B.E., Delhi University
Chair of Advisory Committee: Dr. Kalyan Annamalai

Emissions of oxides of nitrogen (NO_x) from combustion devices is a topic of tremendous current importance. The bulk of the review of NO_x emissions has been in the field of turbulent jet flames. However laminar jet flames have provided much insight into the relative importance of NO_x reaction pathways in non premixed combustion for various flame conditions. The existing models include detailed chemistry kinetics for various species involved in the flame. These detailed models involve very complex integration of hundreds of chemical reactions of various species and their intermediates. Hence such models are highly time consuming and also normally involve heavy computational costs. This work proposes a numerical model to compute the total production of NO_x in a non-premixed isolated circular laminar jet flame. The jet consists of the fuel rich inner region and the O_2 rich outer region. The model estimates both thermal NO_x and prompt NO_x assuming single step kinetics for NO_x formation and a thin flame model. Further the amount of air entrainment by jet depends upon the Sc number of fuel. The higher the Sc number, the higher is the air entrained which lowers the flame temperature and hence NO_x formation. With increasing Sc number, flame volume increases which leads to an increase in the NO_x formation. The effect of the Sc number variation on the net production of NO_x and flame structure is also investigated. The effect of equilibrium chemistry for $CO_2 \Leftrightarrow CO + 1/2\ O_2$ and $H_2O \Leftrightarrow H_2 + 1/2\ O_2$ on total NO_x emission is studied. Also the effect of both CO_2 and H_2O equilibrium is considered simultaneously and the net NO_x formation for propane is 45 ppm. The split between pre-flame and post-flame regions is also investigated. For Propane, 96% of

NO_x emissions occur in the pre-flame region and about 4% in the post-flame region. The model predictions are compared with experimental values of NO_x missions reported elsewhere.

TO MY PARENTS:

FOR THE LOVE, SUPPORT, ENCOURAGEMENT, GUIDANCE AND FOR

HELPING MAKE MY DREAM A REALITY

ACKNOWLEDGEMENTS

I would like to express my sincere gratitude to several people who made this thesis possible. First, I would like to thank my Committee Chair and Advisor, Dr. Kalyan Annamalai, for giving his time and sharing his knowledge on the subject with me. I would also like to thank Dr. Je Han and Dr. Sharath Girimaji for their valuable input as members of my graduate committee.

In closing, I want to thank my parents, Dr. Kartar Singh and Mrs. Saroj Siwatch, my sister, Sujata, and my friend, Tanya Mohan, for encouraging me to pursue higher education and providing the necessary means to make my education possible and converting my dreams into reality. My parents have been a pillar of support for me throughout my stay in the university and stood by me in all times. Without their strength and support, I believe I would have never finished this degree and my thesis.

TABLE OF CONTENTS

Page

ABSTRACT iii

DEDICATION v

ACKNOWLEDGEMENTS vi

TABLE OF CONTENTS vii

LIST OF FIGURES ix

LIST OF TABLES xii

CHAPTER

I INTRODUCTION 1

1.1. Organization of Thesis 6

II LITERATURE REVIEW 8

III OBJECTIVE AND METHODOLOGY 33

3.1. Purpose of Research 33
3.2. Objectives of Research 33

IV MODELING OF A CIRCULAR LAMINAR JET FLAME 35

4.1. Governing Differential Equations for Circular Jet 36
4.1.1. Boundary Conditions for Circular Jet 39
4.2. Normalization of Governing Differential Equations 40
4.3. Similarity Variables for Circular Jet 42
4.4. Solution 43
4.4.1. Summary of Solutions 44
4.4.2. Flame Structure 47
4.4.3. Solution for Flame Height 47
4.4.4. Solution for Air Entrainment for Circular Jet 48
4.4.5. Excess Air 49
4.5. Procedure for NO_x Modeling in Isolated Circular Laminar Jet 49
4.6. Solution Procedure 55

V RESULTS AND DISCUSSIONS 56

5.1. Results of Modeling 56
5.1.1. Complete Combustion 56

CHAPTER Page

5.1.2. CO_2 Equilibrium 65
5.1.3. H_2O Equilibrium 65
5.1.4. Both CO_2 and H_2O Equilibrium 72
5.1.5. Discussion of Results 73
5.2. Effect of Sc Number Variation on NO_x Production 73
5.2.1. Discussion of Results 76
5.3. Validation of Model 81
5.3.1. Conclusions 82

VI CONCLUSIONS AND RECOMMENDATIONS 87

6.1. Conclusions 88
6.2. Recommendations for Future Work 89

NOMENCLATURE 91
REFERENCES 96
APPENDIX A 99
APPENDIX B 127
APPENDIX C 136
APPENDIX D 164
APPENDIX E 165
VITA 169

LIST OF FIGURES

FIGURE Page

I.1 Gas Turbine Engines: (a) Aircraft Turbojet Propulsion, (b) Electric Power Production. 3

I.2 Schematic of Different Burner Geometries a) 2D Jet (d_i << W), b) Circular Jet (Diameter'd')....7

II.1 A Schematic of the Laboratory Diffusion Burner by Tuteja et al. [4] 12

II.2 (Radial Distance) x (ppm in Dry Gas) vs. Radial Distance in Doped Laminar H_2 Diffusion Flames. Hydrogen is Doped With Pyridine (C_5H_5N) Burning in Air [5]....17

II.3 Schematic of the Apparatus Used for Measurement of Total Oxides of Nitrogen Produced by a Diffusion Flame [6]....18

II.4 Schematic of Laboratory Burner Used by Mitchell and Sarofim [7]. 20

II.5 Temperature and NO Profiles by Mitchell and Sarofim [7]....21

II.6 Schematic of Combustor Used by Hahn and Wendt in their Experiments [8]....22

II.7 NO Profile of a $CH_4/N_2/O_2$ Opposed Diffusion Flame With Strain (α = 3.62 sec^{-1}) by Hahn and Wendt [8]....23

IV.1 The Axial Velocity Profile and Fuel and Oxygen Mass Fraction Profiles for a Circular Jet Under Mixing Conditions. The Momentum of the Jet Entrains the Necessary Oxygen for Combustion. A Stoichiometric Region is Formed From the Mixing of the Entrained Air and the Fuel Issuing from the Jet. A Qualitative Illustration of the Mass Fraction of Oxygen and Fuel is Shown on the Figure. 51

IV.2 Schematic of an Elemental Volume Used for Integration 54

V.1 The Production of Total $z = (d\dot{\omega}_{NO}/dx)$ (g/GJ per Unit Dimensionless Height) vs. (x^*) for the Case of Complete Combustion. 59

V.2 Variation of Total NO_x (g/GJ) and T_{max} With Axial Distance x* for the Case of Complete Combustion....60

V.3 Variation of Y_{N_2}, Y_{O_2} and T With Radial Distance r^* at a) x^* = 57, b) x^* = 15 and c) x^*=70 for the Case of Complete Combustion....61

V.4 The Production of Total $z = (d\dot{\omega}_{NO}/dx)$ (g/GJ per Unit Dimensionless Height) vs. (x^*) for the Case of $CO_2 \Leftrightarrow CO + 1/2\ O_2$ Dissociation. 62

FIGURE Page

V.5 Variation of Total NO_x (g/GJ) and T_{max} With Axial Distance x* for the Case of $CO_2 \Leftrightarrow CO + 1/2\ O_2$ Dissociation 63

V.6 Variation of Y_{N_2}, Y_{O_2} and T With Radial Distance r^* at a) $x^* = 45$ and b) $x^* = 15$ for the Case of $CO_2 \Leftrightarrow CO + 1/2\ O_2$ Dissociation 64

V.7 The Production of Total $z = (d\dot{\omega}_{NO}/dx)$ (g/GJ per Unit Dimensionless Height) vs. (x^*) for the Case of $H_2O \Leftrightarrow H_2 + 1/2\ O_2$ Dissociation 66

V.8 Variation of Total NO_x (g/GJ) and T_{max} With Axial Distance x* for the Case of $H_2O \Leftrightarrow H_2 + 1/2\ O_2$ Dissociation.....67

V.9 Variation of Y_{N_2}, Y_{O_2} and T With Radial Distance r^* at a) $x^* = 45$ and b) $x^* = 15$ for the Case of $H_2O \Leftrightarrow H_2 + 1/2\ O_2$ Dissociation 68

V.10 The Production of Total $z = (d\dot{\omega}_{NO}/dx)$ (g/GJ per Unit Dimensionless height) vs. (x^*) for the Case of Simultaneous CO_2 and H_2O Dissociation 69

V.11 Variation of Total NO_x (g/GJ) and T_{max} With Axial Distance x* for the Case of Simultaneous CO_2 and H_2O Dissociation 70

V.12 Variation of Y_{N_2}, Y_{O_2} and T With Radial Distance r^* at a) $x^* = 45$ and b) $x^* = 15$ for the Case of Simultaneous CO_2 and H_2O Dissociation ……...71

V.13 Comparison of Total NO_x (g/GJ) Production for the Four Different Cases. 74

V.14 Variation of Excess Air Fraction With Sc Number.....76

V.15 Variation of Total NO_x (g/GJ) With Sc Number for the Case of Complete Combustion. 77

V.16 Variation of Total NO_x (g/GJ) With Sc Number for the Case of $CO_2 \Leftrightarrow CO + 1/2\ O_2$ Dissociation. 78

V.17 Variation of Total NO_x (g/GJ) With Sc Number for the Case of $H_2O \Leftrightarrow H_2 + 1/2\ O_2$ Dissociation.....79

V.18 Variation of Total NO_x (g/GJ) with Sc Number for the Case of Simultaneous CO_2 and H_2O Dissociation. 80

FIGURE Page

V.19 A Comparison of the Calculated $EINO_x$ (g/ Kg of fuel)Values and the Experimental Values for d_o of 10 mm, Sc=1. 83

V.20 A Comparison of the Calculated $EINO_x$ (g/ Kg of fuel) Values and the Experimental Values for d_o of 20.5 mm, Sc=1. 84

V.21 A Comparison of the Calculated $EINO_x$ (g/ Kg of fuel) Values and the Experimental Values for d_o of 29.5 mm, Sc =1. 85

LIST OF TABLES

TABLE Page

II.1 Studies of NO_x in Laminar Diffusion Flames [1] 13

IV.1 Summary of Solutions to the Governing Differential Equations for Laminar Circular Jets.....44

V.1 Inlet Conditions for Fuel Utilized for Modeling of NO_x in the Study. 57

V.2 Comparison of Calculated $EINO_x$ (g/Kg of fuel) Values and Experimental Values for d_o = 10 mm, Sc =1 for Methane (CH_4).....86

CHAPTER I

INTRODUCTION

Scientists have recognized nitrogen oxides as some of the most harmful and most difficult to control of the man-made pollutants. Part of the difficulty of dealing with nitrogen oxides resides in the complexity of the chemistry that the components participate in. The term "nitrogen oxides (NO_x)" encompasses an entire class of compounds that possess different chemical and physical properties. To complicate matters further, most can spontaneously react to change their identity, becoming a different member of the NO_x family. Nitrogen oxides have many characteristics similar to other man-made gaseous pollutants [1]. They often arise as by-products from other processes, damage the environment, and can be harmful to the health of humans, especially respiratory diseases and lung cancer. Until recently, companies particularly emitting such compounds have largely escaped with these negative impacts to the environment and humans. Despite the similarities between nitrogen oxides and other gaseous pollutants, nitrogen oxides, as a class, provide special challenges, as well as opportunities, that require further research and understanding.

This document follows the style of the ASME Journal of Heat Transfer.

By all accounts, energy consumption in the United States has reached staggering proportions. Till the latter half of the twentieth century, the base-load electrical generation in the country was provided by large coal and nuclear plants. However, since the late 1970s there has been a shift toward using natural gas turbines to produce energy. The turbines present several advantages over the coal and nuclear power plants as they have higher efficiencies, lower capital costs, short installation times and lower emission characteristics compared to coal. The construction costs are roughly half the cost of a conventional fossil-fuel steam power plant.

The gas turbine, shown schematically in Figure I.1, is an internal combustion engine that is able to operate continuously [2]. Gas turbine engines have two main applications: aircraft propulsion and electric power generation and three main components: a compressor, combustor and turbine. Gas turbines operate by drawing a working fluid (typically air) into a compressor which compresses the gas. The compressed gas then enters a combustion chamber where fuel is burned and energy is added to working fluid. Next gas expands through a turbine which extracts power from the hot gases. For aircraft propulsion, the exhaust gases are accelerated through a nozzle producing thrust (Figure I.1a) whereas for electrical power production, the shaft of turbine is connected to an electrical generator (Figure I.1b). Producing power in gas turbine engines has drawbacks. Specifically, burning hydrocarbon fuels in the combustion chamber of gas turbine engines lead to emissions such as CO, CO_2, SO_2, NO and NO_x. These combustion products can harm humans and the environment, and have strict federal legislations governing their release. In addition to gas turbines, many practical systems such as residential gas burners and boilers contribute to the formation of NO_x.

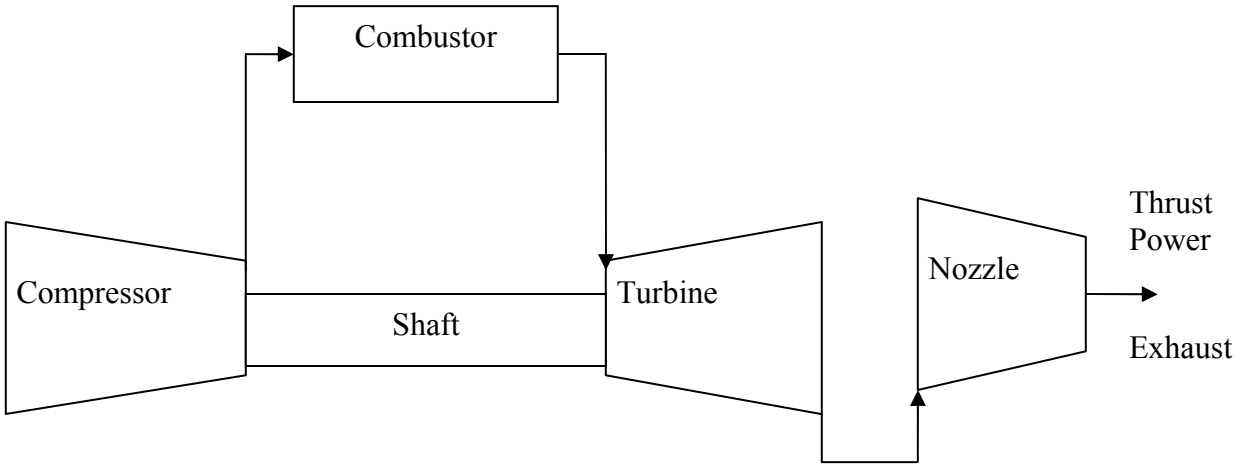

(a)

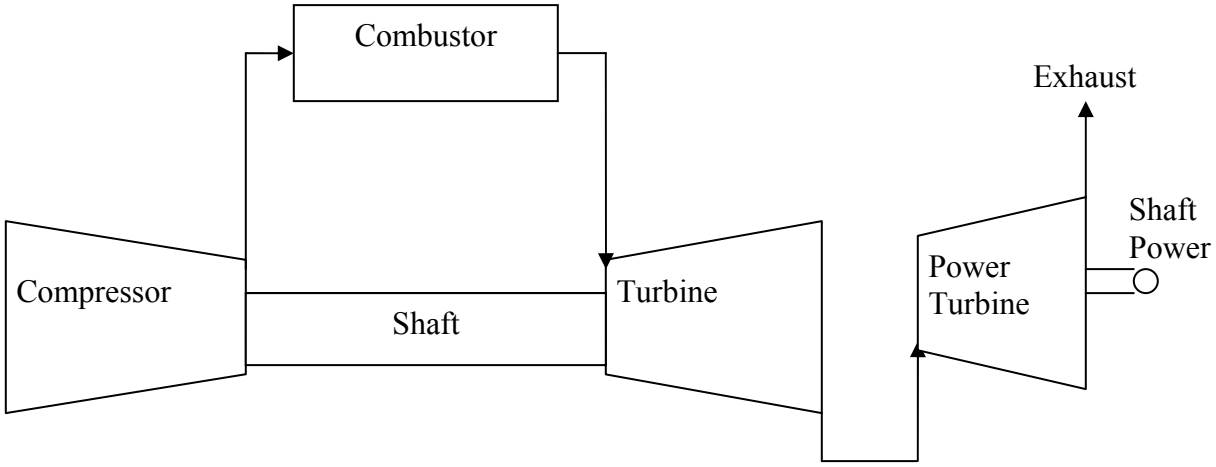

(b)

Figure I.1: Gas Turbine Engines: (a) Aircraft Turbojet Propulsion, (b) Electric Power Production.

Environmental regulations have been the only driver forcing industry to install systems to control NOx emissions. The Clean Air Act Amendments of 1990, and in particular, Title I (Ozone Attainment), Title IV (Acid Rain) and New Source Review requirements have resulted in various State Implementation Plans aimed at reducing NO_x. Recently, limits have been placed on the amount of NO_x that can be released into atmosphere (NO_x < 10 ppm). In light of this legislation, gas turbine manufacturers are exploring ways to reduce NO_x emissions [2].

Nitrogen oxides (NO_x), the term used to describe the sum of NO, NO_2, and other oxides of nitrogen, play a major role in the formation of ozone, particulate matter, haze, and acid rain. While EPA tracks national emissions of NO_x, the national monitoring network measures ambient concentrations of NO_2 for comparison to national air quality standards. The major sources of man-made NO_x emissions are high-temperature combustion processes, such as those that occur in automobiles and power plants. Home heaters and gas stoves can also produce substantial amounts of NO_2 in indoor settings.

Based on annual Arithmetic average, NO_2 air quality improved by 24 % from 1982 to 1991. The average concentration of NO_2 changed from 0.044 ppm in 1982 to 0.035 in 1991. Then there was an 11% decrease from 1991 to 2001 and NO_2 concentration changed from 0.035 ppm in 1991 to 0.031 ppm in 2002. In terms of total NO_x emissions, there was a 9% increase in NO_x emissions from 22500 thousand short tons to 24550 thousand short tons of NO_x in 1991. Then there was a decrease of 3% in NO_x emissions from 24550 thousand short tons of NO_x in 1991 to 23800 thousand short tons of NO_x in 2001.

With government agencies and regulations now providing companies with ever increasing economic “incentives” to reduce waste emissions, work must be done on the

specific problems to keep all waste products “below reg.” With these regulations becoming more and more stringent, simple rules of thumb for reducing waste, though still needed, will not complete the task. In-depth research in order to find solutions to these numerous problems.

The existing models include detailed chemistry kinetics for various species involved in the flame. These detailed models involve very complex integration of hundreds of chemical reactions of various species and their intermediates. Hence such models are highly time consuming and also normally involve heavy computational costs. In order to understand the basic processes leading to NO_x formation, simplified studies must be performed in order to ascertain the important parameters governing NO_x behavior. A model is presented for obtaining flame structure in a simple laminar jet flame which is then used to develop a model to compute total production of NO_x in a non-premixed circular laminar jet flame. The model is based on solutions to the governing differential equations of mass, momentum and species for a circular laminar jet flame. The model estimates both thermal NO_x and prompt NO_x assuming single step kinetics for NO_x formation and a thin flame model. The effect of equilibrium chemistry for $CO_2 \Leftrightarrow CO + 1/2\ O_2$ and $H_2O \Leftrightarrow H_2 + 1/2\ O_2$ on total NO_x emission is studied. The model predictions are compared with experimental values of NO_x emissions reported elsewhere to help validate the model. Recently two flame models have been developed for turbulent flames that incorporate a combination of laminar flamelets representing the outer flame zone of the jet and a well stirred reactor, which represents the core of the jet. These are the two stage Lagrangian model of Lutz and two zone asymptotic model of Rokke. The laminar flamelet simplification of flowfield allows detailed kinetics to be employed with modest computing power [1].

Most of the existing models are typically for M*= 1 and J* =1. In these the relations can not be used for cases when body forces are present in the boundary layer conservation

equations, e.g. if buoyancy is considered, M* >1 and J* >1. However in this model, the effect of M* and J* not equal to one can be modeled.

The laminar jet is further divided into two categories [3]:

(1) The 2D laminar jet having a rectangular slit (of width'd') as shown in (Figure I.2 a) and

(2) The circular laminar jet having a circular slit (of diameter'd').as shown in (Figure I.2 b)

The 2D laminar jet is characterized by a rectangular slit with breadth 'w' and a width'd' (Figure I.2a). The aspect ratio ($d_i/w<<<<<1$) is usually very small. The circular jet is characterized by a slit of diameter'd'. (Figure I.2b). Fuel and air mixes and typically mixture is rich in region R and lean in region L. Along ABCDE the air flow ratio is stoichiometric once ignited; typically reaction occurs rapidly along stoichiometric surface ABCDE. Then a flame is formed along ABCDE once the flame is formed O_2 diffuses from region II towards ABCDE while fuel diffuses from region R towards ABCDE. Since reaction rates are rapid along ABCDE, then almost no O_2 crosses from L into region R. No fuel crosses from region I to II. Then mass fractions of O_2 and fuel Y_{O_2}, $Y_F = 0$ along ABCDE.

1.1 Organization of Thesis

Chapter II provides an overview of the pertinent literature for circular laminar jet flames whereas Chapter III provides the overall objective and tasks proposed under current work. Chapter IV provides equations and the solution procedures used to model an isolated circular laminar jet flame and the methodology adopted for modeling the formation of NO_x using a thin flame model and single step NO kinetics. The results of modeling and comparison with experimental results published elsewhere are found in Chapter V. Finally, a summary of findings and recommendations for future work are provided in Chapter VI.

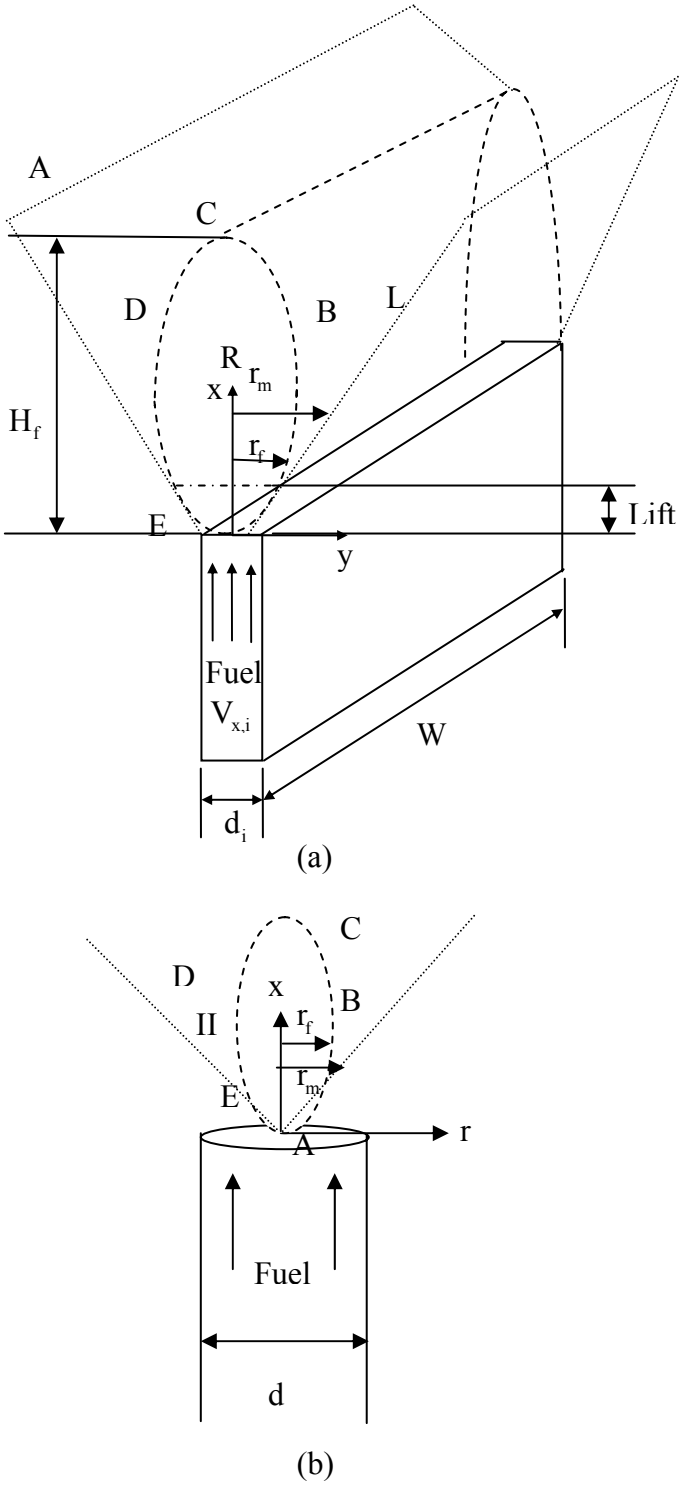

Figure I.2: Schematic of Different Burner Geometries a) 2D Jet (d_i << W), b) Circular Jet (Diameter'd').

CHAPTER II
LITERATURE REVIEW

Emissions of oxides of nitrogen (NO_x) from combustion devices is a topic of tremendous current importance. Environmental concerns related to NO_x emissions are ambient ozone levels, acid rain, and depletion of ozone in the stratosphere. Various clean Air Act Amendments have created intensified interest in NO_x control because of their aggressive program to achieve ambient air quality standards for ozone [2]. To attain the ozone standard, legislation focuses on the control of NO_x and volatile organic compounds. With regard to acid rain, NO_x contributes 25 – 30 % to rain acidity. The third major concern, stratospheric ozone depletion, is believed to be linked to NO_x emissions from aircraft flying at high altitudes. The development of future generations of high speed civil transport aircraft hinges critically on the design of low NO_x engine combustors. The information provided in this chapter summarizes some of the relevant work on laminar diffusion flames. Particular interest has been paid on the production of NO_x in isolated circular laminar jets. The main objective of this review is to examine studies of simple laminar flames.

In primary, nitrogen oxides (NO_x) are divided into the following three categories [1]:

1) *Thermal* NO_x -Reaction of the atmosphere (molecular) nitrogen and oxygen, the latter formed by splitting of molecular oxygen under high temperature in an oxidation atmosphere. (Also called the "Zeldovich" NO_x). In the present study, for calculating the rate of volumetric production of thermal NO_x , the following global relation is assumed [Annamalai, K., 2004]

$$\dot{\omega}_{NO}''' = \frac{d[NO]}{dt} = \frac{A_{NO} M_{NO} (\rho_{mix})^{1.5}}{(M_{N_2})(M_{O_2})^{0.5}} \exp\left(\frac{-E}{RT}\right) \frac{(Y_{N_2})(Y_{O_2})^{0.5}}{T^{0.5}} \ , \frac{kg}{m^3 s} \qquad (2.1)$$

Where $\rho_{mix} = \frac{PM_{mix}}{RT}$

2) *Prompt* NO_x -Reaction of atmosphere (molecular) nitrogen and hydrocarbons or hydrocarbon fragments that originated in the thermal decomposition in a reducing atmosphere. (Also called the Fennimore NO_x). For calculating the volumetric rate of production of prompt NO_x , an empirical rate relation presented by [De Soete, 1975] is used:-

$$\dot{\omega}_{prompt\ NOx}''' = A \frac{M^{1+b}}{\rho^{1+b}} C_{O_2}^{b} C_{N_2} C_{CH_4} \exp\left(\frac{-E_a}{RT}\right) \qquad (2.2)$$

Where pre-exponential factor A = 9.2 x10^6 (1/s), b=0.5 and $\frac{E_a}{R}$ = 30000 (K) respectively.

3) *Fuel* NO_x -Formed by the oxidation of nitrogen compounds in the fuel.

In non premixed combustion of hydrocarbons, the first two mechanisms are responsible for the majority of NO_x formed.

Values of NO_x can be reported in various different units. NO_x is more commonly reported in ppm (particles per million), g/GJ of fuel and EI NO_x (emission index) as g/ kg of fuel. These methods are briefly described as follows [3]:

1) Reporting as ppm

Many analyzers yields gas composition in mole % (or volume %) on dry basis. Since pollutants are in trace amounts, they are reported in parts per million (ppm). For the pollutant species k,

Species k in ppm = $X_k * 10^6$, (interpreted as molecules per million dry molecules).

(Note that for fuels like coal, Hg is also expressed in ppm, here the ppm indicates the mass of species in g per million g of solid fuel.

2) Emissions in mass units Per Unit Heat Value (g /GJ)

Pollutant species NO can be reported as

$$\text{NO in } \frac{g}{GJ} = \frac{c\ X_{NO}}{(X_{CO_2} + X_{CO})} \frac{M_{NO_2} * 1000}{M_F\ HHV_F\ (GJ/kg)} \tag{2.3}$$

or

$$\text{NO in } \frac{g}{GJ} = \frac{Y_c\ X_{NO}}{(X_{CO_2} + X_{CO})} \frac{M_{NO_2} * 1000}{12.01\ x\ M_F\ HHV_F\ (GJ/kg)} \tag{2.4}$$

Where Y_c is the mass fraction and c is the number of moles of CO_2 in the combustion reaction. Note that NO eventually oxidizes to NO_2 and hence molecular weight of NO_2 is used to express in mass unites.

3) Emission Index ($EINO_x$) (g/kg of fuel)

Sometimes emission index is used to report the total production of pollutant species NO.

EINO (g /kg of Fuel) = $\{c^* X_{NO}/ (X_{CO2}+X_{CO})\}$ M_{NO_2} (kg/ kmol) 1000/ M_F (kg/kmole)

Where M_F =c* 12.01+ h*1.01+n*14.01+0*16+s*32 kg/ kmole of fuel

For reporting NO emission, the EPA stipulates that M_k for NO should be that of NO_2 (M_{NO2} = 46.01) instead of 30 since NO is eventually converted into NO_2 in atmosphere which plays a major role in destruction of O_3.

Perhaps the earliest report of NO measurements in non premixed combustion is that by Hanson and Egerton in 1937 [1]. In this study, gas samples were withdrawn from the exhaust of a firing diesel engine at various crank angles, and peak NO concentrations of about 500 ppm were measured. This work was motivated by the concern that NO promotes gumming of engine oil. Following recognition that NO from combustion sources relates to photochemical smog, measurements of NO from a variety of combustion devices were reported in the1950s. Since then, NO formation has been studied in a wide range of non premixed combustion systems, ranging from very simple to quite complex. Laminar studies, in particular, have provided much insight into the relative importance of NO reaction pathways in non premixed combustion for various flame conditions. At the opposite end of the complexity spectrum are investigations of NO in turbulent swirling and recirculating flows and in practical devices, such as diesel engines and gas turbine combustors. Here, complex turbulent systems are not dealt with, but rather, briefly examined as our second focus. These flames provide a well-defined and relatively simple flow field, yet retain the complexity of the interaction between the turbulent flow and chemical reactions.

Tuteja and Newhall [4] studied the formation of nitric oxide in laminar diffusion flames. Their experimental setup consisted of a vertical coaxial diffusion flame burner as shown schematically in Figure II.1, which was designed to produce an enclosed steady laminar diffusion flame at pressures ranging from one to ten atmospheres. Table II.1 Summarizes the various studies of NO_x in laminar diffusion flames.

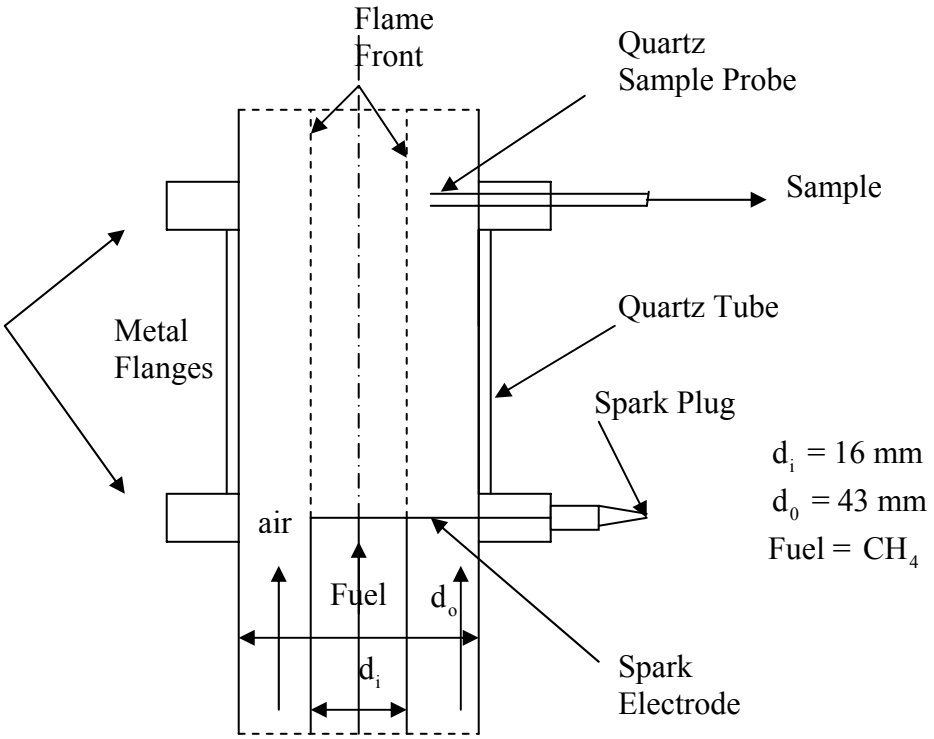

Figure II.1: A Schematic of the Laboratory Diffusion Burner by Tuteja et al. [4]

Table II.1: Studies of NO_x in Laminar Diffusion Flames. [1]

Reference	**Fuel**	**Configuration**	**Comment**
Tuteja &Newhall 1972, 1973	CH_4	Jet with coflow	Sonic microbe sampling; measured NO higher than by equilibrium.
Bracco 1973	CH_2OH	Spherical droplet	Zeldovich mechanism with equilibrium O and steady state N atoms.
Ludwig *et al.* 1975	CH_2OH	Porous sphere	Measured NO higher than prediction even though T's lower.
Fenimore 1976	$CH_4/H_2/N_2$	Jet with coflow	Fuels doped with pyridine (C_5H_5N); conversion time for fuel N calculated as 1 ms.
Maahs & Miller 1979	CO	Jet with coflow	Studies at 1-50 atm; NO rates higher than predicted with equilibrium O atoms.
Mitchell *et al.* 1980	CH_4	Jet with coflow	Calculated 25% thermal NO and 15-30% prompt NO (via cyanides).
Hahn & Wendt 1981	CH_4	Flat opposed jet	Applied detailed kinetics; studied NH_3 addition and flame stretch.
Drake & Blindt 1989	$CO/H_2/N_2$	Opposed flow	NO decreases with stretch; effects linked to T, O-atom, and mechanism
Drake & Blindt 1991	CH_4/N_2	Opposed flow	NO decreases with stretch all mechanisms.
Turns *et al.* 1993	HC's $/N_2$	Jet with coflow	$EINO_x$ unaffected by fuel dilution up to 50%
Takeno and Nishioka 1993	H_2	Generic counterflow	Method to calculate $EINO_x$; illustrated decreasing $EINO_x$ with stretch.
Nishioka *et al.* 1993-1994	CH_4	Counterflow double	Thermal NO falls rapidly with stretch while prompt increases and then falls.

Air was metered in a similar manner and is fed to the burner thorough the outer tube of 43 mm. diameter, surrounding and concentric with the fuel tube. Fuel and air flow rates were regulated by adjusting pressures upstream of the sonic nozzles. An automotive-type ignition system was modified to produce a continuous spark discharge as an ignition source. The flame was enclosed in vertical quartz tubing elements interposed with steel flanges providing for sample probe insertion at number of prescribed axial locations. Combustion gas samples were extracted from localized positions within the flame by means of a quartz microbe introduced through the flange. The microprobe had an inside diameter of the order of 0.5 mm and outside diameter of 0.5 mm at the probe tip. Radial position of the sampling probe was adjusted and measured by means of a micromanipulator with a least count of 0.1 mm.

The extracted samples were analyzed for NO as well as for the species CO, CO_2, N_2, O_2, CH_4 which was the fuel employed. Following this method, detailed radial profiles for each of the above species was established. Concomitant temperature profiles were also established through the use of a 0.25 mm diameter Pt/Pt- 10% Rh thermocouple.

The experimental results of the researchers indicated that in diffusion flames, the NO formation occurs in a narrow region corresponding to that of maximum temperature. It was also observed that the prompt NO formation within highly reactive flame zone was absent.

Bracco et al. [1] conducted a theoretical study on the formation of NO for a spherical (no gravity, no forced convection) diffusion flame around an ethanol drop burning in air. The Zeldovich chemical kinetic mechanism for the formation of NO was used, together with standard equations for the diffusion flame. Bracco concluded that diffusion flames around hydrocarbon fuel drops, burning in high temperature air, could be significant sources of NO. The computed concentrations of NO were very small. The mole fraction

of NO reached a maximum of 20 ppm just outside the maximum temperature region. It was also found that NO diffusion must be considered in order to calculate properly its concentration that the mass of NO produced per unit mass of fuel burned increases with the droplet radius since reaction zone volume increases with drop radius. This was attributed to be the reason as to why finer fuel sprays produce less NO than course ones (all other conditions being the same) and that fuel bound nitrogen could enhance the production of NO at lower air temperatures.

Bracco and Ludwig [1] measured the composition of major stable species, including nitric oxide, and the temperature within the diffusion flames around simulated ethanol droplets burning in air at atmospheric conditions. Nitric oxide measurements were made with ethanol seeded with various percentages of a nitrogen containing compound (pyridine). The fuel droplet was simulated by a 1.2 mm porous carbon sphere supported by a fine stainless steel fuel line. Quartz microprobes, quartz coated thermocouples of platinum/platinum-13% rhodium, a gas chromatograph, and a chemiluminescent analyzer were used by the researchers in their experiment. Their results included documentation of significant oxygen penetration to the simulated droplet surface, and pyrolysis and partial oxidation of ethanol near the surface. The measured nitric oxide concentrations for both pure ethanol and pyridine seeded ethanol were greater than expected in spite of measured flame temperatures considerably lower than predicted. Also they concluded that diffusion flames can be significant sources of NO particularly when the fuel contains nitrogen.

Fenimore [5] measured the yield of NO and the effect of diluents and mixing on nitric oxide from fuel-nitrogen species in diffusion flames. In his experimental setup, a fuel stream composed of various proportions of CH_4, H_2 and diluents, and doped with fuel-N, was fed to one of the three interchangeable Mache-Hebra nozzles of ID = 0.504, 0.318, 0.127 cm. A large proportion of H_2 was used in order to suppress soot formation in laminar flames, and extend the range of flow before blow off. The nozzle stood in a

quartz chimney, 5 cm diameter, which was fed with a smoothed flow of air. A mixing plate above the top of any flame studied, 75 cm above the nozzle, gave well mixed products in the upper part of the chimney. These were drawn thorough a probe which is described below, or thorough a quartz probe, partly dried by passage through a trap at zero $°C$, and analyzed for NO by chemi-luminescence. Radial traverses of NO, HCN, and NH_3 were made across laminar H_2 flames. CH_4 was omitted in the runs to prevent clogging of the probe with soot. A shorter chimney was used and stainless steel probe, mounted on a micromanipulator reached down into the flame from the top of the chimney. The probe was 0.64 cm OD by 30 cm long. An orifice 0.06 cm in its rounded tip led to an inner tube which carried away the sample.

Fenimore observed that the yield of NO from fuel-N was independent of nozzle size and flow velocity as long as the flames remained laminar, but increased abruptly at the onset of turbulence due to rapid mixing of O_2 with fuel N. The yield was also increased by inert diluents. Manipulators which increased the yield of NO from fuel-N decreased the amount of NO formed from N_2. These findings suggested, that given time enough in very rich parts of the flame, fuel-N converts to form little NO converts to N_2. But if fuel-N does not convert in very rich gas (because the temperature is lowered by inert diluents, or because of rapid turbulent mixing) it escapes into regions which are not so rich, and gives a larger yield through laminar flames. Figure II.2 shows the variation of NO with the radial distance. Fenimore concluded that characteristic conversion time of fuel-N is always of the order of one millisecond in the laminar flames. Thus, assuming a constant conversion time of one millisecond, once can predict the yield of NO in laminar flames fairly well.

Jaasma and Borman [6] studied the peculiarities associated with the measurement of oxides of nitrogen produced by diffusion flames. Their experimental setup is shown in Figure II.3. The apparatus was designed to measure the total oxides of nitrogen produced by diffusion flames produced by liquid fuels.

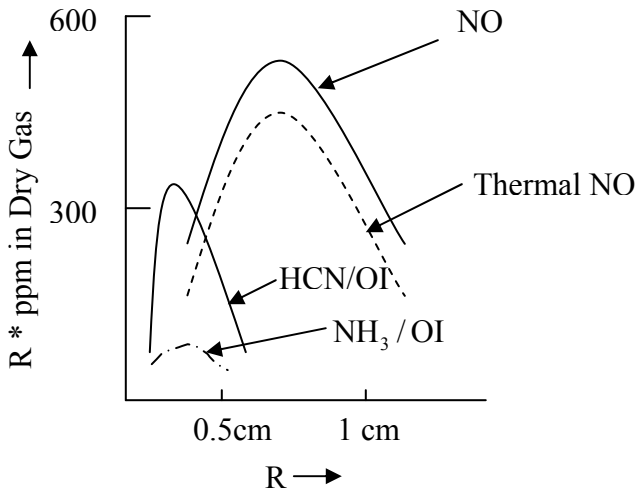

OI means oxygen index = mole ratio $O_2/(O_2+N_2+CO_2)$ in air stream. Here OI = 0.168.

Figure II.2: (Radial Distance) x (ppm in Dry Gas) vs. Radial Distance in Doped Laminar H_2 Diffusion Flames. Hydrogen is Doped With Pyridine (C_5H_5N) Burning in Air [5].

Normal heptane fed to the center of the horizontal porous metal cylinder produced a fuel wetted surface of cylindrical geometry. The porous cylinder was located in a cross-flow of low velocity (less than 1 m/s), ambient temperature and pressure air. The ignition of fuel and adjustment of fuel produced an envelope flame, the forward half of which was laminar and relatively steady. The flow through the collection system was adjusted by means of a valve so that all the combustion products entered the system. The products were mixed with enough additional air from the air supply system and surroundings in order to prevent condensation in any part of the system. A sharp edged orifice was used to measure the flow rate through the collection system. A part of the collector flow was

drawn off for measurement of NO and NO_x concentrations by a Thermo Electron Model 10A chemi-luminescent analyzer with a stainless steel converter.

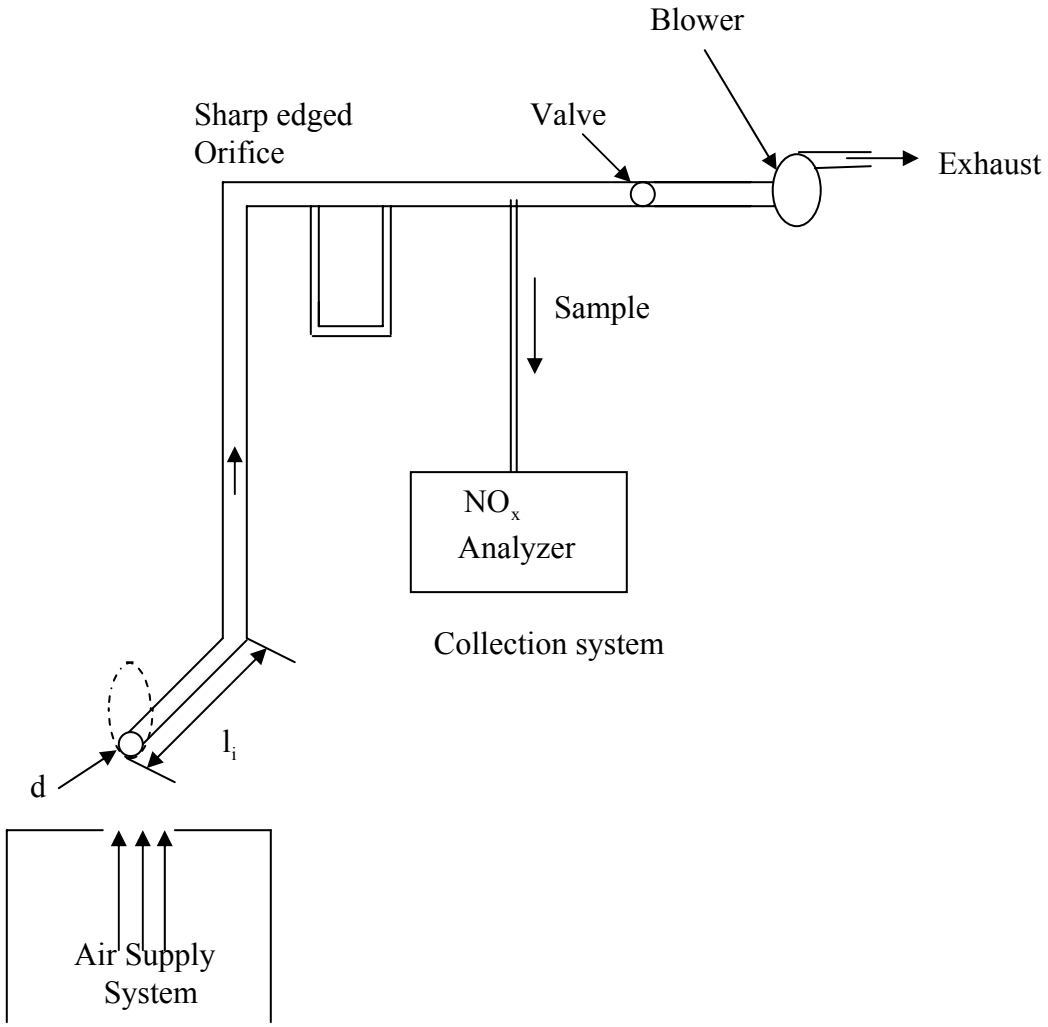

Figure II.3: Schematic of the Apparatus Used for Measurement of Total Oxides of Nitrogen Produced by a Diffusion Flame [6].

Three experiments were conducted by, Jaasma and Borman during the measurements of oxides of nitrogen produced by liquid fuel diffusion flames. In each of their experiments, a diffusion flame at one atmospheric pressure was formed around a horizontal fuel wetted cylinder. In the first experiment a porous metal cylinder of 5.2 mm diameter was wetted by normal heptane and placed in a low velocity stream of ambient air. Soot escaping from the turbulent wake of the diffusion flame was deposited on the surfaces of a large collection system located above the flame. This collection system drew in all of flame products plus some entrained ambient air. The soot was found to give off NO slowly at ambient temperature and more rapidly when heated. The NO from the soot amounted to 20 percent of the gas phase NO produced by the flame. In the second experiment, a quartz microprobe was used to take samples along a horizontal line perpendicular to the cylinder axis. The cause of high NO readings indicated by chemi-luminescent analyzer for samples taken near liquid surface were traced to sensitivity of the analyzer to pyroysis products. In the third experiment, the fuel wetted surface was a horizontal moving thread. It was found that the presence of unburned hydrocarbons in the air around the flame promoted the conversion of NO to NO_2 without changing the total amount of NO_x produced.

Mitchell and Sarofim [7] studied nitric oxide and hydrogen cyanide formation in laminar methane/ air diffusion flames. In their experiments, the researchers analyzed nitric oxide and hydrogen cyanide concentration distributions established in unseeded, laminar, atmospheric methane-air diffusion flames in order to gain insight into the role various nitrogen containing species play in influencing NO formation in such flames. Their experimental data indicated that HCN and NO formation are strongly dependent on local stoichiometry within the flame region. Figure II.4 shows the schematic of laboratory burner used by Mitchell and Sarofim in their experiments. Cyanide formation occurred only within the fuel-rich luminous flame core, presumably via reaction between hydrocarbon radicals and molecular nitrogen or nitric oxide. The cyanide species were subsequently partially converted to nitric oxide on the fuel-lean side of the primary

reaction zone, contributing 15-30 percent of the total nitric oxide production by the flame (i.e. thermal NO_x . The nitric oxide concentration profiles peaked on the fuel-lean side of the flame in the zone where the thermal production of NO by the extended Zeldovich mechanism occurs. Figure II.5 shows temperature and NO profiles vs. radial distance at 1.2, 2, 4 and 5 cm from the burner surface.

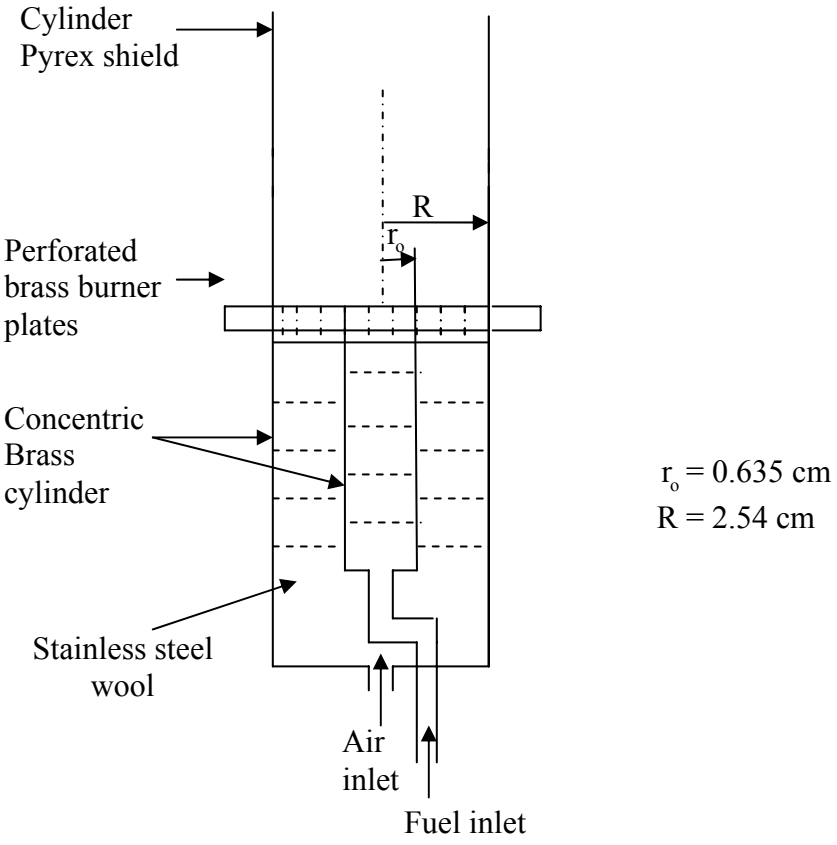

Figure II.4**:** Schematic of Laboratory Burner Used by Mitchell and Sarofim [7].

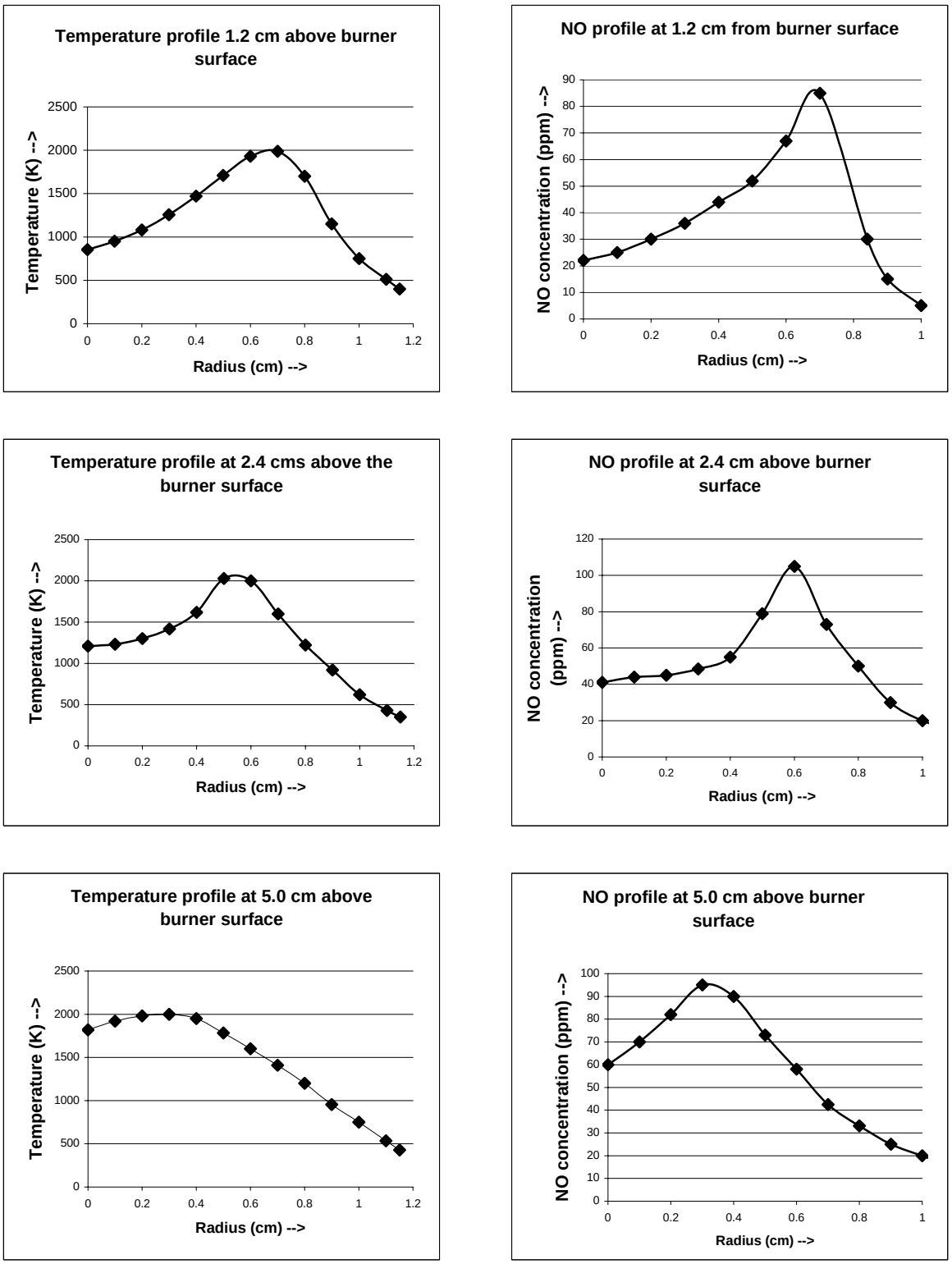

Figure II.5: Temperature and NO Profiles by Mitchell and Sarofim [7].

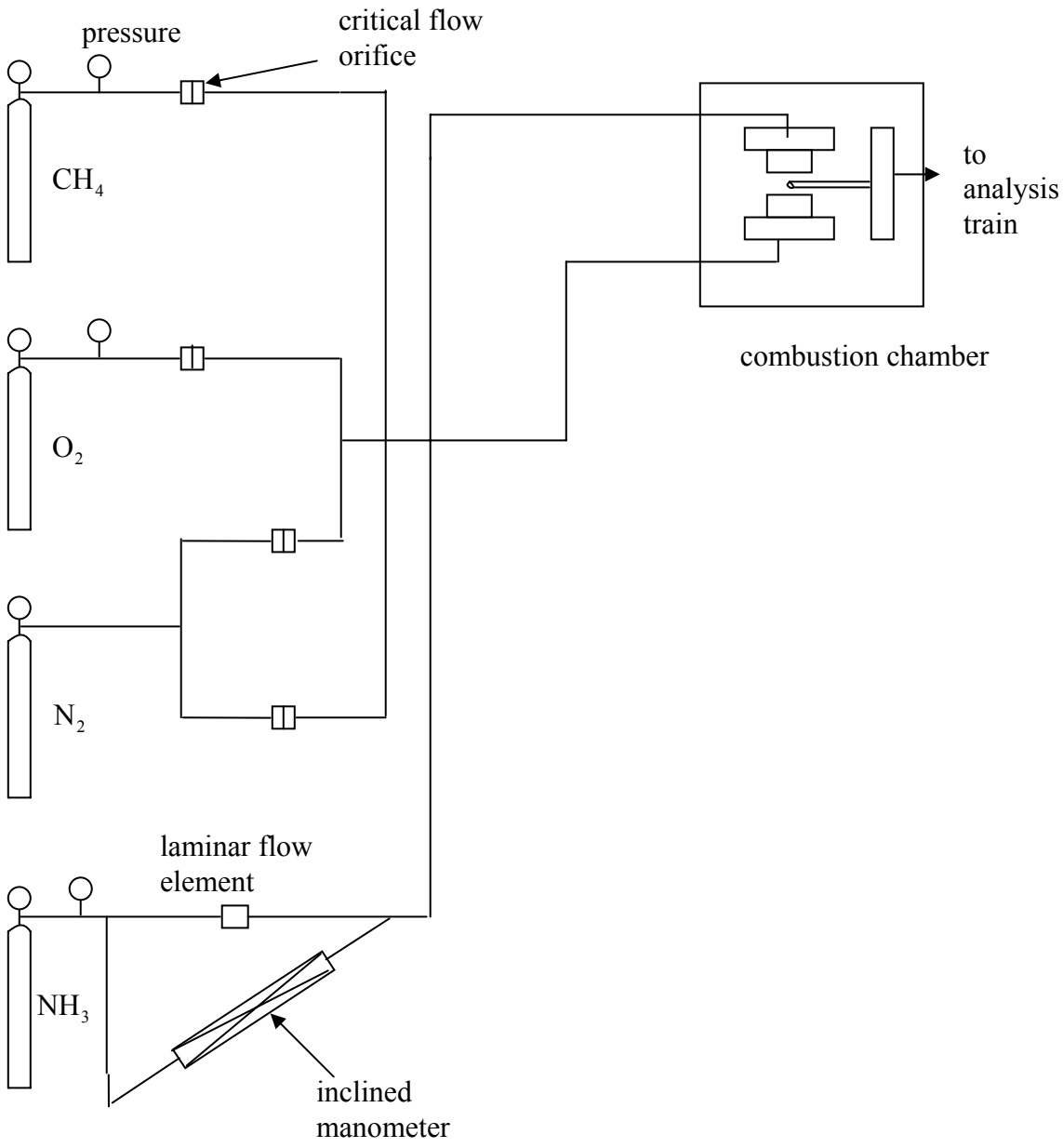

Figure II.6: Schematic of Combustor Used by Hahn and Wendt in their Experiments [8].

Hahn and Wendt [8] studied the formation of NO_x in flat, laminar, opposed jet methane diffusion flames. The experimental setup used by Hahn and Wendt used a combustion chamber. The combustion chamber was a 2x2x2-ft, sealed aluminum box which contained two vertically mounted opposed burners,

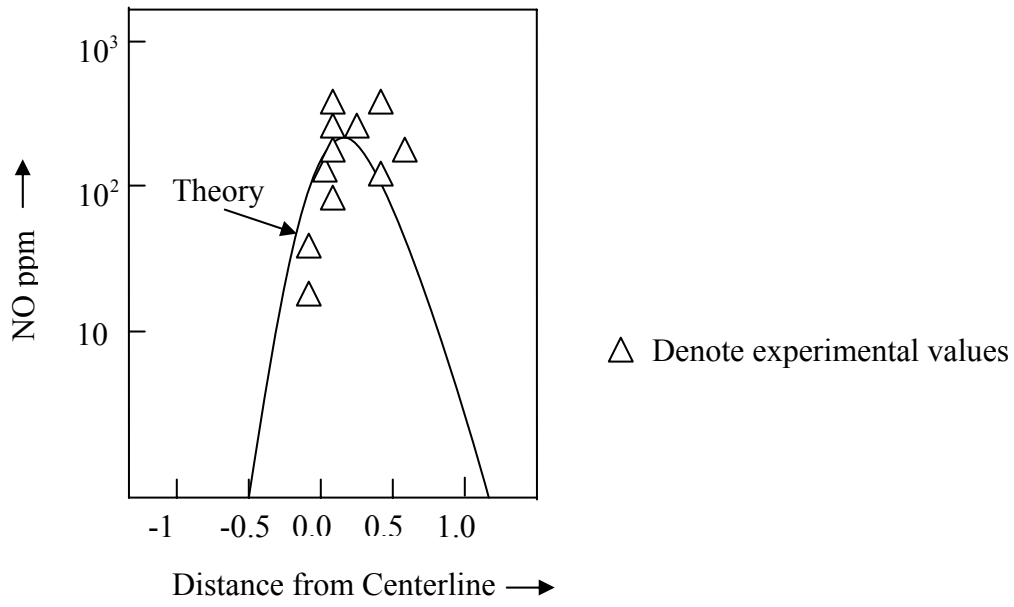

Figure II.7: NO Profile of a $CH_4/N_2/O_2$ Opposed Diffusion Flame With Strain (α = $3.62\,sec^{-1}$) by Hahn and Wendt [8].

an uncoiled quartz probe, I.D. = 0.6 cm, a platinum ignition wire, and a Pt, Pt/ 10% Rh thermocouple, which was mounted on the probe. The bead of the thermocouple used was approximately 0.002 inches in diameter and was uncoated. Figure II.6 shows a schematic of apparatus used by Hahn and co-workers in their experiments. The two burners were

made of 2.5-inch diameter stainless steel tubes filled with glass beads and sealed at the end with a stainless steel sintered disk. Feed lines mixed fuel (CH_4), oxygen and nitrogen and the mixture was fed to the two opposing burners described in Figure II.6.

It was shown by Hahn and Wendt that the detailed structure of a flat laminar jet diffusion flame can be modeled, by properly coupling the momentum and energy conservation equations and by using finite rate combustion kinetics. In the experiment, a laboratory $CH_4/N_2/O_2$ opposed jet diffusion flame was realized and gave good agreement with predictions with respect to both, one dimensionality and temperature and species profiles within the reaction zone. However, the actual location of the reaction zone is displaced by a small distance. The theoretical/ experimental tool developed in this study was utilized to test kinetic mechanisms of NO formation from fuel nitrogen. Also the qualitative dependence of the NO profile of flame stretching was correctly predicted by the model of Hahn and Wendt. This allowed the prediction of reaction zone thickness and the rate of formation of NO as a function of stretching rate and these results could be related to NO formation in strained laminar diffusion flamelets as they occur in turbulent diffusion flames. Figure II.7 shows NO profile of a $CH_4/N_2/O_2$ opposed diffusion flame with strain ($\alpha = 3.62\,\mathrm{sec}^{-1}$) where $\alpha = (du_\infty / dx)$.

Drake and Blint [9] studied the formation of thermal NO_x in stretched laminar opposed diffusion flames with $CO/H_2/N_2$ fuel. The researchers studied the effect of flame stretch (variations in velocity and concentration gradients) on thermal NO_x formation has been studied in laminar opposed-flow diffusion flames. Their detailed chemistry-transport model calculations showed agreement (within 150 K for peak flame temperature and within 3 ppm for peak thermal nitric oxide concentrations) with previous experimental measurements in $CO/H_2/N_2$ laminar opposed-flow diffusion flames at three different velocity gradients (α = 70, 180, and $330\,\mathrm{s}^{-1}$). Major corrections were required to account for the finite spatial resolution of the probe sampling measurements. For their study the

researchers used additional model calculations obtained over a wider range of stretch (α = 0.1-5000 s^{-1}). Calculated NO_x concentrations were found to decrease dramatically as flame stretch was increased (with peak NO_x values of 2300, 1100, 280, 20, and ≤ 1 ppm obtained for flames with α = 0.1, 1, 10, 100, and >500 s^{-1}, respectively). As flame stretches, u_∞ increases residence time in high temperature flame zones (proportional to α^{-1}) and in the net NO_x formation rates. The net NO_x formation rate was found to be affected by flame stretch due to decrease in peak flame temperature (as reaction time will increase due to lower T) and residence time, super equilibrium O atom concentrations, NO destruction reactions, and N_2O formation reactions. Most of the NO_x in flames at low stretch is formed by the Zeldovich mechanism, while the N_2O pathway dominates NO_x formation in flames at very high stretch where the peak flame temperatures are lower. Reactions involving the formation and destruction of NO_2 occurred in lean flame zones, but the amount of NO_2 formed was small (≤ 10 ppm). Both experiments and model calculations showed that a very effective way to reduce thermal NO_x formation in the forward stagnation regions of laminar opposed-flow diffusion flames (and possibly in turbulent diffusion flames as well) is to increase flame stretch.

In another research, Drake and Blint [10] studied the relative importance of nitric oxide formation mechanisms in laminar opposed-flow diffusion flames. The relative importance of the Zeldovich, N_2O, and Fenimore mechanisms for nitric oxide formation in stretched laminar opposed-flow diffusion flames with CH_4/N_2 fuel was determined using model calculations that included detailed chemical kinetics (213 reactions and 45 molecular species) and realistic multi-component transport effects. The model calculations were compared with previous measurements in laminar opposed-flow CH_4/N_2 diffusion flames at three values of stretch (α = 42, 70, and 140 s^{-1}). The NO

values calculated by the model were 110, 65 and 14 ppm respectively for α = 42, 70, and 140 s^{-1}. The model-experiment agreement (within 50 K for peak temperature and within a factor of 2 for peak NO_x formed) supported the validity of the detailed chemical kinetic mechanism used. Drake and Blint concluded that the Fenimore mechanism is expected to dominate NO formation in many laminar and turbulent hydrocarbon diffusion flames.

In a brief discussion Takeno and Nishioka [11] calculated the effect of flame stretch on $EINO_x$ and the effect of flame stretch on fraction of fuel consumed for with hydrogen-air counterflow diffusion air flames. The kinetics adopted by them for thermal NO mechanism constituted of 22 species and 73 elementary reactions. The researchers proposed various ways to calculate emission indices for NO_x in laminar and turbulent diffusion flames. The relation proposed by Takeno et al. is given as follows

$$EI'_{NO} = \frac{\int_0^L M_{NO}\,\dot{\omega}_{NO}\,dx}{\rho_o Y_{F,o}(u_o + V_{F,o})} = \frac{NO_x \text{ production rate}}{\text{fuel feed rate}}\ , \frac{g}{\text{kg of fuel}} \qquad (2.5)$$

However, the researchers further proposed that this remains merely an apparent index since the whole injected fuel is not necessarily consumed in the flame. Hence, if the index is needed to be defined in terms of the fuel actually consumed, then the relation can be given as

$$EI'_{NO} = \frac{\int_0^L M_{NO}\,\dot{\omega}_{NO}\,dx}{-\int_0^L W_F\,\dot{\omega}_F\,dx} = \frac{EI'_{NO}}{I_F} \qquad (2.6)$$

where I_F is defined as

$$I_F = \frac{\int_0^L M_F \dot{\omega}_F \, dx}{\rho_o Y_{F,o}(u_o + V_{F,o})} \tag{2.7}$$

The value of I_F will depend on the flow condition, as well as physical and chemical properties of the fuel and oxidizer.

Perhaps the most comprehensive study of scaling of Nitric Oxide emissions from buoyancy- dominated hydrocarbon jet diffusion flames was done by N.A. Rokke and O.K .Sonju and co-workers [12]. Their work demonstrated that useful scaling laws can be obtained solely from the underlying chemical kinetics, flamelet structure and buoyancy controlled turbulent jet- behavior. The results of theoretical estimates and measurements were reported on the emission of oxides of Nitrogen from methane, propane and natural gas flames under buoyancy controlled conditions.

Their theory employed reduced chemical kinetics mechanisms for the reaction sheet regime along with simplified mass, momentum and mixture fraction balances for the turbulent flame height. Explicit expressions for local, instantaneous NO production rates were derived using rate constants of fourteen elementary steps and a two reaction zone description of laminar flamelets was adopted. This enabled the calculation of average production rates from asymptotics through approximation of a joint probability- density function for mixture fraction and scalar dissipation.

The emission index proposed by Rokke et al. is given by the following relation

$$EINO_x = [H/(\rho_o u_o)](2R/d_o)^2 * (0.65\, \chi_f^{-0.9} + 1.4 \chi_f^{-0.4}) \tag{2.8}.$$

In this relation the first and the second terms represent the prompt and Zeldovich contributions, respectively. Here χ represents the scalar dissipation. The probability

density function P was assumed as a function as $P(Z, \chi)$ or function of the mixture fraction and the scalar dissipation.

The experimental setup consisted of continuous gas analyzers with water cooled quartz and stainless steel suction probes. Methane (purity of 99.5%) and commercial propane were used. A Signal Luminox 4000 chemiluminescent analyzer measured the oxides of nitrogen. The measured ratio of NO_x to CO_2 concentrations was used to calculate the emission index $EINO_x$. The test conditions in the experiments with propane were $2.2 \text{ m/s} \leq u_o \leq 240 \text{ m/s}$ and $4 \text{ mm} \leq d_o \leq 50 \text{ mm}$ and $17 \leq Fr \leq 4.5 \times 10^5$ and for $2 \times 10^4 \leq Re \leq 9 \times 10^5$. For methane $9.5 \text{ m/s} \leq u_o \leq 81 \text{ m/s}$ and $10 \text{ mm} \leq d_o \leq 28 \text{ mm}$ and $600 \leq Fr \leq 4.5 \times 10^5$. Fr is Froude number ($Fr = u_o^2 / gd$) The propane results were reported most extensively for $\rho_o = 2 \text{kg/m}^3$. Since the theory was based on flamelet models, comparisons were made with computational and experimental results for stretched laminar flames. The computations predict a Zeldovich contribution lower by about a factor of 3 (compared with the prompt NO_x mechanism) than predicted in the study and a Nitrous – oxide contribution at least an order of magnitude greater than the flamelet model. The differences may arise from the use of different elementary rate constants and from the fact that a different measure of relative importance was employed in the fact that the computations did not address the Emission indices explicitly.

Also their study included data from various other investigators like Turns and Lovell, Turns and Myhr, Rooke et al, Takagi et al, Buriko and Kuznetsov, Chen and Driscoll, Lovoie and Schiader and Bilger and Beck. The study was mainly restricted to hydrocarbon flames; however some hydrogen flames results were also included.

The theoretical correlations for emission indices of buoyancy- controlled flames were tested experimentally over the Froude number range of $10 \leq Fr \leq 5 \times 10^5$. The

agreement between theory and experiment was within a factor of two, well within theoretical uncertainty. However the predictions roughly equal the prompt and Zeldovich contributions with negligible nitrous oxide contributions at normal atmospheric pressure. Also it was emphasized in this study that the uncertainty in underlying rate constants in the prompt path and adoption of the flamelet structure were sources of error and deserved further investigation.

In yet another important study, which is the most relevant to the work present here, Rokke, N.A. et al. [13] performed a detailed study of partially premixed unconfined propane flames. In this study, unconfined partially premixed propane/ air flames issuing from a straight tube into quiescent air at atmospheric pressure and temperature were investigated. Experiments on lifted flames were performed. Flame height and liftoff were reported together with emission indices for oxides of nitrogen (NO_x). The degree of partially premixing was varied between a fuel mass fraction of 1.0 to 0.15. Six different nozzle diameters, d_o of 3.2, 6, 10, 20.5, 23.3, and 29.5 mm were used. This resulted in outlet velocities, u_o, varying from 1 to 130 m/s, flame heights up to 2.5 m, Froude numbers, Fr, from 3 to 3 $x10^5$, and thermal heat releases up to 350 kW. Flame height and liftoff show a strong dependence upon the ratio of the nozzle outlet velocity to the outlet diameter, the Froude number, and the fuel mass fraction Y_f. Both modified, simplified, and newly developed expressions for height, and NO_x emissions were presented and discussed. All the proposed expressions scaled with $Y_f^a Fr^b$ or $Y_r^a f(u_o, d_o)$. The emission index for NO_x scaled very well with a previously developed expression based on the buoyant flame volume. The agreement between predictions and experimental data was found to be generally good and well within the underlying experimental and theoretical uncertainties.

Rokke and co-workers constructed an experimental rig for measurements of liftoff, flame height and gaseous emissions. The experimental rig consisted of a vertical

telescoping mast, horizontally and vertically movable booms for attaching measuring equipment, and vertically positioned nozzles. Propane of commercial grade (min. 99.85 vol% C_3H_8, rest C_2 and C_4 alkanes) and methane (purity min. 99.5 vol %) were fed to a gas and air metering and mixing station High accuracy rotameters were used for gas and air metering. Propane was supplied by an external evaporator, to give stable temperature and pressure. Pressurized and dried air was mixed with the pure gases in a mixing chamber, the transport distance to the outlet nozzle was approximately 4 m ensuring a uniform mixture of air and gas. The gas and air temperatures were monitored and the differences in gas temperatures are negligible. The gas temperature is typically 288 K. The outlet nozzles were made of high-quality stainless steel, with external tapers of 15 ° to ensure clean flow in the vicinity of the nozzle outlet. The whole experimental setup was surrounded by a fine mesh wire screen, 3.5 m high to lessen effects of room draft. For NO_x measurements, the gas was extracted from the postflame region on the centerline. This has been shown to be sufficient elsewhere, as the $EINO_x$ profiles are constant both radially and axially in the postflame region. This is also true for partially premixed flames. Three independent measurements were made with the mean taken as the measured value. A water-cooled quartz probe was used for NO_x sampling, and a water-cooled stainless-steel probe sampled CO_2, CO, and O_2 with attention paid to inter conversions between NO and NO_2. A Signal Luminox 4000 chemi-luminescent analyzer measured oxides of nitrogen. Water vapor was removed from the sample by a cold trap before it entered the analyzer. The stainless-steel probe was connected to two different analyzers--a Servomex paramagnetic oxygen analyzer measured the O_2 level while the CO and CO_2 were measured with a Hartmann and Braun non dispersive infrared analyzer. The measured ratio of NO_x to CO_2 concentrations was used to calculate the emission index $EINO_x$, relative to NO_2, according to following equation:

$$EINO_x = \frac{n\,[NO_x]\,M_{NO_2}1000}{[CO_2]M_{CnHm}}[\frac{g\ NO_x}{kg\ fuel}] \quad (2.9)$$

Also Rokke et al. proposed a scaling law for the determination of $EINO_x$. The relation is given as follows:

$$EINO_x = 22\ Fr^{3/5}\ Y_f^{-1/5}\ (\frac{d_0}{\rho_0 u_0})\ x\ (0.35^{-0.45} + 0.7\ d_0^{0.2}) \quad (2.10)$$

Some of the experimental values in this study fall in the turbulent regime and some in the laminar regime. The values for which $Y_f = 1$ represents non-premixed inlet fuel conditions. These values which fall in the laminar regime have been utilized in this work for the validation of the model.

Although over time extensive work has been carried out in the field of both laminar and turbulent jet diffusion flames with co flowing air or counter flowing air, however only limited amount of work has been undertaken in laminar flames which involve air entrainment. This involves jets in which fuel is issued through a narrow orifice directly into ambient air. The air gets entrained due to the momentum of the fuel jet. However the air entrained at flame height is more than stochiometrically required air. For both a circular and 2-D jet, no one has performed the effect of Sc number on the solutions of velocity, species and temperature profiles. Excess air as a function of only Sc number has not been studied. The excess air will have a profound influence on the temperature and species profiles which in turn will affect the total NO_x production. It has been shown that that excess air fraction is only a function of Sc number [Annamalai and Tillman, 2000]. Excess air leads to an increased presence of O_2 required for combustion and consequently NO_x production, however excess air also has a cooling effect and leads to drop in temperature. Thermal NO_x is highly sensitive to temperature and decreases

sharply with the reduction in temperature. Thus it is interesting to calculate the overall effect of Sc number on the total production of NO_x. Also, the production of thermal NO_x continues beyond the flame height because of presence of high temperatures. Thus apart from the pre flame region, there is NO_x production in the post flame region of the flame also. This is significant till a point when the temperature consistently falls below 1300 K as the production of thermal NO_x is negligible when T<1300 K. Further the momentum carried by the jet presumes flat velocity profile. If profile is parabolic, momentum of jet is altered. Such a jet will entrain much more air compared to the flat case. Thus momentum of jet is set for an arbitrary profile at burner exit.

The following chapter defines the overall objective of the research and the presents methodology to satisfy the objective of this research.

CHAPTER III

OBJECTIVE AND METHODOLOGY

3.1. Purpose of Research

The overall objective of this research is to model the mixing, combustion and formation of NO_x in circular laminar jet flames.

3.2. Objectives of Research

To satisfy the overall objective of research, the following tasks are proposed:

1. Present governing differential equations for mass, momentum, energy and species for an isolated circular laminar jet issuing from a circular burner. Use these differential equations to solve for mass, momentum, energy and species at various axial and radial coordinates of the flame.

2. Use the thin flame model and obtain explicit solutions for species and T profiles.

3. Treat NO as trace species, obtain an expression for thermal and prompt NO production rate using overall global kinetics.

4. Analyze the effect of considering $H_2O \Leftrightarrow H_2 + 1/2\ O_2$ and $CO_2 \Leftrightarrow CO + 1/2\ O_2$ equilibrium on Thermal NO_x formation.

5. Analyze the effects of Sc number variation on the total NO_x production.

6. Compare the analytical predictions of results with experimental data available.

CHAPTER IV

MODELING OF A CIRCULAR LAMINAR JET FLAME

Jet flames can be divided into (i) laminar and (ii) turbulent jet flames. A large amount of work in this field has been done on turbulent jet flames which emulate more closely various real world phenomenon of combustion for e.g. in turbines and boilers, etc. However laminar jet flames have provided much insight into the basic understanding of flame structure and effect of transport properties and relative importance of NO_x reaction pathways in non premixed combustion for various flame conditions. Because NO_x production is a complicated phenomenon, it is important to first understand the combustion theory for an isolated laminar jet flame. The theory can then further be extended to cover multiple burners and also extrapolated for turbulent flames. The modeling is based on the solutions to the governing differential equations of mass, momentum, energy and species. These solutions are manipulated to yield expressions for the axial and radial gas velocity, the flame height, maximum flame width, the amount of air entrainment and temperature as a function of the injection Reynolds number, Schmidt number and fuel composition. In many practical combustion systems such as the

residential gas burners the jet issues from a straight tube into quiescent air at atmospheric pressure and temperature.

In a circular jet, the equations of mass, momentum, energy and species are presented in the compressible form along with boundary conditions. While 2D jet is amenable for transformation to incompressible form, the conversion of compressible form of equations into the incompressible form is not possible in the case of a circular jet. Hence the properties are assumed to be constant including density so that simple explicit solutions can be presented. The equations of mass, energy, and species are normalized, converted into ordinary differential equation using appropriate similarity variable and then solved using appropriate boundary conditions to give solutions for the axial and radial velocity (v_x and v_r), various species concentrations (Y_F, Y_{O_2}, Y_{N_2}, etc.), the flame height (H_f).A brief summary of relevant steps is presented in the following section. The reader is referred to detailed governing equations for 2D and circular jet, transformations and set of solutions for flame structure, flame height, lift off height etc. are presented by PhD thesis of Tillman [2].

This chapter will be divided into the following sections: (1) Presentation of governing equations and normalized solutions (2) NO_x modeling for an isolated circular laminar jet flame

4.1. Governing Differential Equations for Circular Jet

The conservation of mass, momentum, energy, and species equations for the circular jet in compressible form can be written as follows:

Mass Conservation

$$\partial / \partial x\{\rho v_x r\} + \partial / \partial r\{\rho v_r r\} = 0 \qquad (4.1)$$

Momentum Conservation (x-direction)

$$\partial / \partial x\{\rho v_x r v_x\}+\partial / \partial r\{\rho v_r r v_x\} = \partial / \partial r(\rho \upsilon r \partial v_x / \partial r)+\partial / \partial x(\rho \upsilon r \partial v_x / \partial x) \qquad (4.2)$$

Energy, Species, and Shvab-Zeldovich Conservation

In general, for any property "b"

$$(1/r)\partial / \partial r(\rho v_r r b)+\partial/\partial x(\rho v_x b)=\rho D \partial^2 b/\partial r^2+\rho D \partial^2 b/\partial x^2 \qquad (4.3a')$$

I II III IV

The term b can be Y_k or β_{O_2-F} or β_{h_T-F}.

Using order of magnitude analysis ($\beta \sim 1$ and $r \sim d_i$)

Now on comparison of term III and term IV

$$\rho D/d_i^2 (d_i/d_i) >>> \rho D/H^2 \text{ i.e. } H^2/d^2 >>>1$$

If $H_f >>> d$, then term IV can be neglected in comparison with term III. i.e. lateral diffusion terms are dominant compared to longitudinal diffusion terms.

Hence eq. (4.3a') can be converted into the following equation:

$$\partial / \partial x\{\rho v_x r b\}+\partial / \partial r\{\rho v_r r b\} = \partial / \partial r(\rho D r \partial b / \partial r) \qquad (4.3a)$$

Variable β, with $w_\beta(x,y) = 0$. The Shvab-Zeldovich variables for the single step reaction

given below, Where $b = Y_k, h_T,$ or β. Under mixing conditions, equation (4.3) can be used to solve for Y_k or h_T. For combustion, equation (4.3) must be solved for the Shvab-Zeldovich

$$1 \text{ kg of Fuel} + \upsilon_{O_2} \text{ kg of } O_2 \rightarrow \upsilon_{CO_2} \text{ kg of } CO_2 + \upsilon_{H_2O} \text{ kg of } H_2O$$

The Schvab-Zeldovich variable is defined as:

$$\beta_{O_2\text{-}F} = Y_F - Y_{O_2/\upsilon O_2} \text{ for fuel-oxygen,} \tag{4.3b}$$

$$\beta_{CO_2\text{-}F} = Y_F + Y_{CO_2/\upsilon CO_2} \text{ for fuel-}CO_2, \tag{4.3c}$$

$$\beta_{H_2O\text{-}F} = Y_F - Y_{O_2/\upsilon O_2} \text{ for fuel-}H_2O, \tag{4.3d}$$

$$\beta_{hT\text{-}F} = Y_F + Y_{CO_2/\upsilon CO_2} \text{ for thermal entahlpy fuel} \tag{4.3e}$$

Because b is finite as $y \rightarrow \infty$ (for example, if b = Y_{O_2} for a mixing problem, Y_{O_2} approaches 0.23 at $y = \infty$), equation (4.3a) can be converted as

$$\partial / \partial x\{\rho v_x r b'\} + \partial / \partial r\{\rho v_r r b'\} = \partial / \partial r(\rho D r \partial b' / \partial r), \tag{4.4}$$

Where,

$$b' = b - b_\infty = Y_k - Y_{k,\infty}, h_T - h_{T,\infty}, \beta - \beta_\infty, \text{ etc.} \tag{4.5}$$

and $b' \rightarrow 0$ as $y \rightarrow \infty$ which is similar to the boundary condition for v_x in the x-momentum equation.

4.1.1. Boundary Conditions for Circular Jet

The following three boundary conditions will be applied for the circular jet

Far Field and Symmetric conditions

$$\text{As } r \rightarrow \infty,\ v_x \rightarrow 0,\ b' \rightarrow 0 \tag{4.6}$$

$$\text{At } r = 0,\ \partial b'/\partial r \rightarrow 0,\ \partial v_x/\partial r \rightarrow 0 \tag{4.7}$$

Total Momentum Flux

The integral of momentum is written as M. all momentum comes from the gas leaving the burner as implied by equation (4.7). Thus, the momentum at any given x is simply given by:

$$M = 2\pi \int \rho v_x^2 r dr \tag{4.8}$$

and $M^* = M/M_{ref}$ where $M_{ref} = \{\pi d_i^2 / 4\}\rho_i v_{x,i}^2$ for a flat velocity profile.

If profile is flat, then $M^* = 1$.

Total β flux

The integral of the Shvab-Zeldovich variable, β is written as J. Hence,

$$J = 2\pi \int \rho v_x \beta' r dr \tag{4.9}$$

Where $\beta' = \beta - \beta_\infty$, $J^* = J/J_{ref}$ where $J_{ref} = (\pi d_i^4 / 4)\rho_i v_{x,i}\beta_i'$ assuming a flat velocity and species profile.

4.2. Normalization of Governing Differential Equations

For the isolated circular jet, the equations of mass, momentum, energy and species were normalized with normalized boundary conditions, converted into ordinary differential equations using appropriate similarity variable, and then solved with the appropriate boundary conditions to give solutions for the axial and radial gas velocity (v_x and v_r), the species concentrations (Y_F, Y_{O_2} ,etc.), the flame height (H), the lift off height of the flame (L), and the blow off velocity (v_{blow}). A brief summary of the relevant steps which will be taken is presented here.

To normalize the governing equations and appropriate boundary conditions, the following variables will be used:

$$r^* = r/d_i \tag{4.10}$$

$$x^* = x/d_i \tag{4.11}$$

$$v_x^* = v_x / v_{x,i} \tag{4.12}$$

$$v_r^* = v_r / v_{x,i} \tag{4.13}$$

The normalized SZ variable for laminar jet is defined as:

$$\phi = \beta/\beta = (\beta - \beta_\infty)/(\beta_i - \beta_\infty) \tag{4.14}$$

Using the above non-dimensional groupings allows the governing differential equations of mass, momentum, and Shvab-Zeldovich conservation given in equations (4.1) , (4.2) and (4.3), to be rewritten in the following normalized form:

Mass Conservation

$$\partial / \partial x^* \{v_x^* r^*\} + \partial / \partial r^* \{v_r^* r^*\} = 0 \tag{4.15}$$

Momentum Conservation (x-direction)

$$v_x^* \partial v_x^* / \partial x^* + v_r^* \partial v_x^* / \partial r^* = \{1/Re_i\}(1/r^*)\partial / \partial r^* (r^* \partial v_x^* / \partial r^*) \tag{4.16}$$

Energy, Species and Shvab-Zeldovich conservation

$$v_x^* \partial \phi / \partial x^* + v_r^* \partial \phi / \partial r^* = \{1/(Re_i SC)\}(1/r^*)\partial / \partial r^* (r^* \partial \phi / \partial r^*) \tag{4.17}$$

The boundary conditions must also be updated. The new conditions to be enforced are:

$$\text{As } r^* \rightarrow \infty, v_x^* \rightarrow 0, \phi \rightarrow 0 \tag{4.18a}$$

$$\text{At } r^* = 0, \partial v_x^* / \partial r^* \rightarrow 0, \partial \phi / \partial r^* \rightarrow 0 \tag{4.18b}$$

The conservation of momentum and Shvab-Zeldovich variables are rewritten as:

$$M^* = M/M_{ref} = \int_0^\infty v_x^* v_x^* r^* dr^* = 1/8 \text{ where } M_{ref} = \{\pi d_i^2 / 4\} \rho_i v_{x,i}^2 \tag{4.19a}$$

$$J^* = J/J_{ref} = \int_0^\infty v_x^* \phi \, r^* dr^* = 1/8 \qquad \text{where} \quad J_{ref} = (\pi d_i^4/4)\rho_i v_{x,i} \beta_i' \tag{4.19b}$$

4.3. Similarity Variables for Circular Jet

The normalized governing differential equations can be reduced from partial differential equations to ordinary differential equations with the selection of an appropriate similarity variable.

Schliciting (1955) [3] gives the appropriate similarity variable, η as:

$$\eta = r^*/x^* \tag{4.20}$$

The use of this similarity variable allows the momentum equation given in equation (4.16) to be rewritten as:

$$f''' - f''/\eta + f'/\eta^2 - f'^2/\eta + ff'/\eta^2 - ff''/\eta = 0 \tag{4.21}$$

Where,

$$f = \xi^2/(1+\xi^2/4) \tag{4.22a}$$

and,

$$\xi = (\sqrt{3}/8) M^{*1/2} Re_i r^*/x^* = (\sqrt{3}/8) M^{*1/2} Re_i \eta \tag{4.22b}$$

Using the appropriate boundary conditions allows the momentum equations in equation (4.19) to be integrated to give the following solutions:

$$f' = 2(\sqrt{3}/8) M^{*1/2} Re_i \xi/(1+\xi^2/4)^2 \tag{4.23}$$

$$v_x^* = f'/(Re_i r^*) = (3/32)M^{*1/2}(Re_i/x^*)/(1+\xi^2/4)^2 \quad (4.24)$$

$$v_r^* = \{1/(Re_i x^*)\}[f' - f(\eta)/\eta]$$

$$v_r^* = \{1/x^*\}[\{(\sqrt{3}/8)M^{*1/2}\}\xi\{1-\xi^2/4\}/(1+\xi^2/4)^2] \quad (4.25)$$

4.4. Solution

The solution for ϕ will lead to the solution for T and Y_k for mixing problems and β for combustion problems. The coupling function is modified as:

$$\psi(\eta) = \phi x^* \quad (4.26)$$

Selection of this variable allows the species and energy equations, represented by the Shvab-Zeldovich formulation in equation (4.17), to be reduced to the following:

$$\psi_K''\eta + \psi_K' + Sc\ f\psi_K' + Sc\ f'\psi_K = 0 \quad (4.27a)$$

$$\psi_T''\eta + \psi_T' + Pr\ f\psi_T' + Pr\ f'\psi_T = 0 \quad (4.27b)$$

Solutions for the energy, species, and Shvab-Zeldovich conservation equations are given by:

$$\phi = (2Sc+1)(J^*/32)(Re_i/x^*)/\{1+\xi^2/4\}^{2Sc} \quad (4.28)$$

4.4.1. Summary of Solutions

The solutions to the governing differential equations for circular jets are summarized in tabular forming Table IV.1. [2]. The symbols used in the tables are defined in the nomenclature at the front of this document. All the solutions in Table IV.1 are presented in absence of buoyancy forces. If buoyancy forces are included, M^* and J^* listed in #2 and #3, respectively will be larger than the listed values. The solutions for the axial velocity, the lateral velocity and the species/temperature profiles for mixing problems or Schvab-Zeldovich variable profiles for combustion problems are also summarized.

Table IV.1: Summary of Solutions to the Governing Differential Equations for Laminar Circular Jets.

No.	**Parameter**	**Circular Jet**	**Remarks**
1	Properties	Constant	For a circular jet The properties are Assumed to be const.
2	M^*	$M^* = 4/3$ for parabolic $v_{x,i}$ profile at inlet $M^* = 1$ for flat $v_{x,i}$ profile at inlet	$M^*>1$ when Fr>1 or when buoyancy is important.
3	J^*	$J^* = 4/3$ for parabolic $v_{x,i}$ and parabolic b profile. $J^* = 1$ for a parabolic $v_{x,i}$ and flat b profile $J^* = 1$ for flat $v_{x,i}$ and flat b profile	

Table IV.1: Continued.

No.	Parameter	Circular Jet	Remarks
4	Stretched coordinate	$r' = r$ (assumed incompressible)	
5	Similarity coordinate, η	$\eta = r^*/x^*$	r = radial coordinate for the circular jet.
6	Modified similarity variable, ξ	$\xi = (\sqrt{3}/8)M^{*1/2}Re_i r^*/x^*$ $= (\sqrt{3}/8)M^{*1/2}Re_i \eta$	
7	Momentum eq.	$f'''-f''/\eta+f'/\eta^2-f'^2/\eta+ff'/\eta^2$ $-ff''/\eta=0$ $f'=2(\sqrt{3}/8)M^{*1/2}Re_i\xi/(1+\xi^2/4)^2$ $v_x^*=f'/(Re_i r^*)=(3/32)M^{*1/2}$ $=(3/32)M^{*1/2}(Re_i/x^*)/(1+\xi^2/4)^2$ $v_r^*=\{1/(Re_i x^*)\}[f'-f(\eta)/\eta]$	
8	Species eq. in η	$\psi_K''\eta+\psi_K'+Sc\, f\psi_K'+Sc\, f'\psi_K=0$ where $\psi(\eta) = \phi x^*$	
9	axial velocity,	$v_x^* = (3/32)M^{*1/2}(Re_i/x^*)/(1+\xi^2/4)^2$ $v_{x,max}^* = (3/32)Re_i\ M^*/x^*$	
10	radial velocity	$v_r^*=\{1/x^*\}[\{(\sqrt{3}/8)M^{*1/2}\}\xi$ $\{1-\xi^2/4\}/(1+\xi^2/4)^2]$ $v_{r,max}^*=\{1/x^*\}(9/96)M^{*1/2}$	

Table IV.1: Continued.

No.	Parameter	Circular Jet	Remarks
11	Mixing layer thickness	$r_m^* = 48x^*/\{\sqrt{3}Re_i M^{*1/2}\}$	Mixing layer $\propto$ x
12	Mass flow	$\dot{m}(x^*,r^*)/\dot{m}_i = 32(x^*/Re_i)$ $[1/(1+\xi^2/4\}]$	Total mass flow at any x^* between $r = 0$ and $r = r^*$
13	Total mass flow	$\dot{m}(x^*,\infty)/\dot{m}_i = 32(x^*/Re_i)$	Total mass flow between $r = 0$ and $r = \infty$
14a	Air entrained at x^*	$\dot{m}_A/\dot{m}_i = 32(x^*/Re_i) - 1$	Total air at $x = x^*$ between $r = 0$ and $r = \infty$
14b	Air entrained at $x^* = H_{st}^*$	$\dot{m}_A/\dot{m}_i = J^*\{(2Sc+1)/\phi_f - 1\}$ $\dot{m}_A/\dot{m}_i \approx J^*(2Sc+1)/\phi_f$ $\dot{m}_A(Sc)/\dot{m}_A(Sc=1) \approx C$	Total air entrained at $x^* = H_{st}^*$ between $r = 0$ and $r = \infty$
15	Species and non dimensional Shvab-Zeldovich	$\phi(Sc=1) = (3/32)(J^* Re_i/x^*)$ $/\{1+\xi^2/4\}^{2Sc}$ $\phi(Sc \neq 1) = (2Sc+1)(J^*/32)$ $(Re_i/x^*)/\{1+\xi^2/4\}^{2Sc}$	
16	Lift off Height	$L_{Lift}^*/H_{cir}^* = \{(Cv_{x,i}/S)\phi_f\{M^*/J^*\}^{Sc/Sc-1}$ where $C = \{(2Sc+1)/3\}$	

(All the results summarized in the table have been explained in detail in Appendix A.)

4.4.2. Flame Structure

The flame contour is similar to the one shown in Figure IV.3. Let us assume a thin flame model. The fuel exists in the inner region while oxygen exists in the outer region. This is illustrated in Figure IV.3. Only at some distance r_{st}, the fuel mixture will be in stoichiometric proportions. Given these restrictions on the flammability limits, if the mixture is ignited within the region bound by the rich limit and the lean limit, the flame can propagate only within the narrow region, δ, which is called the combustible mixture tube. For this work, it is assumed that the combustible mixture tube is thin and can be represented by the position in space where the fuel and air are in exact stoichiometric proportions. This is the thin flame approximation in this work. Particularly item # 15 of table IV.1 leads to presentation of flame structure Y_k (r,x), k = CO_2, H_2O, O_2, N_2 and fuel. Also T (x) if one assumes thin flame model ($\delta = 0$ in Fig. IV.3).

4.4.3. Solution for Flame Height

The stoichiometric contour for mixing is the same as the flame contour for the case of combustion.

$$\phi_f = f_\infty / \{1 - f_i + f_\infty\} = \{(2Sc+1)/32\}(Re_i J^*)/(x^*)1/\{1+\xi_f^2/4\}^{2Sc} \tag{4.29}$$

Maximum height is obtained by setting $\xi_f = 0$. Then

$$H^*_{cir} = \{(2Sc+1)/(32\phi_f)\} Re_i J^* \tag{4.30}$$

Note that H_{cir}^* for the circular jet is proportional to $1/\phi_f$.

4.4.4. Solution for Air Entrainment for Circular Jet

Total gas entrained at x^* between $r^* = 0$ and $r^* = r$ is given as:

$$\dot{m}(x^*,r^*)/\dot{m}_i = 2\pi\{\int_0^r \rho v_x r dr/\dot{m}\} = 8\{\int_0^{r^*} v_x^* r^* dr^*\} \tag{4.31}$$

Using the expression for velocity

$$v_x^* = f'/(Re_i r^*) = (3/32)M^{*1/2}(Re_i/x^*)/(1+\xi^2/4)^2 \text{ and the definition of } \xi \tag{4.32}$$

$$\dot{m}(x^*,r^*)/\dot{m}_i = \{32x^*/Re_i\}[1/(1+3Re_i^2 r^{*2} M^*/(256x^{*2})\}]$$

or $$\dot{m}(x^*,r^*)/\dot{m}_i = 32(x^*/Re_i)[1/(1+\xi^2/4\}] \tag{4.33}$$

Total air flow is given by subtracting the jet mass flow at burner outlet.

Total gas and air entrained at x = H is obtained by setting $x^* = H^*_{cir}$

$$\dot{m}/\dot{m}_i = 32H^*_{circ}/Re_i = J^*\{(2Sc+1)/\phi_f\} \tag{4.34}$$

Similarly air flow is given as

$$\dot{m}_A/\dot{m}_i = J^*\{(2Sc+1)/\phi_f - 1\} \tag{4.35}$$

Since $\phi = \dfrac{0-\beta_\infty}{\beta_i - \beta_\infty}$ then:

$$1/\phi_f = \{A{:}F\}_{Stoich} + 1,$$

Eq. (4.35) is simplified as :

$$\dot{m}_A/\dot{m}_i = J^*\{(2Sc+1)\{A{:}F\}_{Stoich} + 1\}\text{-}1 \qquad (4.36)$$

4.4.5. Excess Air

This air flow $\dot{m}_A$ at $x = H_{cir}$ is more than stochiometrically required air, $\dot{m}_{a,\,stoichiometric}$ for burning the fuel issued from the jet. Borrowing the term from fire literature [14] where excess fuel is defined when a polymer plate burns under free or forced convection, one can define excess air as:

$$(\dot{m}_{A,\,excess}) = \dot{m}_A - \dot{m}_{A,Stoich.} \qquad (4.37a)$$

Normalizing, the Sc excess air fraction is given as

$$[\dot{m}_A(H^*_{stoich},\infty) - \dot{m}_{A,stoich}]/\dot{m}_{A,stoich} =$$
$$[\{(2Sc+1)J^*_F - 1\}\text{-}1/[A{:}I]_{stoich}[(2Sc+1)J^*_F - 1]$$

$$[\dot{m}_A(H^*_{stoich},\infty) - \dot{m}_{A,stoich}]/\dot{m}_{A,stoich} \approx [(2Sc+1)J^*_F - 1] \approx 2Sc \qquad (4.38)$$

Equation (4.38) shows that excess air fraction is only a function of Sc.

4.5 Procedure for NO_x Modeling in an Isolated Circular Laminar Jet

As shown in previous section 4.4.2. the relations for profiles T (r,x), $Y_{O_2}(r,x)$, Y_{N_2} (r, x) can be obtained. In case of combustion of fuels that do not contain nitrogen bound in

organic material, fuel NO_x is Zero. Hence in the current research, the hydrocarbons dealt with are fuels like propane and methane, the fuel NO_x is zero.

The ambience is the entire region outside the mixing layer. The potential core is assumed to be relatively small and in our analysis, the potential core is not accounted for in the calculations or is neglected. NO_x via the Zeldovich mechanism proceeds in regions where N_2 and O_2 co-exist. If one assumes thin flame model, thermal NO_x is produced only in region L (Figure IV.1). On the other hand if dissociation occurs or equilibrium is assumed then O_2 could be present in trace amounts within region R (Figure IV.1) Thus thermal NO_x could be produced in region R also for cases when equilibrium is assumed. In post flame region, T gradually decreases and rate of decrease depends upon the excess air percentage at $x = H_{cir}$. Higher the excess air (i.e. higher Sc number) faster the decrease of T and lower the post flame region D produces thermal NO_x. Now a model will be developed for NO_x formation including all regions R, L and D. The effect of Sc number variation on the total production of NO_x is modeled and observed. This process is repeated for all four cases mentioned above. Starting from a region out of the potential core, the value of NO_x is calculated at all the radial distances at a particular value of x* or the axial distance. Then the total NO_x production is calculated by integrating these values for various x* till a point beyond the flame height where the temperature consistently falls below 1400 K.

The total NO_x production is calculated for the following four cases:

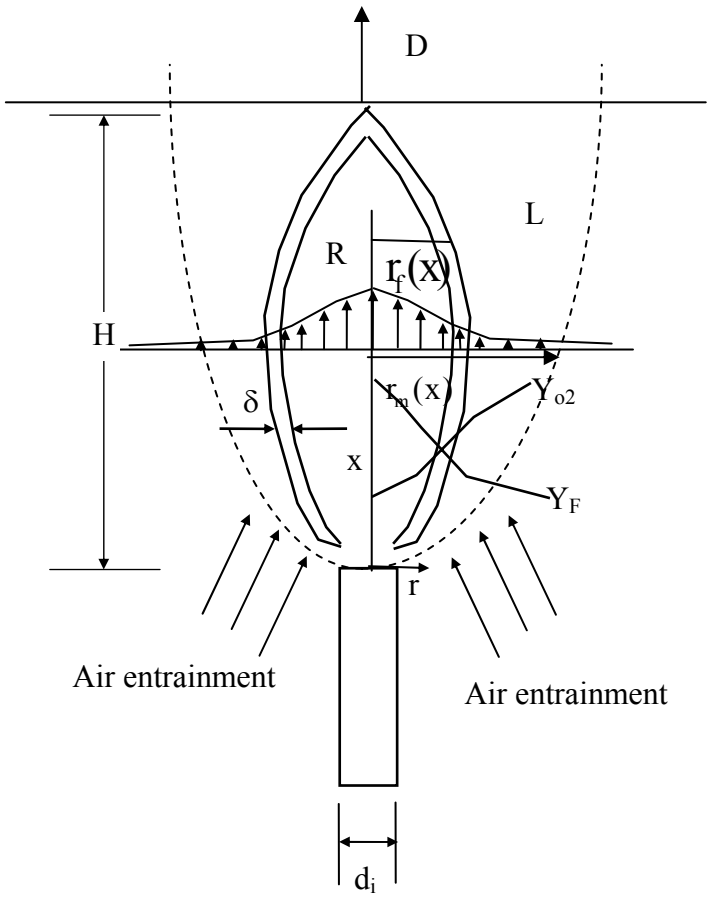

Figure IV.1**:** The Axial Velocity Profile and Fuel and Oxygen Mass Fraction Profiles for a Circular Jet Under Mixing Conditions. The Momentum of the Jet Entrains the Necessary Oxygen for Combustion. A Stoichiometric Region is Formed From the Mixing of the Entrained Air and the Fuel Issuing From the Jet. A Qualitative Illustration of the Mass Fraction of Oxygen and Fuel is Shown on the Figure.

(1) Complete Combustion: In which O_2 is absent in the fuel rich region R and Fuel is absent in the O_2 rich region (fuel rich region, L)

(2) CO_2 Equilibrium: When the equilibrium of the reaction $CO_2 \Leftrightarrow CO + 1/2\ O_2$ is considered there is presence of trace amounts of CO and O_2 in regions R and L.

(3) H_2O Equilibrium: When the equilibrium of the reaction $H_2O \Leftrightarrow H_2 + 1/2\ O_2$ is considered then H_2 and O_2 are present in regions R and L.

(4) CO_2 and H_2O Equilibrium: The equilibrium of both of the above mentioned reactions is considered simultaneously and O_2 contribution will be from both H_2O and CO_2 dissociation.

However CO_2 and H_2 and O_2 produced by equilibrium reactions are assumed to be in trace amounts hence Y_{CO_2} and Y_{H_2O} at various flame locations is relatively unaffected. lean regime is negligible. For the case (1), there is no Y_{O_2} (oxygen mass fraction) in the fuel rich regime. In the case when CO_2 or H_2O or both CO_2 and H_2O equilibrium is used, there is a non zero Y_{O_2} oxygen mass fraction in the fuel rich regime which consequently increases the NO_x production. This Y_{O_2} value in region R is calculated by considering the $CO_2 \Leftrightarrow CO + 1/2\ O_2$ equilibrium at every radial point at a given x* and then integrated over the entire range of x*. The following relation for equilibrium constant is assumed and calculated from standard tables.

$$\ln K = C_1 - \frac{C_2}{T} \qquad (4.39a)$$

A 10 point curve fit of table data yields the following values of C_1 and C_2.

Where C_1 and C_2 are constants. For CO_2, $C_1 = 4.327$ and $C_2 = -14436$.

For H_2O $C_1 = 3.0165$ and $C_2 = -13078.5$. (4.39b)

Hence, the equilibrium constant is a function of the temperature and can be solved at various differential locations and the oxygen mass fraction is ascertained in the fuel rich regime. Similarly one may assume $H_2O \Leftrightarrow H_2 + 1/2\ O_2$ and the combined CO_2 and H_2O equilibrium. For calculating the rate of volumetric production of thermal NO_x, the following global relation is assumed [2]as:

$$\dot{\omega}_{NO}''' = \frac{d[NO]}{dt} = \frac{A_{NO} M_{NO} (\rho_{mix})^{1.5}}{(M_{N_2})(M_{O_2})^{0.5}} \exp\left(\frac{-E}{RT}\right) \frac{(Y_{N_2})(Y_{O_2})^{0.5}}{T^{0.5}} \ , \frac{kg}{m^3 s} \qquad (4.40)$$

$$\text{Where } \rho_{mix} = \frac{PM_{mix}}{RT} \qquad (4.41)$$

An elemental volume of $\pi r^2 dx$ is considered as shown in figure IV.2

$$NO_x \text{ produced} = w_{NO}''' * dx * dr * 1 \qquad (4.42a)$$

Integrating over dr at a given x :

$$d\dot{w}_{NO} / dx = \int_0^{\infty} \dot{w}'''_{NO}\ 2\pi r\ dr \qquad (4.42b)$$

Where $\dot{\omega}_{NO}'''$ is known from eq. (4.40)

$$d\dot{w}_{NO} / dx = 2\pi d_i^2 x^{*2} \int_0^{\infty} \dot{w}'''_{NO}(T, Y_{N_2}, Y_{O_2})\eta\ d\eta \qquad (4.43)$$

$$\text{Where } r^* = \frac{r}{d_i}\ ; x^* = \frac{x}{d_i} \text{ and } \eta = \frac{r^*}{x^*}$$

After obtaining the various species concentrations and temperature profile from eqs. (18, 19, 23), the rate of thermal NO_x can be calculated from eq. (4.40). Then eq. (4.43) is integrated to attain the net rate of thermal NO_x. The final value is reported in ppm, g/GJ and also $EINO_x$ (g/kg of fuel). Methods of conversion to different units is summarized in Appendix.

Production of prompt NO_x formation in hydrocarbon systems involves the multi-step reaction sequence of hydrocarbon radicals first postulated by Fennimore [1]

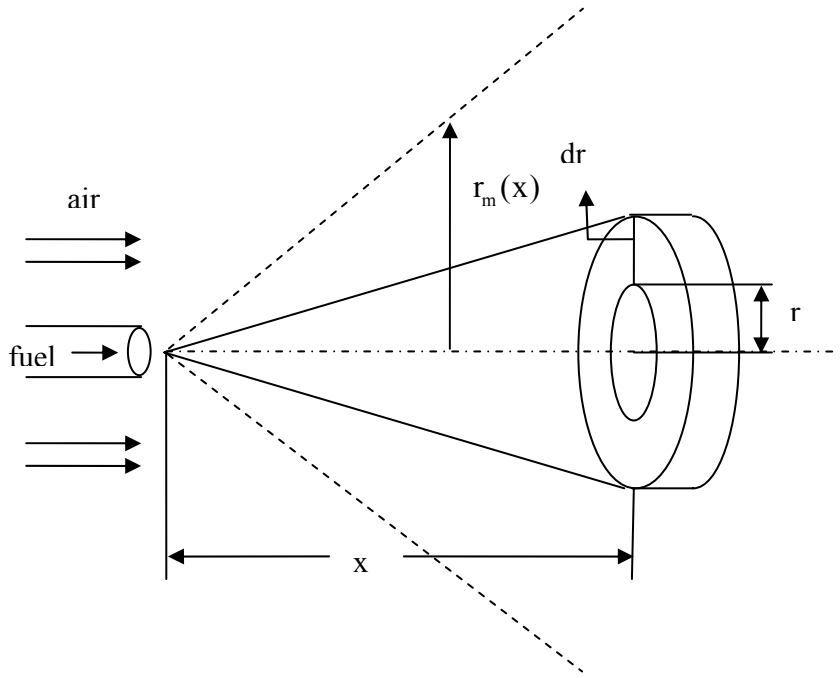

Figure IV.2: Schematic of an Elemental Volume Used for Integration.

The general scheme of the Fennimore mechanism is that hydrocarbon radicals react with molecular nitrogen to form amines or cyano compounds. These are converted to intermediate compounds that ultimately form NO_x. The earlier literature focused on incorporating detailed chemistry involving simultaneous consideration of hundreds of species and intermediate species in the flame [5]. However these studies involve very detailed models and usually the computational cost involved is very large.

For prompt NO_x, an empirical rate relation presented by [15] is used:-

$$\dot{\omega}'''_{\text{prompt NOx}} = A\frac{M^{1+b}}{\rho^{1+b}}C_{O_2}^{b}C_{N_2}C_{CH_4}\exp\left(\frac{-E_a}{RT}\right) \qquad \left(\frac{\text{Kmole}}{m^3 s}\right) \tag{4.44}$$

Where pre-exponential factor A = 9.2 x10^6, b= 0.5 and $\frac{E_a}{R}$ = 30000 (K) respectively.

Using a method similar to thermal NO_x as given above, the total prompt NO_x will be calculated by using eq (4.44) in eq (4.43).

4.6. Solution Procedure

1) With thermo-chemical data input of fuel, geometry of jet and transport properties, flame structure is obtained.
2) For equilibrium cases, the local mass fractions of CO, H_2 and O_2 are computed from known CO_2 and H_2O concentrations.
3) Using global reactions $\dot{\omega}'''_{NO}$ is computed.
4) Integration is continued for $x > H_{cir}$ until T drops to 1300 K.

CHAPTER V

RESULTS AND DISCUSSIONS

This chapter is divided into 3 sections: (1) Results of NO_x modeling, (2) Effect of Sc number on the production of NO_x and (3) Comparison with experimental values. The following section covers the results of numerical modeling of the laminar jet for all of the four cases cited above.

5.1. Results of Modeling

The results reported here are the modeling results for propane with the inlet fuel and transport properties as shown in Table V.1.

5.1.1. Complete Combustion

In this case O_2 is absent in the fuel rich region R, fuel is absent in the O_2 rich region L. The production of thermal NO_x is zero in R due to absence of O_2. The net

Table V.1: Inlet Conditions for Fuel Utilized for Modeling of NO_x in the Study.

Input	Value	Units
Fuel Properties		
Carbon	3	
Hydrogen	8	
Nitrogen	0	
Oxygen	0	
Sulphur	0	
h_c, lower heating value	46357	KJ/Kg
Transport Properties		
λ	7.63E-05	KW/m K
C_p	1.175	KJ/Kg K
υ	0.00001	m^2/s
Sc	1	
Jet Properties		
T_∞	300	K
$Y_{f,i}$	1	
$Y_{O_2,\infty}$	0.23	
T_i	300	K
d_i (m)	0.01	m
v_i (m/s)	0.5	m/s
M*	1	
J*	1	
Molecular weight of fuel	44.11	

NO_x production in the case complete combustion is 4 ppm, 4.61 g/GJ and $EINO_x$ is 0.14.Figure V.1.shows the production of NO_x $z = (d\dot{\omega}_{NO}/dx) = \int_0^\infty \dot{\omega}'''_{NO} 2\pi r\,(x)$ at individual axial points. Whereas Figure V.2 shows how the total NO_x and T_{max} varied with axial distance x*. It is clear that $z \to 0$ at $x^* > 80$ where $T_{max} < 1400$ K . As shown in Table V.1 these results are for Sc =1. In a later section, the effect of varying Sc number is also demonstrated and its effect on the production of NO_x is studied. Figure V.3 shows the Variation of Y_{N_2}, Y_{O_2} and T with Radial Distance r^* at a) x^*= 57, b) x^*=15 and c) x^*=70.The maximum temperature occurs at flame for $x<H_f$ with $T_{max} = T_{adiabatic}$ as the flame moves closer to the axis with rapid radial heat transfer. For x^* = 57, $T_{max} \approx T$ (r =0). For x^*=15, T (r =0) < T_{max}. Physically this can be explained by the fact that near the burner exit, due to higher velocities heat is carried away faster by advection and hence there is more temperature difference in between the flame temperature and the centerline temperature. Also since the flame is located farther away from the axis, this leads to reduced radial heat transfer. Further downstream, T (r =0) comes closer to the $T_{adiabatic.}$ After the flame tip (x> H_f), T_{max} =T (r =0). $\partial T/\partial x$ = 7000 (K/m) thus $\lambda \partial T/\partial x \approx 0.07$ (KW/ m^2) and $\partial T/\partial r$ = 60000 (K/m) at x^* = 65 which is near the flame tip but downstream the flame height. For $x^* < 62.8$, $\partial T/\partial x = \partial T/\partial r \approx 0$ .However $\partial T/\partial r >> \partial T/\partial x$ for x^*>62.8 and thus the assumption of negligible diffusive gradient properties in the x direction is still valid as given by eq. (4.3a'). As x^* >> H_f, $\partial T/\partial r \approx \partial T/\partial x$. These gradients are comparable for x^* >160. However, the production of NO_x is negligible beyond x^*>90 and hence region beyond x* >100 is not of interest. It is interesting to note that the gradient $\partial T/\partial x$ and $\partial T/\partial r$ are both non zero beyond the flame height or in the post flame region. The model represents an unconfined non-premixed propane/ air flames issuing from a straight tube into quiescent air at atmospheric pressure and temperature. It is evident from the graph that highest NO_x production per unit distance takes place at about x*= 57 almost near the flame tip since the flame height in this case is at x*= 62.8.

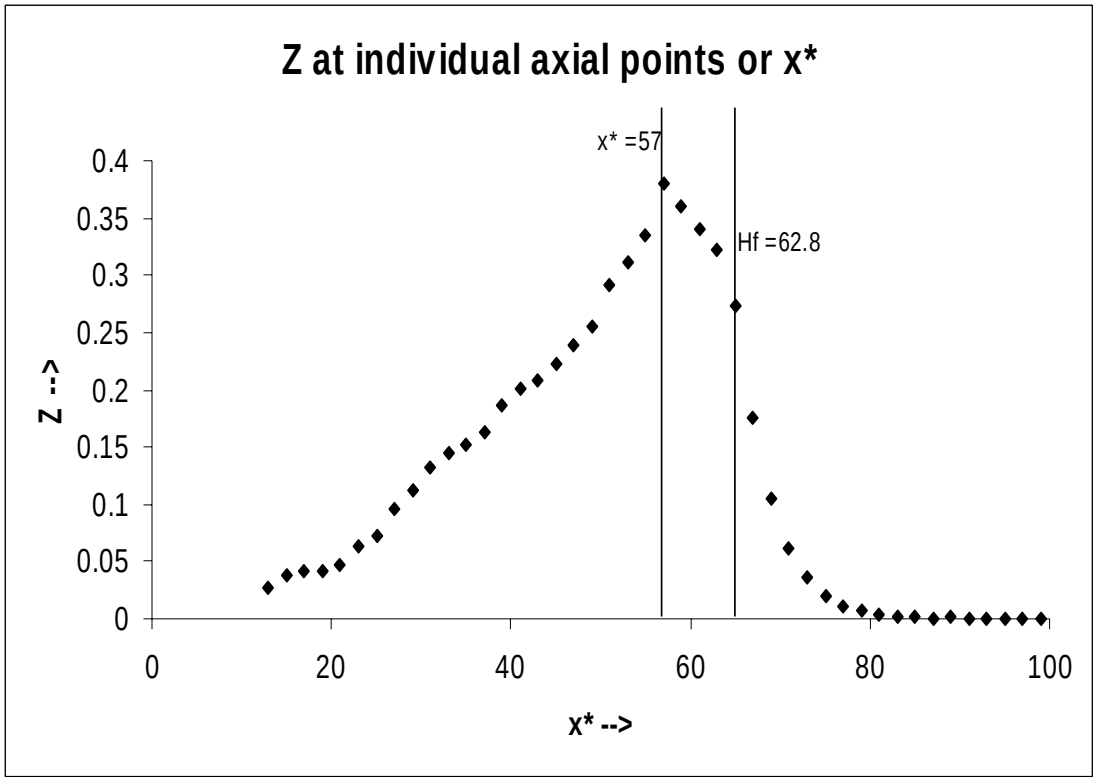

Figure V.1: The Production of Total $z = (d\dot{\omega}_{NO}/dx)$ (g/GJ per Unit Dimensionless Height) vs. (x^*) for the Case of Complete Combustion.

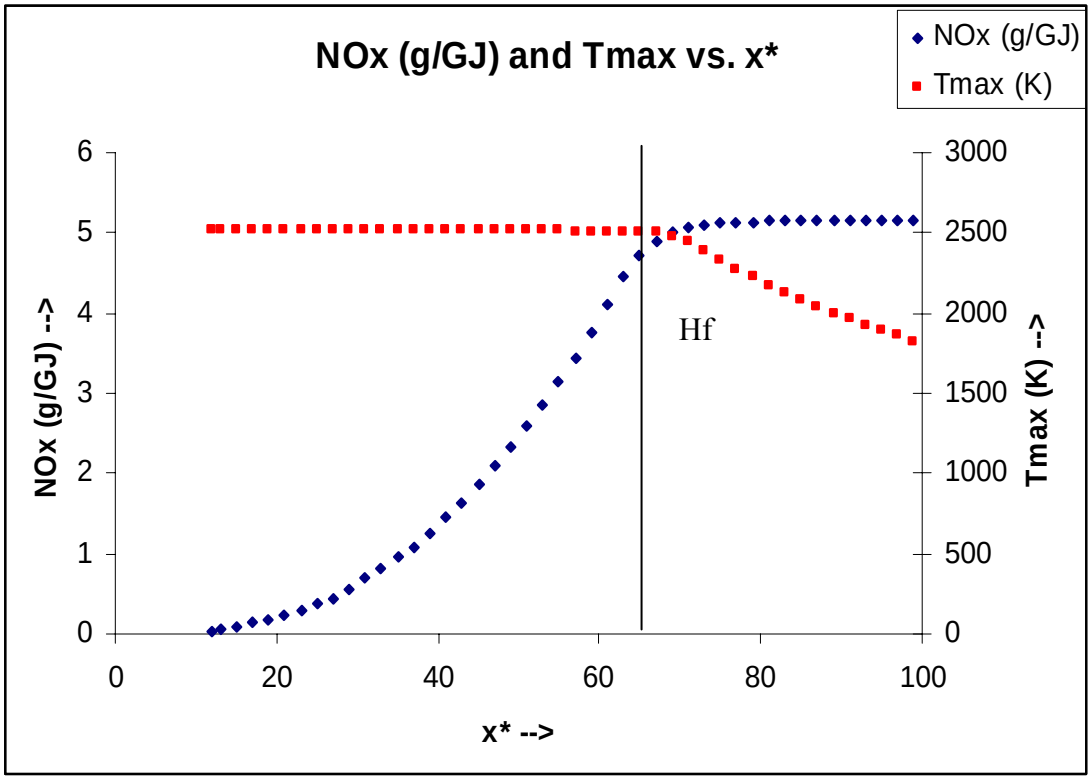

Figure V.2: Variation of Total NO_x (g/GJ) and T_{max} With Axial Distance x* for the Case of Complete Combustion.

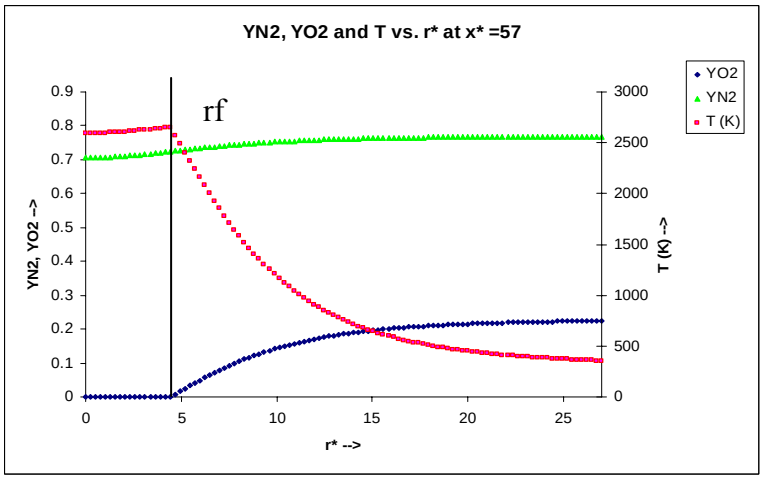

(a)

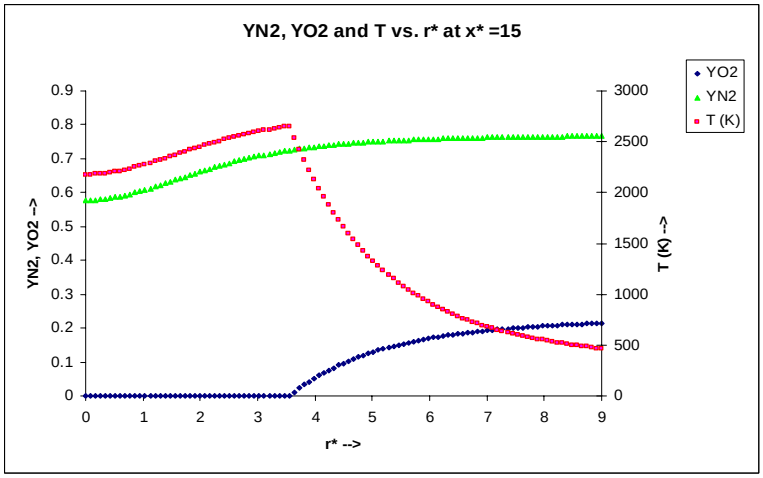

(b)

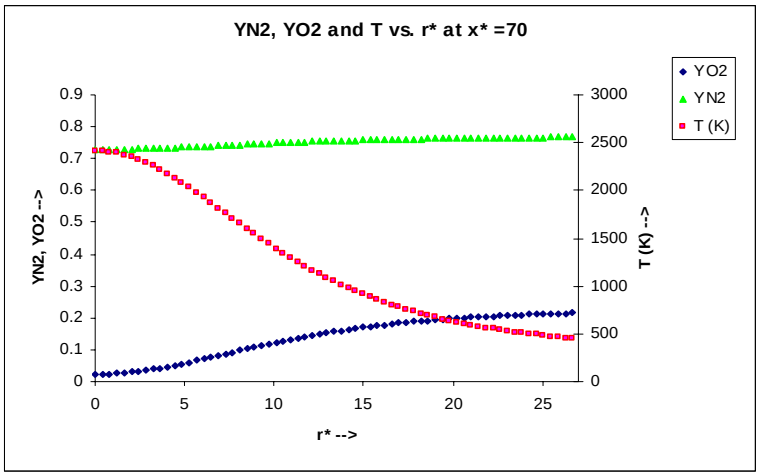

(c)

Figure V.3: Variation of Y_{N_2}, Y_{O_2} and T With Radial Distance r^* at a) $x^* = 57$, b) $x^* = 15$ and c) $x^* = 70$ for the Case of Complete Combustion.

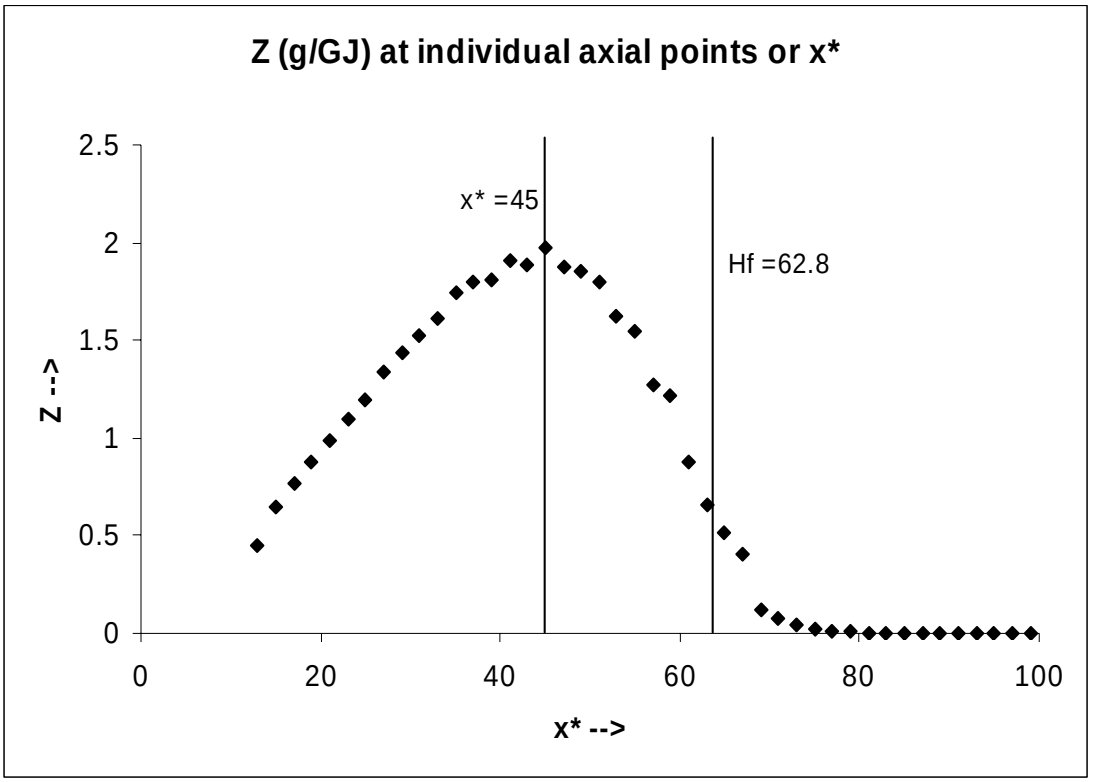

Figure V.4: The Production of Total $z = (d\dot{\omega}_{NO}/dx)$ (g/GJ per Unit Dimensionless Height) vs. (x^*) for the Case of $CO_2 \Leftrightarrow CO + 1/2\ O_2$ Dissociation.

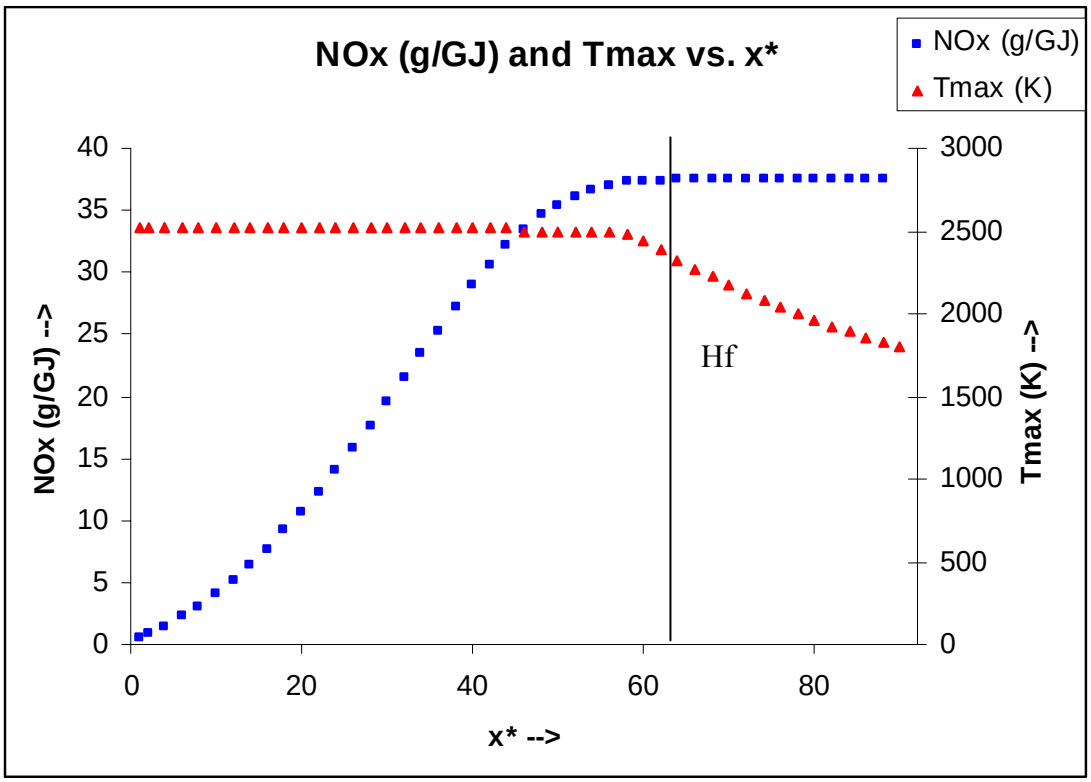

Figure V.5: Variation of Total NO_x (g/GJ) and T_{max} With Axial Distance x* for the Case of $CO_2 \Leftrightarrow CO + 1/2\ O_2$ Dissociation.

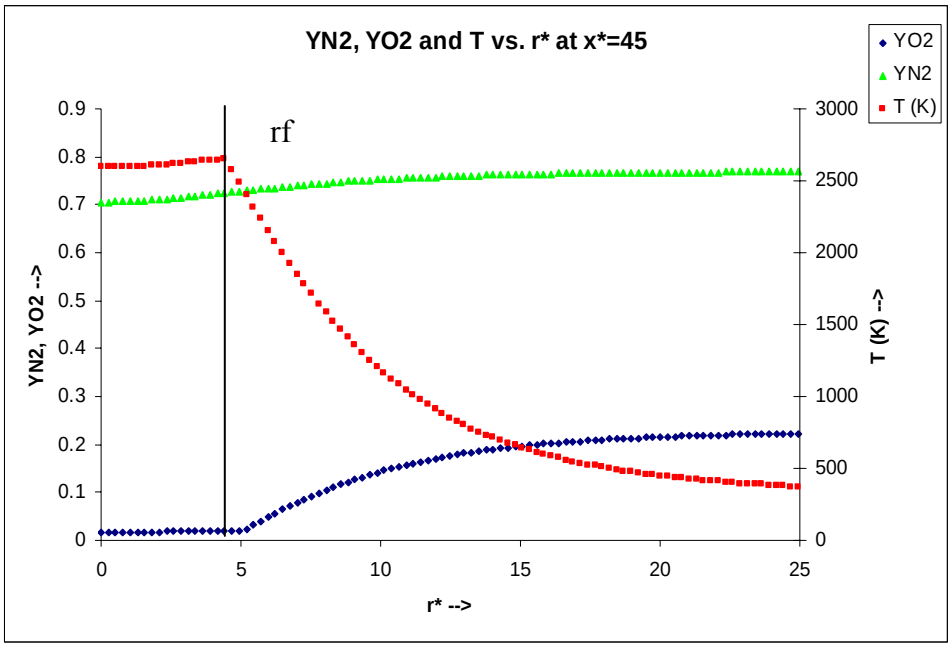

(a)

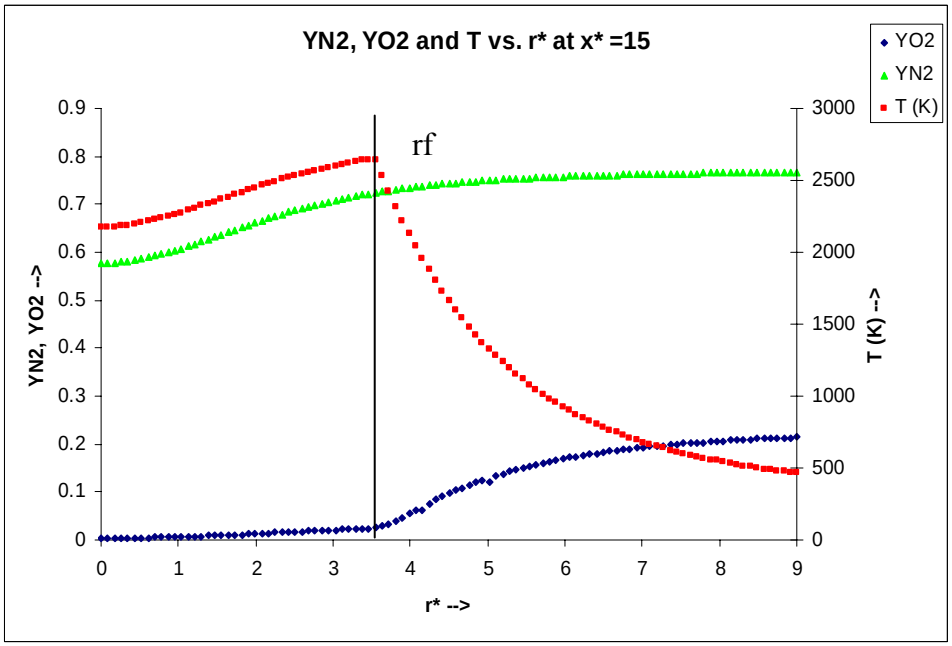

(b)

Figure V.6: Variation of Y_{N_2}, Y_{O_2} and T With Radial Distance r^* at a) $x^* = 45$ and b) $x^* = 15$ for the Case of $CO_2 \Leftrightarrow CO + 1/2\ O_2$ Dissociation.

5.1.2. CO_2 Equilibrium

In this case, there is presence of O_2 in the fuel rich region due to CO_2 dissociation. However CO_2 is treated as a trace species; hence the change in O_2 concentration due to CO_2 dissociation in fuel lean regime is negligible. In this case when the $CO_2 \Leftrightarrow CO + 1/2\ O_2$ dissociation is assumed, the net NO_x is 33 ppm or 37.34 g/GJ and $EINO_x$ of 1.22. Figure V.4 shows the production of NO_x $z = (d\dot{\omega}_{NO}/dx) = \int_0^{\infty} \dot{\omega}'''_{NO} 2\pi r\,(x)$ at individual axial points, whereas Figure V.5 shows how the total NO_x and T_{max} varies with axial distance x*. It is evident from the graph that highest NO_x production takes place at about x*= 45. Figure V.6 shows the Variation of Y_{N_2}, Y_{O_2} and T with Radial r^* at a) $x^* = 45$ and b) $x^*=15$. $T_{max} = T_{adiabatic}$ or the temperature at the flame location. For $x^* = 45$, $T_{max} \approx T\ (r=0)$. For $x^*=15$, $T\ (r=0) < T_{max}$. The flame height in this case is at x*= 62.8. The increase in NO_x is due to CO_2 dissociation which increases the availability of O_2 in the high temperature fuel rich region.

5.1.3. H_2O Equilibrium

In this case, there is the presence of O_2 in the fuel rich region due to H_2O dissociation. However H_2O is treated as a trace species; hence the change in H_2O concentration in L and R region in fuel lean regime are negligible. The net NO_x is 30 ppm or 34.15 g/GJ and $EINO_x$ of 1.1 which is comparable to CO_2 dissociation case. Figure V.7 shows the production of NO_x $z = (d\dot{\omega}_{NO}/dx) = \int_0^{\infty} \dot{\omega}'''_{NO} 2\pi r\,(x)$ at individual axial points, whereas Figure V.8 shows how the total NO_x and T_{max} varied with axial

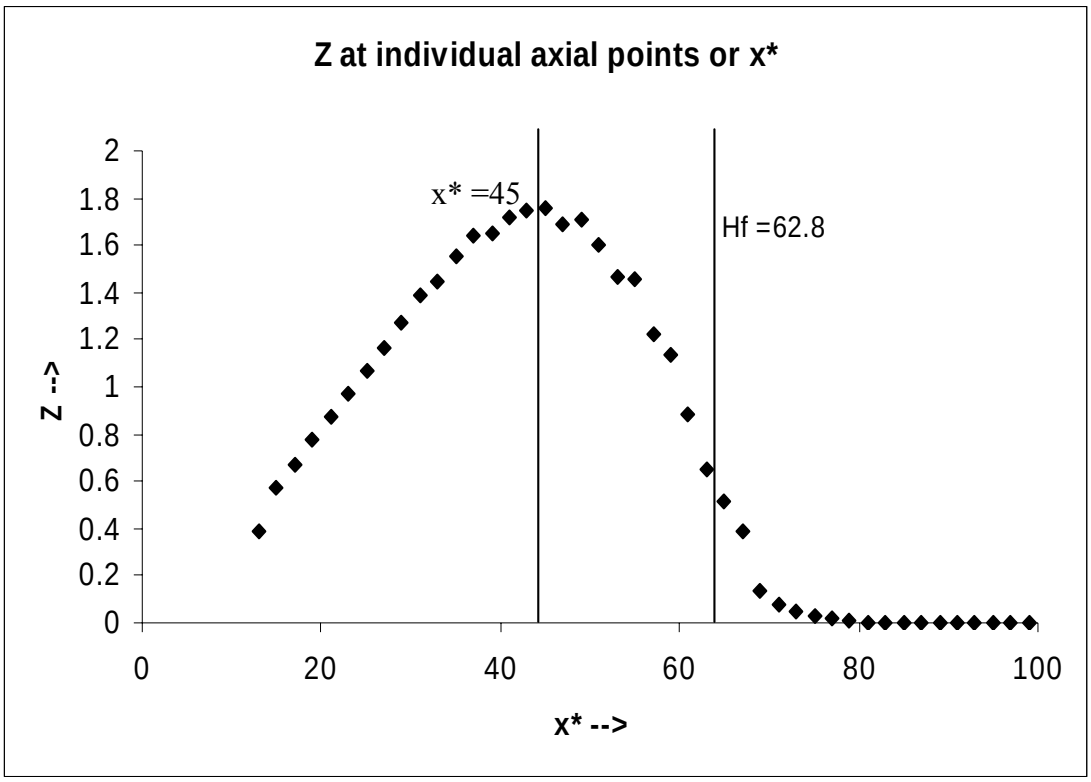

Figure V.7: The Production of Total $z = (d\dot{\omega}_{NO}/dx)$ (g/GJ per Unit Dimensionless Height) vs. (x^*) for the Case of $H_2O \Leftrightarrow H_2 + 1/2\ O_2$ Dissociation.

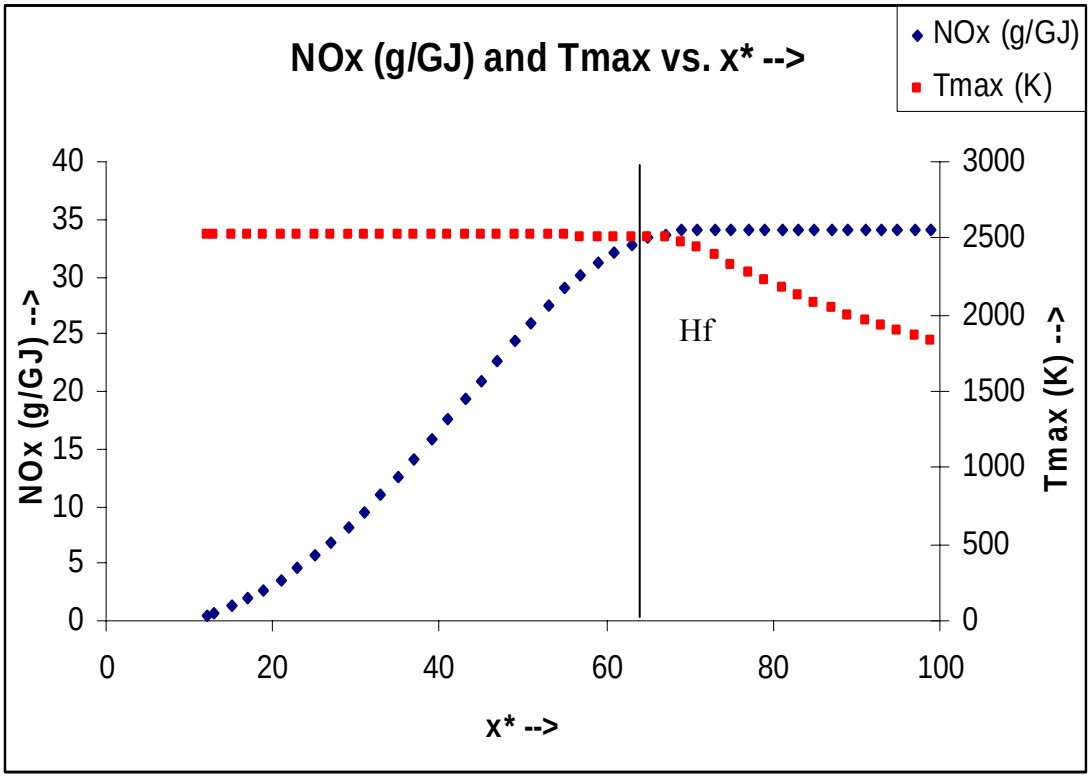

Figure V.8: Variation of Total NO_x (g/GJ) and T_{max} With Axial Distance x* for the Case of $H_2O \Leftrightarrow H_2 + 1/2\ O_2$ Dissociation.

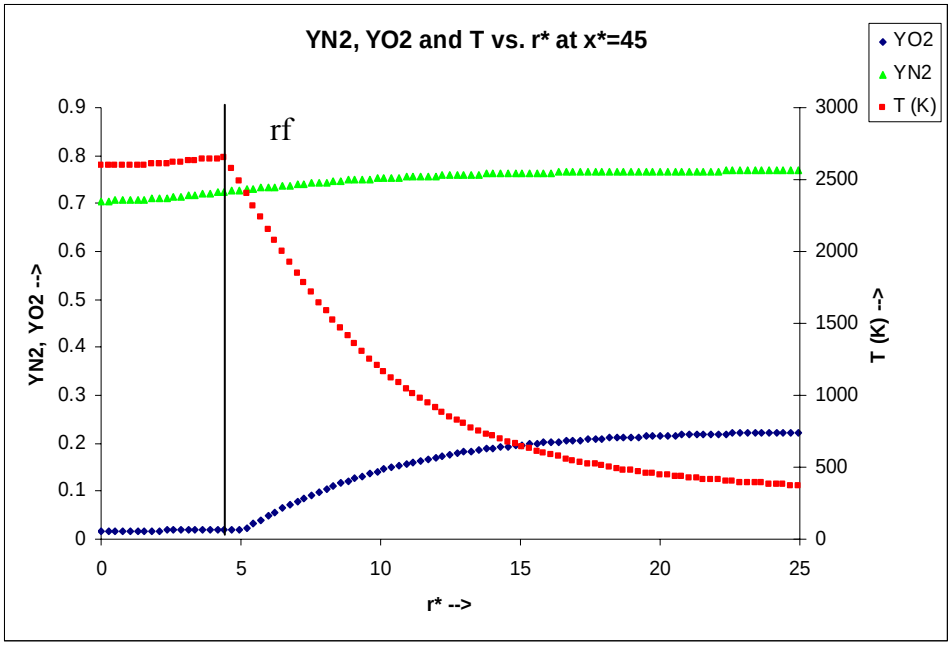

(a)

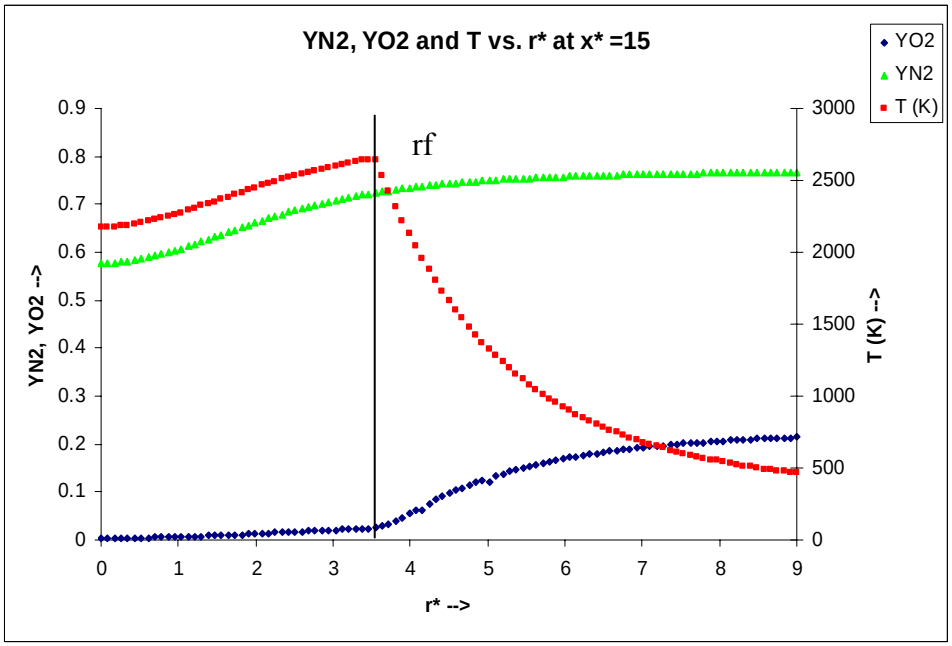

(b)

Figure V.9: Variation of Y_{N_2}, Y_{O_2} and T With Radial Distance r^* at a) $x^* = 45$ and b) $x^* = 15$ for the Case of $H_2O \Leftrightarrow H_2 + 1/2\ O_2$ Dissociation.

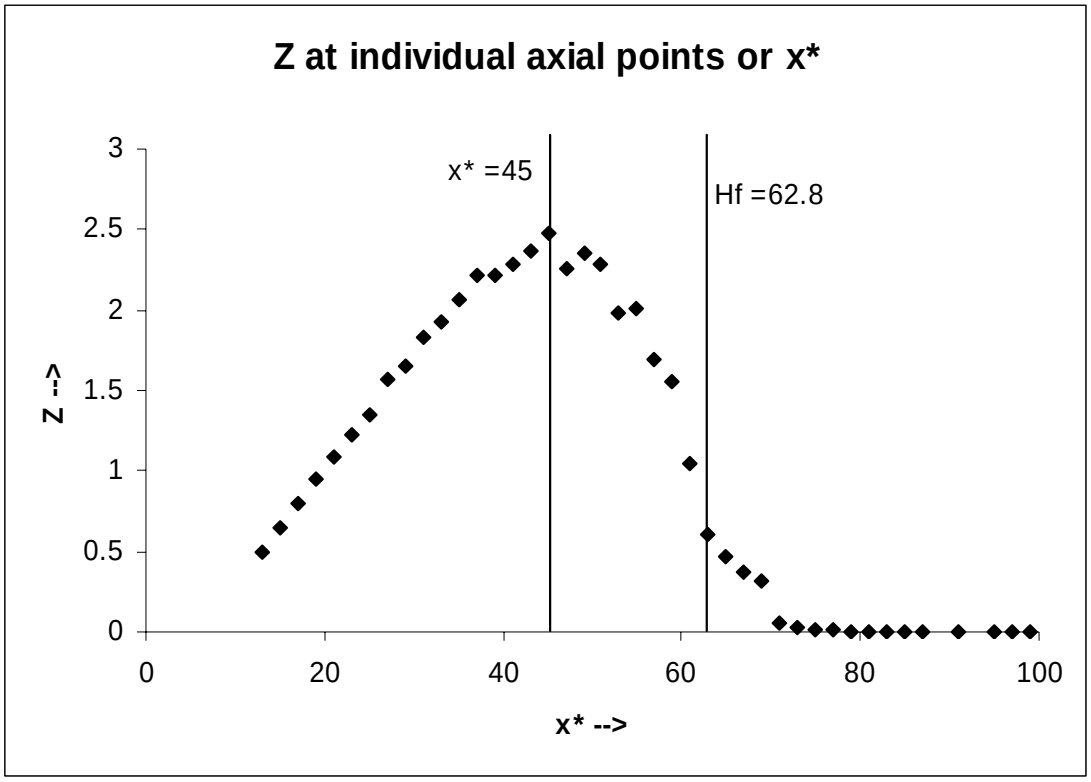

Figure V.10: The Production of Total $z = (d\dot{\omega}_{NO}/dx)$ (g/GJ per Unit Dimensionless Height) vs. (x^*) for the Case of Simultaneous CO_2 and H_2O Dissociation.

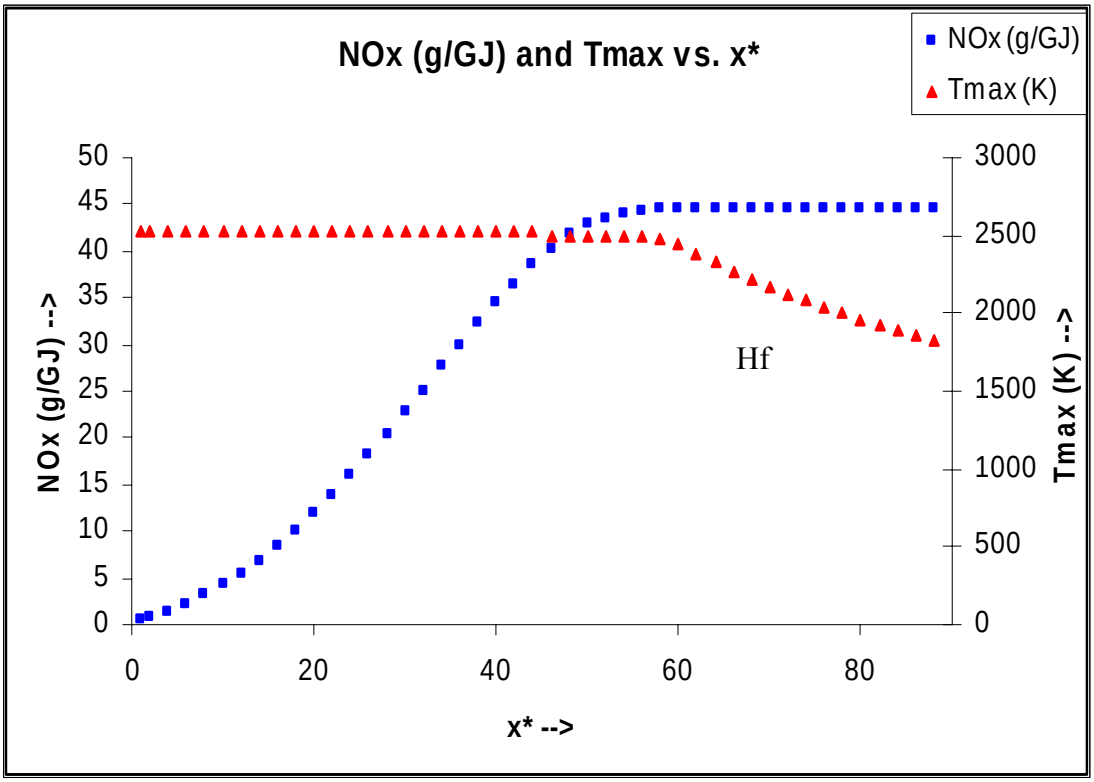

Figure V.11: Variation of Total NO_x (g/GJ) and T_{max} With Axial Distance x* for the Case of Simultaneous CO_2 and H_2O Dissociation.

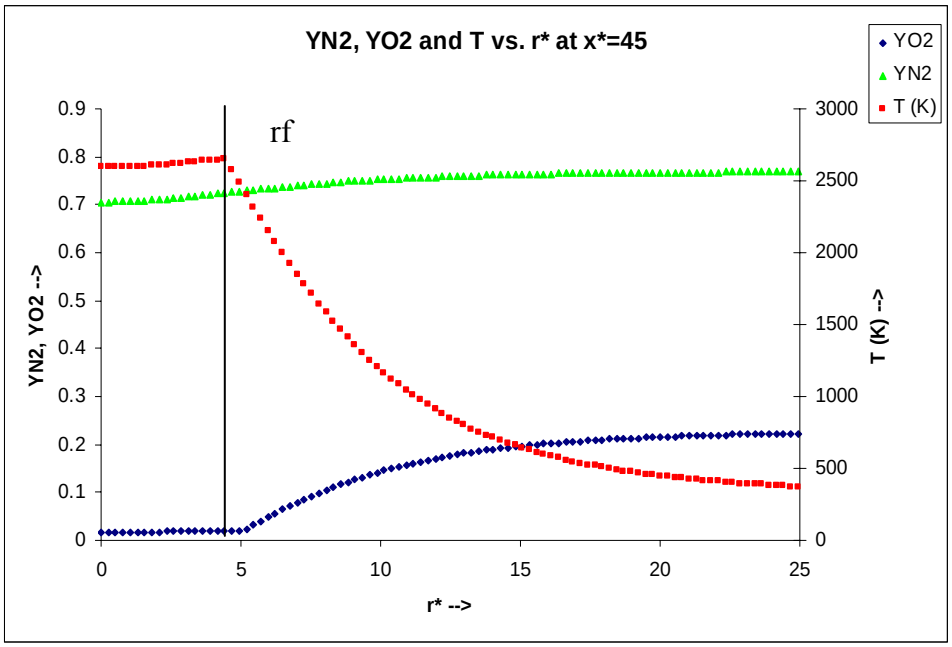

(a)

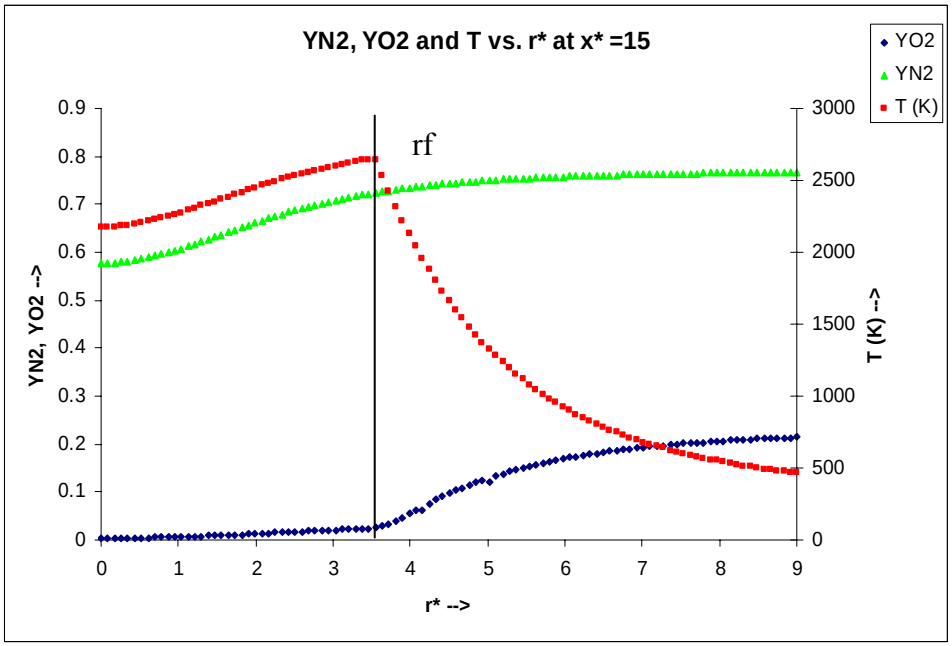

(b)

Figure V.12: Variation of Y_{N_2}, Y_{O_2} and T With Radial Distance r^* at a) $x^* = 45$ and b) $x^* = 15$ for the Case of Simultaneous CO_2 and H_2O Dissociation.

distance x*. It is evident from the graph that highest NO_x production takes place at x*= 45. The flame height in this case is at x*= 62.8. Figure V.9 shows the Variation of Y_{N_2}, Y_{O_2} and T with Radial Distance r^* at a) $x^* = 45$ and b) $x^*=15$. $T_{max} = T_{adiabatic}$ or the temperature at the flame location. For $x^* = 45$, $T_{max} \approx T$ (r =0). For $x^*=15$, T (r =0) < T_{max}.

5.1.4. Both CO_2 and H_2O Equilibrium

In this case both equilibrium reactions $CO_2 \Leftrightarrow CO + 1/2\ O_2$ and $H_2O \Leftrightarrow H_2 + 1/2\ O_2$ is considered simultaneously. Thus there is an increased presence of O_2 in the fuel rich region due to both CO_2 and H_2O dissociation. Again as both CO_2 and H_2O are treated as a trace species; hence the change in CO_2 and H_2O dissociation are assumed to be negligible. The net NO_x is 39 ppm or 44.5 g/GJ and $EINO_x$ of 1.45. NO_x increase in this case is not simply addition of NO_x when CO_2 and H_2O are considered separately. The oxygen produced in these reactions separately is dependent on each other as has been explained in the appendix. Figure V.10 shows the production of NO_x $z = (d\dot{\omega}_{NO}/dx) = \int_0^\infty \dot{\omega}'''_{NO} 2\pi r\,(x)$ at individual axial points, whereas Figure V.11 shows how the total NO_x and T_{max} varied with axial distance x* It is evident from the graph that highest NO_x production takes place at about x*= 45. The flame height in this case is at x*= 62.8 Figure V.12 shows the Variation of Y_{N_2}, Y_{O_2} and T with Radial Distance with Radial Distance r^* at a) $x^* = 45$ and b) $x^*=15$. $T_{max} = T_{adiabatic}$ or the temperature at the flame location. For $x^* = 45$, $T_{max} \approx T$ (r =0). For $x^*=15$, T (r =0) < T_{max}. As it is evident, the NO_x produced is the maximum in this case and is approximately nine times the NO_x produced in the case when complete combustion is

assumed. It signifies that even trace amounts of oxygen in the high temperature fuel rich region lead to a sharp increase in NO_x formation.

5.1.5. Discussion of Results

The following observations can be made from the results of modeling:

(1) Plots of the g/GJ vs. x* were plotted for all of the four cases: (i) complete combustion, (ii) $CO_2 \Leftrightarrow CO + 1/2\ O_2$ equilibrium, (iii) $H_2O \Leftrightarrow H_2 + 1/2\ O_2$ equilibrium and (iv) Both CO_2 and H_2O equilibrium considered together. Figure V. 13 shows that comparison of the total NO_x (g/ GJ) production for the four cases.

(2) There is an approximately nine fold increase in the NO_x production between the case of fuel with no dissociation and when both CO_2 and H_2O equilibrium is assumed.

(3) For all four cases, it is observed that the maximum NO_x production takes place at about x*= 45 which is about $3/4^{th}$ of the flame height which is at $H_f^* =$ 62.8 for all four cases.

(4) In the case of complete combustion, the pre-flame region contributes to 85% of the total NO_x production whereas in the other three cases, the pre-flame region contributes to 96% of the total NO_x production and post-flame region contributes to 4% of the total NO_x production.

5.2. Effect of Sc Number Variation on NO_x Production

The effect of Sc number on total NO_x is investigated. $Sc = \upsilon/D$, thus a higher Sc number implies lower D. Physically; the Schmidt number represents the ratio of the

momentum to the mass diffusion. Increase in Sc number increases the excess air flow. Inceased Sc implies increased υ and hence entrainment of more air by fluid due to increased momentum diffusivity. In case of lighter fuels like Hydrogen, υ is low and it diffuses faster as it is light and hence entrains less air. Fuels like propane have higher Sc and an increased υ and thus entrain more air. Hence more O_2 is available in the post flame region, but there is reduction in temperature due to dilution. If diffusion rate is slower (decreased D, e.g. propane) and correspondingly the burn rate per unit height is expected to be slower. This will lead to an increase in the length of the flame and also the volume of the flame. Hence under equilibrium conditions, thermal NO_x is expected

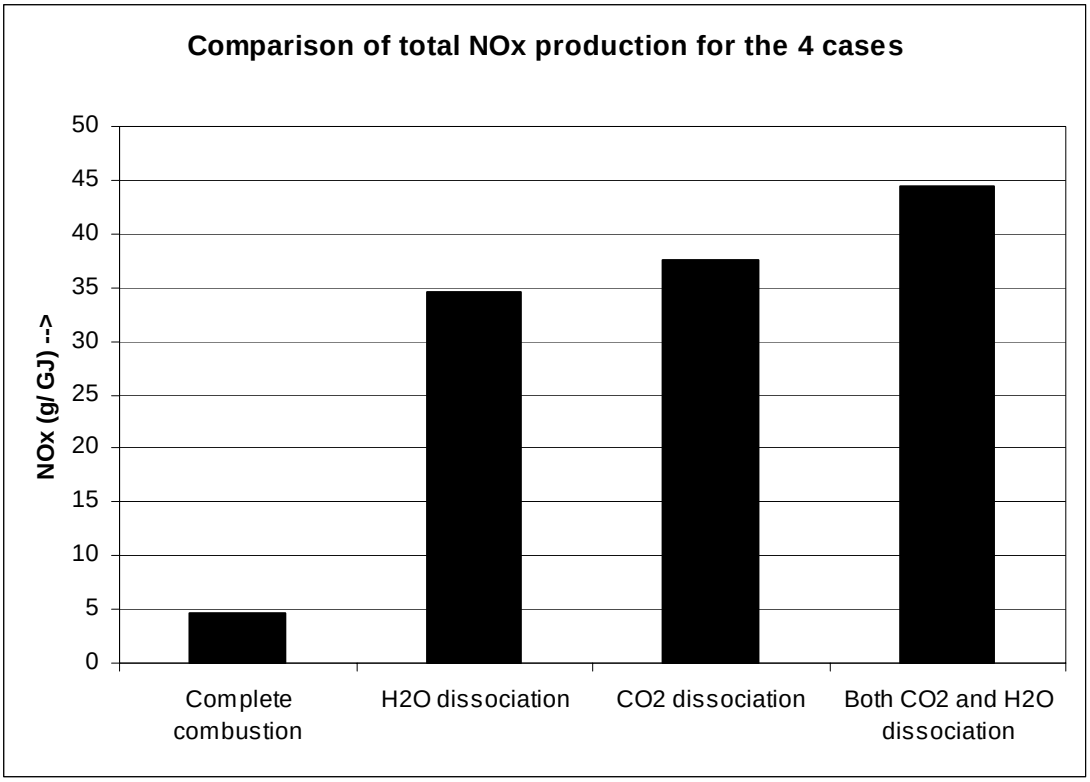

Figure V.13: Comparison of Total NO_x (g/GJ) Production for the Four Different Cases.

to increase. However, on the other hand an increase in the Sc number will lead to increase in the excess air and hence will affect the temperature profile by inducing a cooling effect. Reduced temperatures will lead to a decrease in the thermal NO_x production. Thus, among these opposing phenomenons, the dominating one is ascertained which is typically T. Sc number can be allowed to vary for the same fuel by changing the inlet mass fraction of fuel. Dilution with inert gases like N_2 can change Sc number of a fuel. In the present study, the Sc number is varied between 0.5 and 1.5 and the total NO_x is plotted against Sc number for all four cases, namely: (i) complete combustion, (ii) with CO_2 equilibrium, (iii) with H_2O equilibrium and finally with (iv) both CO_2 and H_2O equilibrium are assumed.

It has already been shown in section 4.4.4. and equations (4.36) and (4.37) that excess air % at the flame tip for circular jets is only a function of Sc number. Figure V.14 shows the variation of excess air fraction vs. Sc number for a circular jet and a 2D jet.

For the case of complete combustion, it is observed that the total NO_x decreases as Sc number is increased from 0.5 to 1.7. Figure V.15 shows the variation of total NO_x (g/GJ) with the variation of Sc number for the case of complete combustion. There is a six fold decrease in NO_x with a three fold increase in Sc number. Figure V.16 shows the variation of total NO_x (g/GJ) with Sc number for the case when $CO_2 \Leftrightarrow CO + 1/2\ O_2$ dissociation is assumed. Figure V.17 shows the variation of total NO_x (g/GJ) with Sc number for the case when $H_2O \Leftrightarrow H_2 + 1/2\ O_2$ dissociation is assumed. Figure V.18 shows the variation of total NO_x (g/GJ) with Sc number for the case when both CO_2 and H_2O equilibrium are assumed simultaneously.

5.2.1. Discussion of Results

Thus in all four cases, a similar trend is seen in which the total NO_x (g/GJ) production decreases while Sc number is increased from 0.5 to 1.7. One can conclude that the increase in excess air has a more dominant effect on NO_x production than does increase in flame volume. This is understandable since NO_x production is highly sensitive to temperature and even a small drop of temperature can drastically

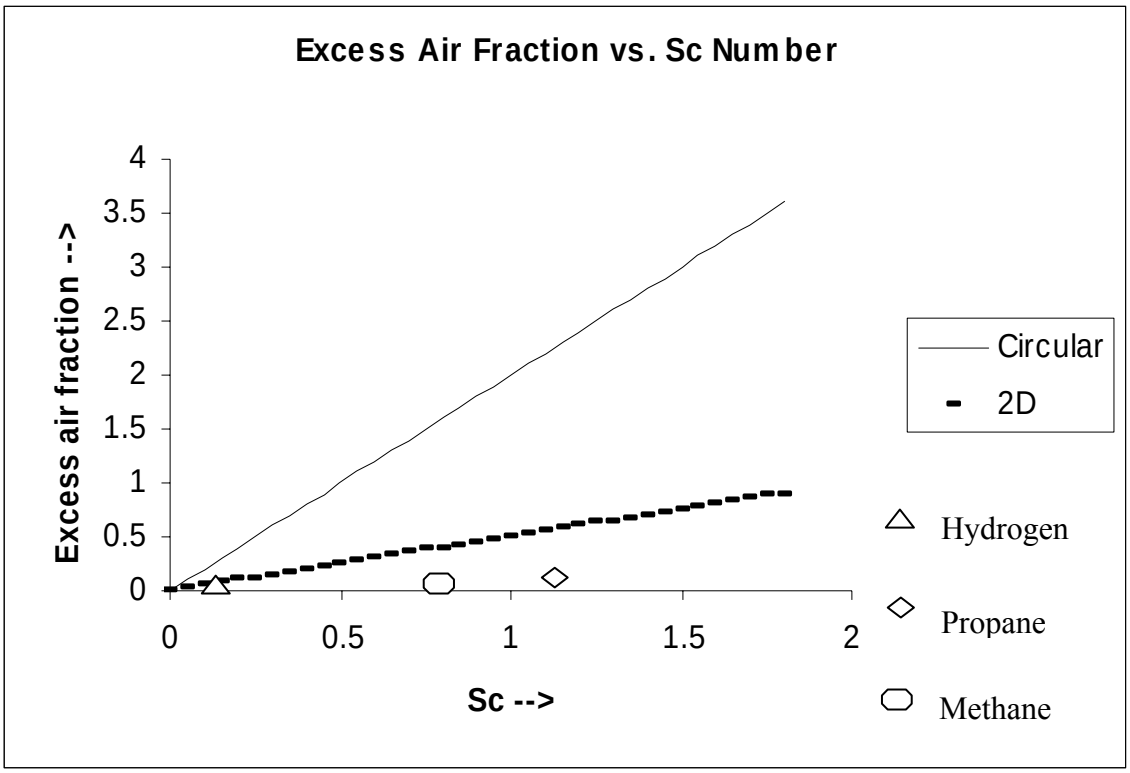

Figure V.14: Variation of Excess Air Fraction With Sc Number. [Tillman, 2000]

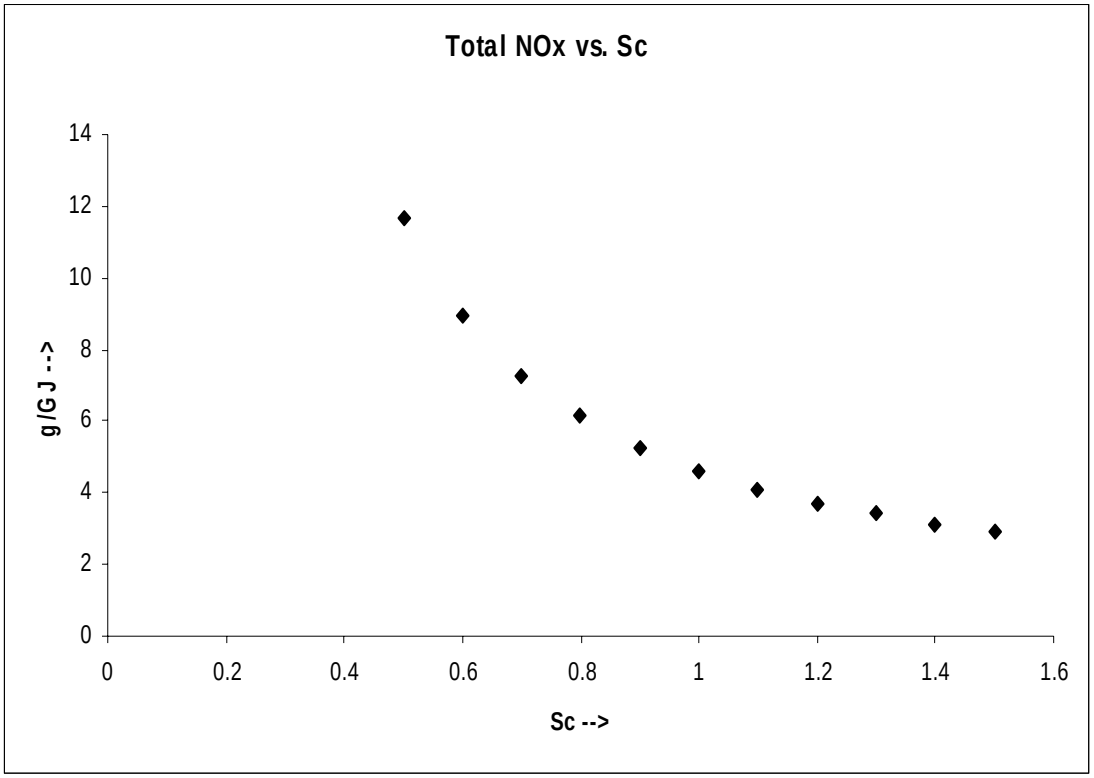

Figure V.15: Variation of Total NO_x (g/GJ) With Sc Number for the Case of Complete Combustion.

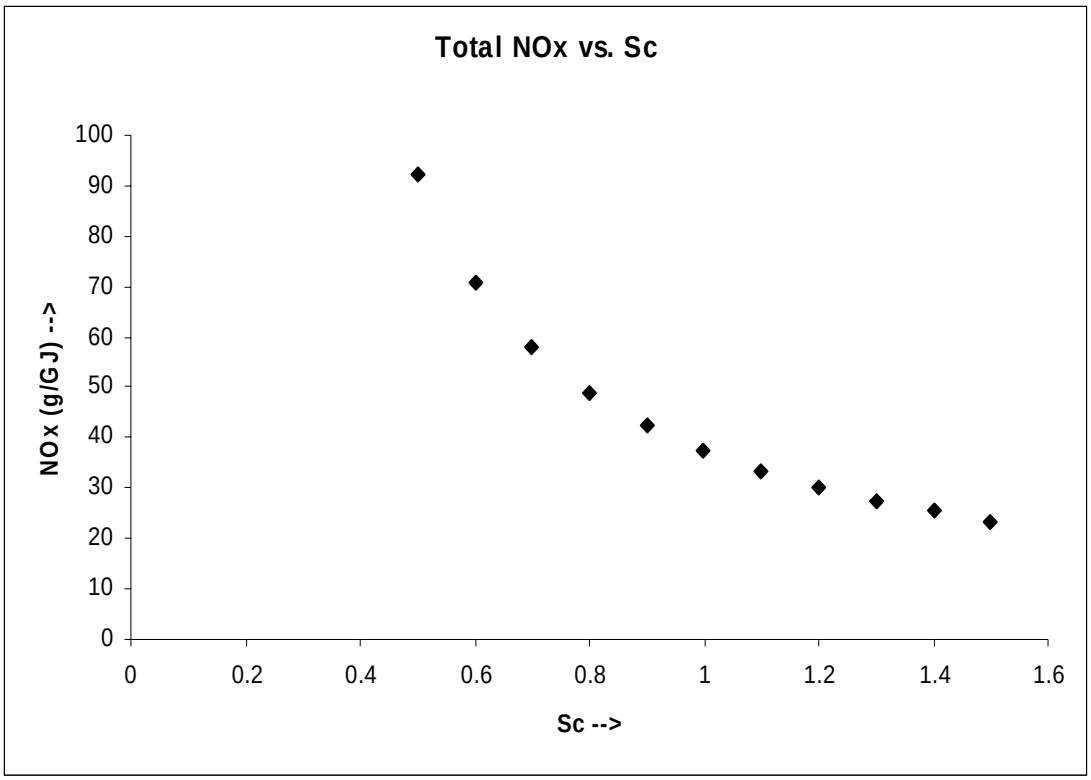

Figure V.16: Variation of Total NO_x (g/GJ) With Sc Number for the Case of $CO_2 \Leftrightarrow CO + 1/2\ O_2$ Dissociation.

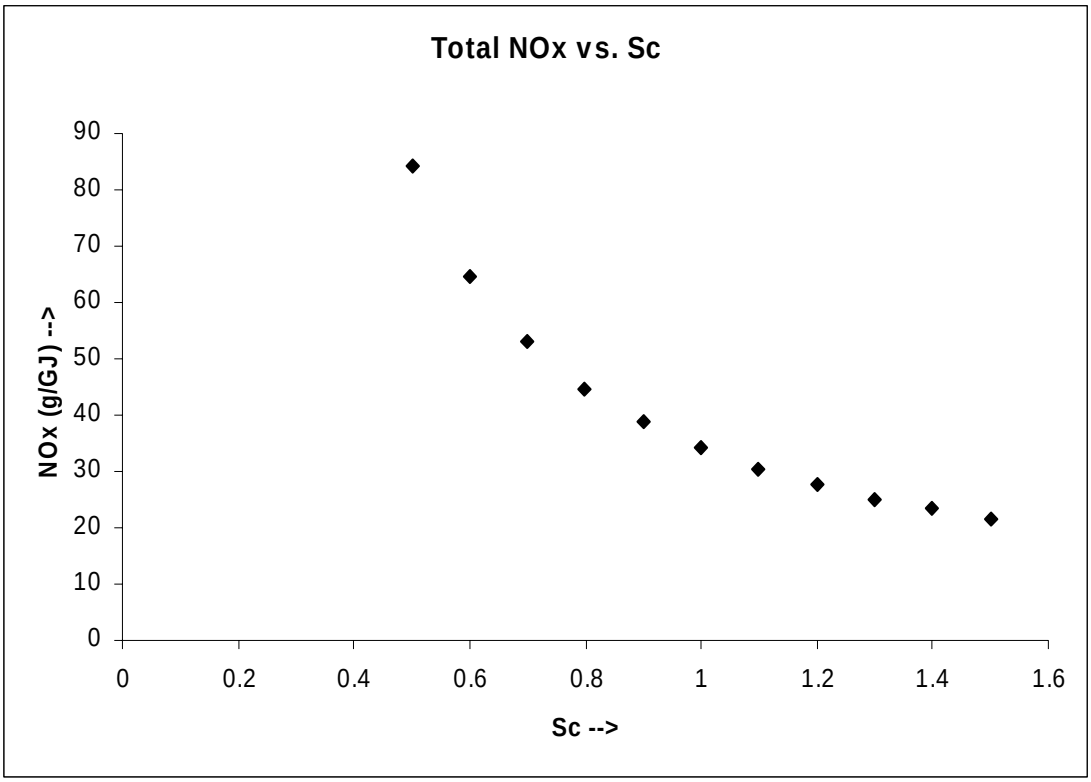

Figure V.17: Variation of Total NO_x (g/GJ) With Sc Number for the Case of $H_2O \Leftrightarrow H_2 + 1/2\ O_2$ Dissociation.

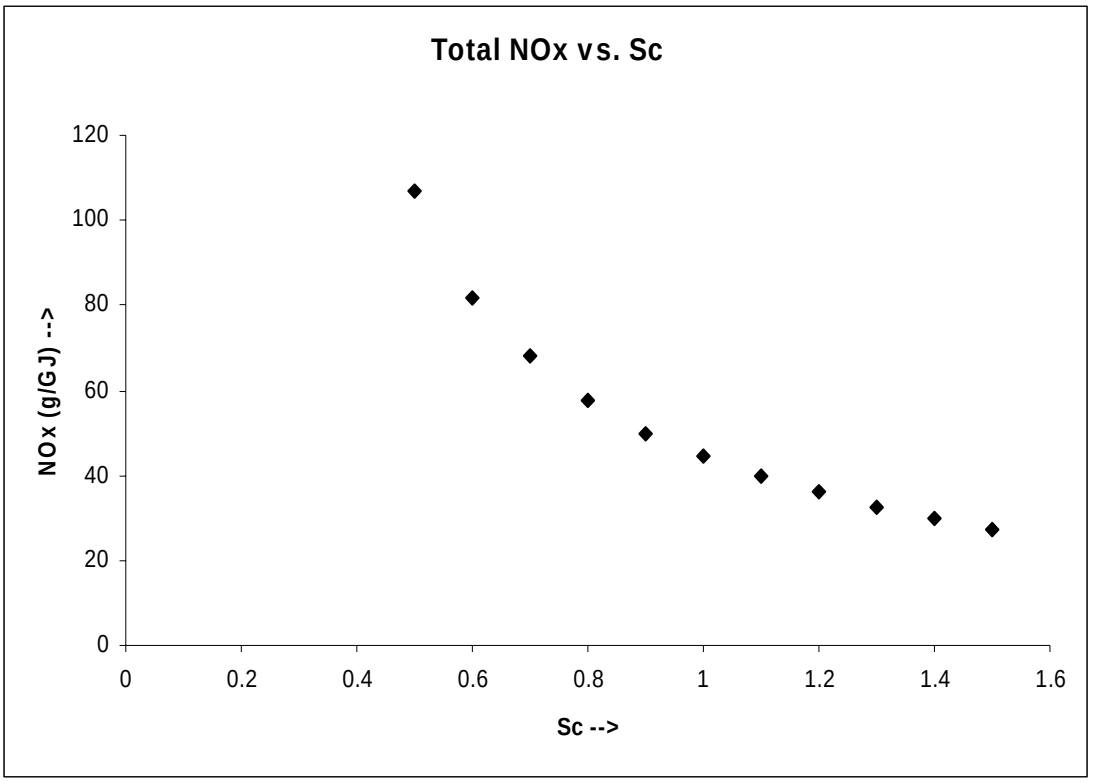

Figure V.18: Variation of Total NO_x (g/GJ) With Sc Number for the Case of Simultaneous CO_2 and H_2O Dissociation.

reduce NO_x formation. When Sc number is increased, the flame volume (both width and height) increase, this should lead to an increase in the NO_x production, however as Sc number is increased, the excess air increases and this decreases the flame temperature.

Further if $M^*<1$, air entrained is less compared to flat velocity case. Flame volume will increase and is expected to increase the total NO_x formation. On the other hand buoyancy will cause $M^*>1$, (parabolic velocity profile) and in this case the NO_x production is expected to be more.

5.3. Validation of Model

Most of the work in this field has been in the field of turbulent jet flames. A limited literature is available on laminar jet flames. The basic flame types that have been studied are envelope flames around spheres of droplets and cylinders, jet flames in co flow and various types of counter flow flames. The closest that a study related to unconfined laminar jet flames with propane as fuel comes from [2].

Rokke et al. used unconfined partially premixed propane/ air flames issuing from a straight tube into quiescent air at atmospheric pressure and temperature. Though some of their data falls into the turbulent flame category, there are data points that fall in the laminar flame regime. The extensive work covers experimental values with different fuel mass fractions Y_f. The range of Y_f varies from 1 to 0.15. This variation of inlet fuel mass fraction were brought into effect by addition of inert N_2. The values that have Y_f of 1 are useful for comparison with the values predicted by the present model as $Y_f = 1$ signifies a non- premixed propane/ air flame. Six different nozzle diameters d_0 of 3.2, 6, 10, 20.5, 23.3 and 29.5 mm were used. Also the nozzle outlet velocity varied from 1 m/s to 130 m/s and Re number varying from 40 to 12000. The scaling law proposed by the

researchers is as follows:

$$EINO_x = 22\ Fr^{3/5}\ Y_f^{-1/5}\ \left(\frac{d_0}{\rho_0 u_0}\right) \times (0.35^{-0.45} + 0.7\ d_0^{0.2})\ \left[\frac{g\ NO_x}{kg\ fuel}\right] \qquad (5.6)$$

Where Y_f is the fuel mass fraction, Fr is the Froude number, d_o is the inlet diameter and u_0 is the initial jet velocity.

The present model was tested for propane as fuel, for d_o values of 10mm, 20.5 mm and 29.5 mm and inlet velocity varying from 0.1 m/s to 5 m/s and a fuel mass fraction $Y_f = 1$. The jet issues into quiescent air at atmospheric pressure and temperature (300 K) and the $Sc = 1$ for comparison with the experimental values. The present model does not incorporate for buoyancy effect. Here $M^* = 1$ and in order to include the effect of buoyancy M^* has to be modified. Figure V.15 shows a comparison of the calculated $EINO_x$ values and the experimental values for d_o of 10 mm. Buoyancy effect will increase air flow and decrease the temperature. Figure V.16 shows a comparison of the calculated $EINO_x$ values and the experimental values for d_o of 20.5 mm and Figure V.17 shows a comparison of the calculated $EINO_x$ values and the experimental values for d_o of 29.5 mm. Table V.2 shows the comparison of calculated $EINO_x$ (g/Kg of fuel) values and experimental Values for d_o = 10 mm, Sc =1 for methane (CH_4) referenced from Turns [1].

5.3.1. Conclusions

It is seen that the model is more accurate for u_0 less than 0.5m/ s and under predicts the experimental values by an average error of $\pm$ 8%. However, it tends to over predict the $EINO_x$ values for higher inlet velocities or with $u_0 \geq$ 1 m/ s. The model is accurate for smaller diameters and tends to over predict $EINO_x$ values for $d_o \geq 20$ mm.

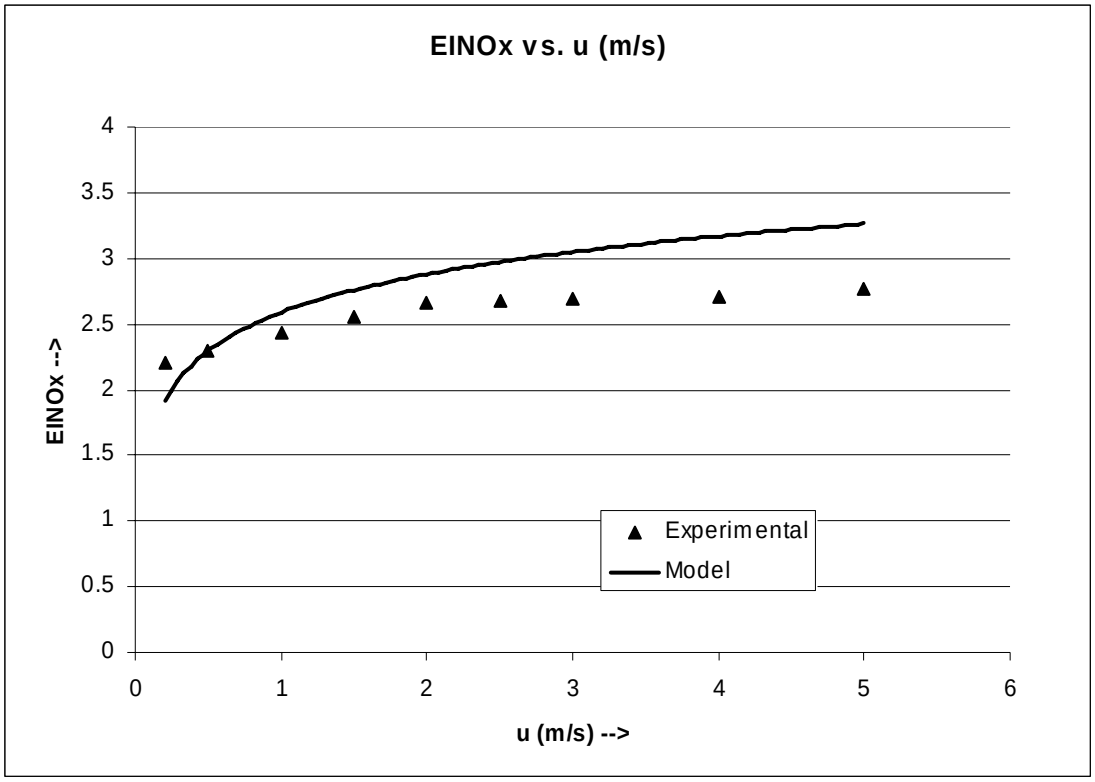

Figure V.19: A Comparison of the Calculated $EINO_x$ (g/ Kg of fuel) Values and the Experimental Values for d_o of 10 mm, Sc=1.

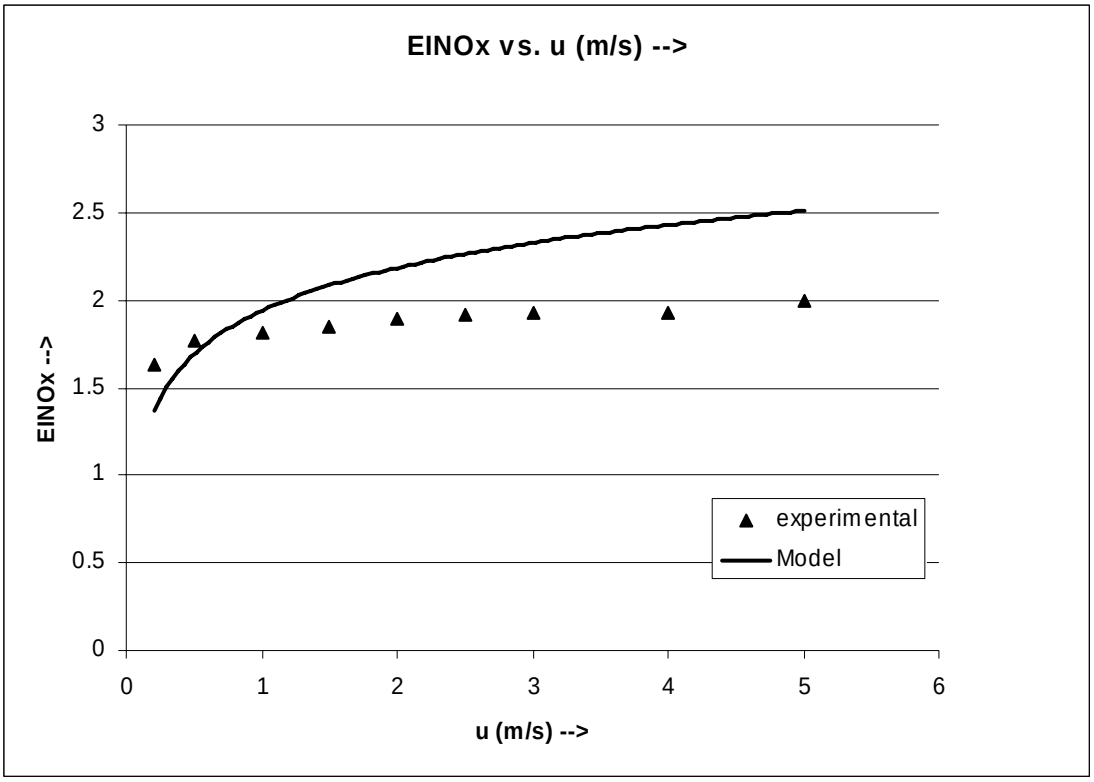

Figure V.20: A Comparison of the Calculated $EINO_x$ (g/Kg of fuel) Values and the Experimental Values for d_o of 20.5 mm, Sc=1.

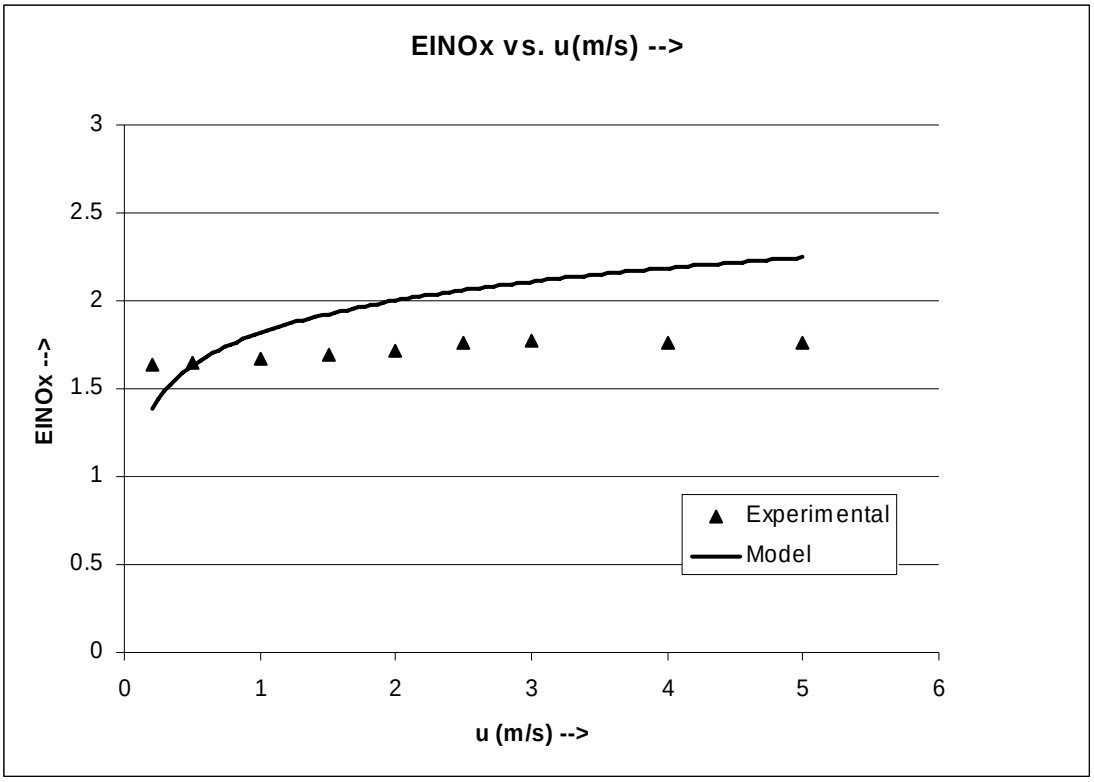

Figure V.21: A Comparison of the Calculated $EINO_x$ (g/Kg of fuel) Values and the Experimental Values for d_o of 29.5 mm, Sc =1.

Figure V.19 shows a comparison of the calculated $EINO_x$ (g/ Kg of fuel) values and the experimental values for d_o of 10 mm and Sc=1. Figure V.20 shows a comparison of the calculated $EINO_x$ (g/ Kg of fuel) values and the experimental values for d_o of 20.5 mm and Sc=1. Figure V.21 shows a comparison of the calculated $EINO_x$ (g/ Kg of fuel) values and the experimental values for d_o of 29.5 mm and Sc=1.

Table V.2: Comparison of Calculated $EINO_x$ (g/Kg of fuel) Values and Experimental Values for d_o = 10 mm, Sc =1 for Methane (CH_4).

d (mm)	**u_o (m/s)**	**$EINO_x$ (Experimental)**	**$EINO_x$ (Model)**
10	0.1	1	0.9
10	0.25	0.75	0.74
10	0.5	0.52	0.53
10	0.75	0.46	0.48
10	1	0.41	0.44
10	1.5	0.31	0.37
10	2.1	0.21	0.291

CHAPTER VI

CONCLUSIONS AND RECOMMENDATIONS

This work proposes a numerical model to compute the total production of NO_x in a non-premixed circular laminar jet flame. The model estimates both thermal NO_x and prompt NO_x assuming single step kinetics for NO_x formation and a thin flame model. Unlike various existing models, this model does not involve very complex integration of hundreds of chemical reactions of various species and their intermediates. Such models are highly time consuming and also normally involve heavy computational costs. Although the model was run for propane as fuel, it can also be used for other fuels. The model predicts the axial and radial gas velocities, visible flame height, the maximum flame width, amount of air entrainment and the total NO_x production along with the axial NO_x production. The model also demonstrates the effect of Sc number on the total production of NO_x. Comparisons with experimental values reported elsewhere were done to help validate the model. Several observations, conclusions and recommendations for future work are listed below.

6.1. Conclusions

(1) Solutions for the compressible form of the governing equations of mass, momentum, energy, and species for a single laminar circular jet have been obtained earlier to give explicit solutions for flame height and width, mixing layer growth, lift off height and blow off velocity. Using these results, the volumetric rate of thermal NO_x is calculated using the species and temperature profiles derived from the governing equations of mass, momentum, energy and species and a single step reaction for formation of thermal NO_x.

(2) Using a single step empirical co-relation for prompt NO_x [De Soete, 1975] and a method similar to thermal NO_x, the net production of prompt NO_x is calculated and net NO_x formation can be summarized as the sum of both thermal NO_x and prompt NO_x with Fuel NO_x being zero for the case of hydrocarbon fuels containing no bound nitrogen. With Propane as fuel, the net NO_x production is reported in ppm, g/GJ and EI NO_x for the all the four cases of: (i) complete combustion; total NO_x is 4 ppm, 4.61 g/GJ and $EINO_x$ is 0.14. (ii) With CO_2 equilibrium; net NO_x is 33 ppm or 37.34 g/GJ and $EINO_x$ of 1.22. (iii) With H_2O equilibrium; net NO_x is 30 ppm, 34.15 g/GJ and $EINO_x$ of 1.1. Finally with (iv) Both CO_2 and H_2O equilibrium; assumed; net NO_x is 39 ppm or 44.5 g/GJ and $EINO_x$ of 1.45.

(3) The model NO_x predictions compare favorably with experimental data collected for a single circular laminar jet. [2]. The case in which both CO_2 and H_2O equilibrium is assumed provides values of $EINO_x$ that match most closely with the experimental values. However the model seems to be more accurate for fuel inlet velocity, $u_0 \leq 1$ m/s and inlet diameter $d_0 \leq 20$ mm and

tends to over predict $EINO_x$ values for higher velocities. The error is of the order of $\pm$ 10 %.

(4) An increase in Sc number leads to a decrease in the total NO_x production. From this it follows that the increase in excess air has a more dominant effect on NO_x production than does increase in flame volume. A three fold increase in Sc number reduces NO_x by six times.

6.2. Recommendations for Future Work

(1) This model was validated for experimental results for propane and methane only. In future, other fuels, especially those with low Schmidt numbers such as hydrogen ($Sc \approx 0.2$) should be tested.

(2) The model should be extrapolated to include high velocity, turbulent regimes in addition to laminar regimes studied.

(3) For the calculation of NO_x a more detailed chemistry model involving multiple step kinetics for the formation of NO_x should be incorporated for both thermal NO_x and prompt NO_x mechanism. It would be interesting to see how close the values of a detailed model are to the present model.

(4) CO_2 dissociation results in production of CO and O_2. Their effect on flame structure and change in temperature must be included. Further, the O_2 so produced gets transported to the locations and hence local Y_{O_2} will change not only due to dissociation but also due to transport.

(5) In the present work, $\dot{\omega}'''_{NO}$ is calculated using only the forward reaction in the species conservation relation given as follows:

$$\rho v \partial Y_{NO}/\partial x + \rho v \partial Y_{NO}/\partial r = (1/r)\partial/\partial D(\rho Dr \partial Y_{NO}/\partial r) + \dot{\omega}'''_{NO} \qquad (6.1)$$

In future work, in order to obtain Y_{NO_2} vs. (x, r), backward reaction of eq. (6.1) can be considered.

NOMENCLATURE

(A: F) = air to fuel ratio (Kg air/Kg fuel)

b = Y_K for mixing, β for combustion

C = Sc number dependent constant
= (2Sc+1)/3

D = mass diffusion coefficient (m^2 / s)

d_i = diameter of circular jet (m)

f = stream function

h_c = Higher heating value of fuel

H = flame height (m)

h = enthalpy (J/Kg)

J = species flux (Kg/s)

J' = species flux per unit width (Kg/s-m)

J^* = non- dimensional species flux
= $J' / (\rho v_{x,i} b_i' d_i)$

L = lift off height

Le = Lewis number = Sc/Pr

M = momentum flux (N)

M' = momentum flux per unit width (N/m)

M^* = non-dimensional momentum flux
$= M'/(\rho_i v_{x,i}^2 d_i)$

$\dot{m}$ = mass flow rate (Kg/s)

$\dot{m}'$ = mass flow per unit width (Kg/s-m)

Pe = Peclet number = Re Pr

Pr = Prandtl number = υ / α

r = radial coordinate (m)

R = Universal gas constant,
8.314 (KJ/Kmole K)

Re = Reynolds number = $v_{x,i} d_i / \upsilon_i$

$s = Y_{O_2,\infty}/(\upsilon_{O_2} Y_{F,i})$

= vol. of air/ vol. of gas
for complete combustion

Sc = Schmidt number = υ / D

T = temperature (K)

v = velocity (m/s)

$\dot{w}'''$ = Rate of species generation
by chemical reaction

x = axial coordinate (m)

Y = mass fraction

Greek Letters

α = thermal diffusivity (m^2 / s)

β = Schvab Zeldovich variable

ξ = Dimensionless radial co-ordinate

η = similarity variable

υ = Kinematic viscosity (m^2 / s)

υ_K = stoichiometric coefficient of species k (kg of k/ kg of fuel)

ψ = Streamline function = $\phi x^{*1/3}$

ϕ = Normalized species and Shvab Zeldovich variable = $(b-b_\infty)/(b_i-b_\infty)$

ϕ_f = flame profile = s/ (1+s)

ρ = density (kg/m^3)

Subscripts

A = air

b = species, Schvab-Zeldovich

c = combustion

cir = circular

ent = entrained

equiv = equivalent

F = fuel

f = flame

i = condition at burner exit (injection)

k = species; (k= fuel, O_2, CO_2 etc.)

max = maximum

mix = mixture

r = radial distance

st = stoichiometric

v = velocity

x = axial distance

Greek subscripts

* = Normalized variable

. = rate

REFERENCES

[1] Turns, S.R., 1995, **"**Understanding NO_x Formation in Non Premixed Flames: Experiments and Modeling,**"** Combustion and Flame, **21**, pp.361-385.

[2] Tillman, S.T., 2000, "Flame Structure and Flame Stability Characteristics of Interacting 2D and Circular Laminar Jets in a Linear Triple Burner Array," Ph.D Dissertation, Texas A&M University, College Station, TX.

[3] Annamalai, K., and Puri, I.K., 2004, *Combustion Science and Engineering*, Final draft, CRC Press LLC, Boca Raton, FL.

[4] Tuteja, A.D., and Newhall, H.K., 1972, "Nitric Oxide formation in Laminar Diffusion Flames," *Proceedings of the Symposium on Emissions from Continuous Combustion Systems*, General Motor Research Laboratories, Warren, MI, p. 109-122.

[5] Fennimore, C. P., 1976, "Effects of Diluents and Mixing on Nitric Oxide from Fuel-Nitrogen Species in Diffusion Flames," *Sixteenth Symposium (International) on Combustion*, The Combustion Institute, Pittsburg, p. 1065.

[6] Jaasma, D., and Borman, G., 1980, "Peculiarities associated with the Measurement of Oxides of Nitrogen Produced by Diffusion Flames," Combustion Science and Technology, **23**, pp. 83-88.

[7] Mitchell, R.E., and Sarofim, A.F., 1980, "Nitric Oxide and Hydrogen Cyanide Formation in Laminar Methane/ Air Diffusion Flames," Combustion Science and Technology, **21**, pp. 157-167.

[8] Hahn, W.A., and Wendt, J.O.L., 1981, "NO_x Formation in Flat, Laminar, Opposed Jet Methane Diffusion Flames," *Eighteenth Symposium (International) on Combustion,* The Combustion Institute, Pittsburg, p. 121.

[9] Drake, M. C. and Blint, R. J., 1989, "Thermal NO_x in Stretched Laminar Opposed-Flow Diffusion Flames with $CO/H_2/N_2$ Fuel," Combustion and Flame, **76**, p.151.

[10] Drake, M. C., and Blint, R. J., 1991, "Relative Importance of Nitric Oxide Formation Mechanisms in Laminar Opposed-Flow Diffusion Flames," Combustion and Flame, **83**, p. 185.

[11] Takeno, T., and Nishioka, M., 1993, "Species Conservation and Emission Indices for Flames Described by Similarity Solutions," Combustion and Flame, **92**, pp. 465-468.

[12] Rokke, N.A., Hustad, J.E. and Sonju, O.K., 1976, "Scaling of Nitric Oxide Emissions from Buoyancy- Dominated Hydrocarbon Turbulent- Jet Diffusion Flames" *Twenty-fourth Symposium (International) on Combustion,* The Combustion Institute, Pittsburg, pp. 385 – 393.

[13] Rokke, N.A., Hustad, J.E. and Sonju, O.K., 1994, **"**A study of Partially Premixed Unconfined Propane Flames,**"** Combustion and Flame, **97**, pp. 88-106.

[14] Annamalai, K., and Sibulkin, M., 1979, "Flame Spread over Combustion Surfaces for Laminar Flow Systems," Combustion Science and Technology, Part I, **19**, pp. 167-183.

[15] DeSoete, C.G., 1975, "Overall Reaction rates of NO and N_2 Formation from Fuel Nitrogen," *Fifteenth Symposium (International) on Combustion*, The Combustion Institute, Pittsburgh, pp. 1093-1102.

[16] Solving Quartic Equations, 1999, Copyrighted 1728 Software Systems, Available: http://www.1728.com/quartic2.htm.

APPENDIX A

CONSERVATION EQUATIONS AND SUMMARY OF DERIVATIONS FOR CIRCULAR LAMINAR JET

For the isolated circular jet, the equations of mass, momentum, energy and species were normalized with normalized boundary conditions, converted into ordinary differential equations using an appropriate similarity variable and then solved with the appropriate boundary conditions to give solutions for the axial and radial gas velocity (v_x and v_r), the species concentrations (Y_F, Y_{O_2} ,etc.) , the flame height (H), the lift off height of the flame (L), and the blow off velocity (v_{Blow}). Derivations of the relevant steps which were taken are provided here [2].

A.1. Conservation Equations

A.1.1. Introduction

Variable properties can not be handled if a closed form solution is desired. Hence, constant properties are assumed.

A.1.2. Flame Height Analysis

The fuel issuing from the jet entrains the surrounding air. Thus air and fuel are mixed. Once ignited, a flame of height H is formed. The flame contour is similar to the one shown in Fig.III.3. Let us assume a thin flame model. The fuel exists in the inner region while oxygen exists in the outer region.

Diffusion rate of fuel per unit flame area $\approx \rho D Y_{F,O}(x)/r_f(x)$

Where $Y_{F,O}$ is the fuel concentration along axis.

Total diffusion rate of fuel over whole flame $= H*2\pi r_f(x)*\rho DY_{F,O}(x)/r_f(x)$

The burn rate of fuel must be equal to the fuel rate $\dot{m}_F = H*2\pi*\rho DY_{F,O}(x)$

If it is assumed that $Y_{F,O}(x)$ scales with $Y_{F,i}$

$$\dot{m}_F = H*2\pi*\rho DY_{F,i}$$

Hence

$$H=\dot{m}_F/\{2\pi*\rho DY_{F,i}\}$$

Thus, H is proportional to the flow rate of fuel for laminar jets and for a given flow rate it is independent of the jet size.

A.1.3. Derivations of Conservation Equations

Mass

$$\partial/\partial x\{\rho v_x r\}+\partial/\partial r\{\rho v_r r\} = 0 \qquad \text{(A.1 a)}$$

X-Momentum

$$\partial/\partial x\{\rho v_x r v_x\}+\partial/\partial r\{\rho v_r r v_x\} = \partial/\partial r(\rho \upsilon r \partial v_x/\partial r) \qquad \text{(A.1 b)}$$

Shvab Zeldovich

$$\partial/\partial x\{\rho v_x r\beta\}+\partial/\partial r\{\rho v_r r\beta\} = \partial/\partial r(\rho Dr\partial\beta/\partial r) \qquad \text{(A.1 c)}$$

Total momentum flux

$$M = 2\pi\int \rho v_x^2 r dr=(\pi d_i^4/4)\rho_i v_{x,i} v_{x,i} \qquad \text{(A.1 d)}$$

Where, $M^* = M/M_{ref}$, $M_{ref} = \{\pi d_i^2 / 4\}\rho_i v_{x,i}^2$

Total β flux

$$J = 2\pi \int \rho v_x \beta' r dr = (\pi d_i^4 / 4)\rho_i v_{x,i} \beta_i' \qquad \text{(A.1 e)}$$

Where $\beta' = \beta - \beta_\infty$

For no buoyancy and for flat profiles at the burner exit, $M^*=1$ since $M=(\pi d_i^4 / 4)\rho_i v_{x,i}^2$. If profiles for velocity v_i and "b" are not flat, then J_b^* and $M^* \neq 1$.

The governing differential equations can be normalized using the following variables

$$r^* = r/d_i \qquad \text{(A.1 f)}$$

$$x^* = x/d_i \qquad \text{(A.1 g)}$$

$$v_x^* = v_x / v_{x,i} \qquad \text{(A.1 h)}$$

Particularly eqs (A.1d) and (A.1e) become

$$\int_0^\infty \{\rho / \rho_i\} v_x^* v_x^* r^* dr^* = 1/8 \qquad \text{(A.1 i)}$$

$$\int_0^\infty \{\rho / \rho_i\} v_x^* \phi \, r^* dr^* = 1/8 \qquad \text{(A.1 j)}$$

There appears to be no transformation available for conversion from compressible to the incompressible form. Hence we assume constant properties in obtaining the solution. Thus ρ / ρ_i=1.

A.2. Solutions for Velocity

Mass:

$$\partial / \partial x\{v_x r\}+\partial/\partial r\{v_r r\} \qquad \text{(A.2 a)}$$

Normalizing using equations (A.1f) to (A.1h),

$$\partial / \partial x^*\{v_x^* r^*\}+\partial/\partial r^*\{v_r^* r^*\} = 0 \qquad \text{(A.2 b)}$$

x-Momentum

$$v_x \partial v_x / \partial x+v_r \partial v_x / \partial x=(\upsilon/r)\partial/\partial r(r)\partial v_x / \partial r \qquad \text{(A.3)}$$

Normalizing using equations (A.1f) to (A.1h),

$$v_x^* \partial v_x^* / \partial x^* +v_r^* \partial v_x^* / \partial r^* =(\upsilon/u_i d_i)(1/r^*)\partial/\partial r^* (r^* \partial v_x^* / \partial r^*)$$

$$v_x^* \partial v_x^* / \partial x^* +v_r^* \partial v_x^* / \partial r^* =\{1/Re_i\}(1/r^*)\partial/\partial r^* (r^* \partial v_x^* / \partial r^*) \qquad \text{(A.4)}$$

Define stream function such that

$$v_x^* r^* = \{\partial \psi / \partial r^*\} \qquad \text{(A.5a)}$$

$$v_r^* r^* = -\{\partial \psi / \partial x^*\} \qquad \text{(A.5 b)}$$

Introduce the similarity variable

$$\eta = r^* / x^* \qquad \text{(A.6 a)}$$

$$f(\eta) = \psi(r^*, x^*) / \{Cx^*\} \qquad \text{(A.6 b)}$$

or $$\psi(r^*, x^*) = f(\eta) * \{Cx^*\} \qquad \text{(A.6c)}$$

Then from (A.5a) and (A.6c),

$$v_x^* r^* = \{Cf' / x^*\} x^* = f'C$$

$$v_x^* = Cf' / r^* \qquad \text{(A.7 a)}$$

Similarly

$$v_r^* r^* = -[f(\eta)C - Cf' r^* / x^*] = -[f(\eta)C - Cf'\eta]$$

$$v_r^* = -[f(\eta)C - Cf'\eta] / r^* = (C/x^*)[f' - f(\eta)/\eta] \qquad \text{(A.7 b)}$$

In order to convert Eq. (A.4) into an ordinary differential equation the following steps are carried out:

$$\partial v_x^* / \partial r^* = C\{-f'/r^{*2} + f''/(r^* x^*)\} \qquad \text{(A.8 a)}$$

$$r^* \partial v_x^* / \partial r^* = C\{-f'/r^* + f''/x^*\} \qquad \text{(A.8 b)}$$

$$\partial v_x^*/\partial x^* = C\{-f''/x^{*2}\} \qquad \text{(A.8 c)}$$

$$[\partial/\partial r^*][r^*\partial v_x^*/\partial r^*]=C\{-f''/(x^*r^*)+f'/r^*+f'''/x^{*2}\} \qquad \text{(A.8 d)}$$

Inserting (A.7a), (A.7b), (A.8a), (A.8b), (A.8c) and (A.8d) into (A.4),

$$\begin{aligned}&\{Cf'/r^*\}C\{-f''/x^{*2}\}+C(f'/x^*-f/r^*)C\{-f'/r^*+f''/(r^*x^*)\}\\&\quad=(1/Re_i)(1/r^*)C\{-f''/(x^*r^*)+f'/r^*+f'''/x^{*2}\}\end{aligned} \qquad \text{(A.9)}$$

Multiply (A.9) by r^* and use (A.6a)

$$\begin{aligned}&-\{f'f''/x^{*2}\}+(f'\eta-f)\{-f'/(\eta^2x^2)+f''/(\eta x^{*2})\}\\&\quad=\{1/CRe_i\}\{-f''/(\eta x^{*2})+f'/(\eta^2x^{*2})+f'''/x^{*2}\}\end{aligned} \qquad \text{(A.10)}$$

Let $C=1/Re_i$. Then, (A.11.a)

$$v_x^*=f'/(Re_ir^*) \qquad \text{(A.11 b)}$$

$$v_r^*=\{1/(Re_ix^*)\}[f'-f(\eta)/\eta] \qquad \text{(A.11 c)}$$

Multiply (A.10) by x^{*2} . Then

$$-\{ff''\}+(f'\eta-f)\{-f'/\eta^2+f''/\eta\}=\{-f''/\eta+f'/\eta^2+f'''\}$$

$$-\{ff''\}+f'\eta\{-f'/\eta^2+f''/\eta\}-f\{-f'/\eta^2+f''/\eta\}=\{-f''/\eta+f'/\eta^2+f'''\}$$

Simplifying

$$-f'^2/\eta+ff'/\eta^2-ff''/\eta=-f''/\eta+f'/\eta^2+f''' \qquad \text{(A.12)}$$

Thus

$$f'''-f''/\eta+f'/\eta^2-f'^2/\eta+ff'/\eta^2-ff''/\eta=0$$

Since

$$d/d\eta\{(\eta f''-f')/\eta\} = (1/\eta)\{\eta f'''+f''-f''\}-(1/\eta^2)(\eta f''-f') \\ =f''-f''/\eta+f'/\eta^2 \qquad \text{(A.13 a)}$$

And

$$d/d\eta\{ff''/\eta\} = f^2/\eta+ff''/\eta-ff'/\eta^2 \qquad \text{(A.13 b)}$$

Then the RHS of (A.12) could be replaced by (A.13a) and LHS of (A.12) could be replaced by (A.13b)

$$d/d\eta\{ff''/\eta\} = d/d\eta\{(\eta f''-f')/\eta\}$$

Integrating,

$$-\{ff'/\eta\}=\{(\eta f''-f')/\eta\}+A$$

As $\eta \to \infty, f''' \to 0,$ hence A=0

Hence

$$-ff'=(\eta f''-f') \qquad \text{(A.15)}$$

Rewriting

$$f'(1-f)=\eta f''$$

$$-df/d\eta(f-1)=d/d\eta\{\eta f'-f\}$$

$$-d/d\eta[\{f-1\}^2/2]=d/d\eta\{\eta f'-f\}$$

Integrating

$$-(f-1)^2/2=\{\eta f'-f\}+B'$$

Simplifying

$$-f^2/2+f-1/2=\{\eta f'-f\}+B'$$

$$-f^2/2+2f=\eta f'+B'$$

As $\eta \to 0, f \to 0$;hence B=0

$$-f^2+4f=2\eta f'$$

$$-[f-2]^2=2\eta f'-4 \qquad \text{(A.16)}$$

Let [f-2]=F

$$-F^2=2\eta F'-4$$

$$-\{F^2-4\}=2\eta F'$$

$$-2dF/\{F^2-4\}=d\eta/\eta$$

$$\{2/4\}[1/(F+2)]-[1/(F+2)]dF=\ln\eta$$

$$\ln\{(F+2)/(F-2)\}=\ln\eta^2+C$$

$$f/(f-4)=D\eta^2$$

$$f=D\eta^2 f-4D\eta^2$$

$$f(1-D\eta^2)=-4D\eta^2$$

$$f=-4D\eta^2/(1-D\eta^2)$$

If $D=-E^2/4$, then

$$f=(E^2\eta^2)/\{1+E^2\eta^2/4\}$$

Which is exactly the same as Schlichting (1955) [2] solution

Let

$$E\eta=\xi \qquad \text{(A.17)}$$

$$f=\xi^2/(1+\xi^2/4) \qquad \text{(A.18)}$$

$$f' = df/d\eta=2E^2\eta/(1+\xi^2/4)-(2E^2\eta/4)E^2\eta^2/(1+E\eta/4)^2 \qquad \text{(A.19 a)}$$

or $$f=2E\xi/(1+\xi^2/4)^2 \qquad \text{(A.19 b)}$$

Recall from equation (A.11b),

$$v_x^* = f'(\eta)/(Re_i r^*) \qquad \text{(A.11 b)}$$

$$v_x^* r^* = f'(\eta)/(Re_i) \qquad \text{(A.20)}$$

$$\eta = r^*/x^* \qquad \text{(A.6 a)}$$

$$\int v_x^{*2} r^* dr^* = M^*/8 \qquad \text{(A.21)}$$

where

$$M^* = M/[\rho_i v_{x,i}^2 (\pi d_i^2/4)] \qquad \text{(A.22)}$$

and typically $M^* = 1$

With (A.11b) in (A.21)

$$= \int f'^2 d\eta/\eta = [M^*/8]Re_i^2 \qquad \text{(A.23)}$$

With (A.19a)

$$= \int [(2E^2)^2/(1+E^2\eta^2/4]^2 \eta d\eta = (M^*/8)Re_i^2$$

$$= -(4/3)(2E^2)\{1/(1+E^2\eta^2/4)\}_0^\infty = (8/3)E^2 = (M^*/8)Re_i^2$$

Thus

$$E^2 = (3/64)M^* Re_i^2$$

$$E=(3/64)^{1/2}M^{*1/2}Re_i \qquad (A.24)$$

Now let us summarize the results

$$E=(\sqrt{3}/8)M^{*}Re_i \qquad (A.24)$$

$$\eta = r^{*}/x^{*} \qquad (A.6\ a)$$

$$\xi = E\eta=(3/64)M^{*}Re_i r^{*}/x^{*}$$

$$f^{'}=2(3/64)M^{*1/2}Re_i\eta/(1+E^2\eta^2/4)^2 \qquad (A.25\ a)$$

or $$f^{'}=2(\sqrt{3}/8)M^{*1/2}Re_i\xi/(1+\xi^2/4)^2 \qquad (A.25\ b)$$

$$f=\xi^2/(1+\xi^2/4) \qquad (A.25\ c)$$

Using (A.25a), (A.11b) and (A.11c),

$$v_x^{*}=f^{'}/(Re_i r^{*})=(3/32)M^{*1/2}(Re_i/x^{*})/(1+\xi^2/4)^2 \qquad (A.26)$$

$$v_r^{*}=\{1/(Re_i x^{*})\}[f^{'}-f(\eta)/\eta]$$

$$v_r^{*}=\{1/x^{*}\}[2(\sqrt{3}/8)M^{*1/2}\xi/(1+\xi^2/4)^2-(\sqrt{3}/8)M^{*1/2}\xi^2/(1+\xi^2/4)\}]$$

$$v_r^{*}=\{1/x^{*}\}[\{(\sqrt{3}/8)M^{*1/2}\}\xi\{1-\xi^2/4\}/(1+\xi^2/4)^2] \qquad (A.27)$$

Note that

$v_r^*=0$ at $\xi=0$ (axis),$v_r^*>0$, $0<\xi<2$,

$v_r^*=0$ at $\xi=2$, $v_r^*<0$, $2<\xi<4$,

$v_r^*=\{1/x^*\}\{\sqrt{3}/2M^{*1/2}Re_i\}\{1/\xi\}$ as $\xi\to\infty$ and $v_r^*=0$ at $\xi=0$

Differentiating with respect to ξ and equating to zero, the maximum radial velocity can be found. Thus,

$dv_r^*/d\xi=\{1-\xi^2/4\}+\xi\{-2\xi/4\}=1-3\xi^2/4=0$

Solving, $\xi=2/\sqrt{3}$

Using (A.27a)

$$v_{r,max}^*=\{1/x^*\}\{\sqrt{3}/8M^{*1/2}\}2/\sqrt{3}(1-4/(3*4)\}/(1+4/(3*4)^2] \\ =\{9/96\}(1/x^*)M^{*1/2} \qquad \text{(A.27 b)}$$

Mixing layer

For a circular jet the velocity profile is given as

$$v_x/v_{x,i}=(3/32)M^*(Re_i/x^*)/(1+\xi^2/4)^2 \qquad \text{(A.27 c)}$$

The maximum velocity occurs at $r^*=0$ and is given by

$$v_x/v_{x,i}=(3/32)(Re_i/x^*) \qquad \text{(A.28)}$$

Hence

$$v_x/v_{x,i}=1/(1+\xi^2/4)^2 \qquad \text{(A.29)}$$

if $v_x=0.01v_{x,max}$ then the mixing layer profile is given as

$$0.01=1/(1+\xi^2/4)^2$$

$$\{1+\xi^2/4\}^2=100$$

$$\xi^2=9*4=36$$

$$\xi_{mix}=\sqrt{3}/8Re_iM^{*1/2}r^*/x^*=6 \qquad \text{(A.30 a)}$$

$$r^*_{mix}=\{48x^*/\sqrt{3}M^{*1/2}Re_i) \qquad \text{(A.30 b)}$$

In Schilchting (1955): $r_{mix}=\{16x^*/(\sqrt{3}M^{*1/2}Re_i)\}$; recall that $v^*_r=0$ at $\xi=2$; if we use this definition for the mixing layer, then $\xi=2$ and hence $r^*_{mix}=\{16x^*/\sqrt{3}M^{*1/2}Re_i)$

Hence mixing layer grows linearly with x^*. Using ξ in Eq. (A.27a), the radial velocity at ξ^*_{max} is given as (called entrainment velocity)

$$v^*_{r,ent}=[\{1/(Re_ix^*)\}\{\sqrt{3}/8M^{*1/2}Re_i\}\xi_{mix}\{1-\xi^2/4\}/\{1+\xi^2/4\}^2]$$

Then

$$v^*_r/v^*_{r,ent}=\{\xi/\xi_{mix}\}[\{(1-\xi^2/4)/(1-\xi^2_{mix}/4)\}]\{1+\xi^2_{mix}/4\}/[(1+\xi^2/4)^2] \qquad \text{(A.31 a)}$$

$$v_r^*/v_{r,ent}^* = -\{\xi/6\}[(1-\xi^2/4)/(-8)](100)/[(1+\xi^2/4)^2] \quad \text{(A.31 b)}$$

$$= -(100/48)\{\xi\}[\{1-\xi^2/4\}/(1+\xi^2/4)^2] \quad \text{(A.31 c)}$$

x^* at which the two layers intersect

If multiple burners are spaced apart by l^*, the mixing layers will intersect at (using (A.31 c)),

$$l^*/2 = \{48x^*/\sqrt{3}\,Re_i\,M^{*1/2}\}$$

$$x_{int}^* = l(\sqrt{3}\,Re_i\,M^{*1/2})/96 \quad \text{(A.32)}$$

If an infinite series of burners surrounds the central burner, then the gas entrained by the central burner is within $l^*/2$ and $0<x^*<x_{int}^*$.

Gas entrained within r^* and x^*

$$\dot{m}(x^*,r^*)/\dot{m}_i = 2\pi\{\int_0^r \rho v_x r dr/\dot{m}\} = 8\{\int_0^{r^*} v_x^* r^* dr^*\}$$

Using v_x^* from (A.26) and using the definition of ξ,

$$\dot{m}(x^*,r^*)/\dot{m}_i = 16\{\int_0^{\xi} (3/32x^*)M^* Re_i\}\{1/(1+\xi^2/4)\}/$$
$$\{(3/64)Re_i^2 M^*/x^{*2}\}\{\xi d\xi\}/2$$

$$\dot{m}(x^*,r^*)/\dot{m}_i = \{32x^*/Re_i\}[1/(1+3Re_i^2 r^{*2}M^*/(256x^{*2}))] \quad \text{(A.33)}$$

or

$$\dot{m}(x^*,r^*)/\dot{m}_i = 32(x^*/Re_i)[1/(1+\xi^2/4\}]$$

Gas entrained within $r^*=l^*/2$ is given as

$$\dot{m}(x^*,l^*/2)/\dot{m}_i = \{32x^*/Re_i\}[1/(1+3Re_i^2 l^{*2}M^*/(1024x^{*2})\}] \quad (A.34)$$

As $r^* \to \infty$ or gas entrained within mixing layer up to x^*

$$\dot{m}/\dot{m}_i = 32x^*/Re_i \quad (A.35)$$

If an infinite series of burners surrounds the central burner, then the gas entrained by the central burner within $l^*/2$ and $0<x^*<x^*_{int}$ is given as

$$\dot{m}/\dot{m}_i \approx 32x^*/Re_i = \{32/Re_i\}[l^*(\sqrt{3}M^{*1/2}Re_i)/96] = [l^*M^{*1/2}/\sqrt{3}] \quad (A.36)$$

And the air entrained within $l^*/2$ if all the burners are surrounding the central burner is given as

$$\{\dot{m}_A/\dot{m}_i\} = [l^*M^{*1/2}/\sqrt{3}] - 1 \quad (A.37)$$

A.3. Solutions for Species, Temperature and φ

Species

Consider the species conservation equation:

$$v_x \partial\phi/\partial x + v_r \partial\phi/\partial r = (D/r)\partial/\partial r(r)\partial\phi/\partial r \quad (A.38)$$

Normalizing

$$v_x^* \partial\phi / \partial x^* + v_r^* \partial\phi / \partial r^* = (D/v_i d_i)(1/r^*) \partial/\partial r^* (r^* \partial\phi / \partial r^*)$$

$$v_x^* \partial\phi / \partial x^* + v_r^* \partial\phi / \partial r^* = \{1/(Re_i SC)\}(1/r^*) \partial/\partial r^* (r^* \partial\phi / \partial r^*) \quad \text{(A.39)}$$

Let

$$\phi = \psi(\eta) / x^* \quad \text{(A.40)}$$

$$\partial\phi / \partial x^* = \psi'(-r^*/x^{*3}) - \psi/x^{*2} = -\psi'\eta/x^{*2} - \psi/x^{*2} \quad \text{(A.41)}$$

$$\partial\phi / \partial r^* = \psi'/x^{*2} \quad \text{(A.42)}$$

$$r\partial\phi / \partial r^* = \{\psi'\eta/x^*\} \quad \text{(A.43)}$$

$$v_x^* = f'/(Re_i r^*) \quad \text{(A.11 b)}$$

$$v_r^* = 1/(Re_i x^*)[f' - f(\eta)/\eta] \quad \text{(A.11 c)}$$

Using (A.11b),(A.11c),(A.41),(A.42), (A.43) and (A.39)

$$\{f'/(Re_i r^*)\}\{-\psi'\eta/x^{*2} - \psi/x^{*2}\} + 1/(Re_i x^*)[f' - f(\eta)/\eta]\{\psi'/x^{*2}\}$$
$$= (1/r^*)(1/(Re_i Sc))\{\psi''\eta/x^{*2} + \psi/x^{*2}\}$$

Simplifying

$$Scf'\{-\psi'\eta\} - Sc\{f'\psi\} + Sc(f'\eta - f)\{\psi'\} = \{\psi''\eta + \psi'\}$$

$$-Sc\, f'\psi'\eta - Sc\, f'\psi + Sc\, f'\psi'\eta - Scf\psi' = \psi''\eta + \psi'$$

$$-\mathrm{Sc}\, f\psi' - \mathrm{Sc}\, f'\psi = \psi''\eta + \psi' \qquad \text{(A.44)}$$

Rewriting

$$d/d\eta\{\psi'\eta\} = -d/d\eta\{\mathrm{Scf}\psi\}$$

Integrating

$$\psi'\eta = -\mathrm{Sc}\, f\psi + G$$

As $\eta \to 0,\ f \to 0$, G=0

$$d\ln\psi/d\eta = -\mathrm{Scf}/\eta$$

$$= -\mathrm{Sc}\, E^2\eta/(1+E^2\eta^2/4)$$

Since

$$E\eta = \xi$$

Then

$$\ln\psi = -\mathrm{Sc}\ 2\ln\{1+\xi^2/4\} + H'$$

$$\psi = G/\{1+\xi^2/4\}^{\mathrm{Sc}} \qquad \text{(A.45)}$$

Where G needs to be evaluated

$$\int_0^\infty \phi_v\ \phi\ r^* dr^* = J^*/8 \qquad \text{(A.46)}$$

Where

$$\phi_v = v_x/v_{x,i}=(3/32)M^*(Re_i x^*)/(1+\xi^2/4)^2 \quad \text{(A.26)}$$

$$\phi = \psi / x^* =(G/x^*)/\{1+\xi^2/4\}^{2Sc} \quad \text{(A.47)}$$

$$\int_0^\infty [(3/32)M^*(Re_i/x^*)/(1+\xi^2/4)^2](G/x^*)/\{1+\xi^2/4\}^{2Sc} r^* dr^* = J^*/8$$

$$\int_0^\infty (3/32)M^*(Re_i)/(1+\xi^2/4)^2](G)/\{1+\xi^2/4\}^{2Sc} \{E\eta\} d\{E\eta^*\} = E^2 J^*/8$$

$$\int_0^\infty (3/32)M^*(Re_i)/(1+\xi^2/4)^2](G)/\{1+\xi^2/4\}^{2Sc} \{\xi\} d\{\xi\} = E^2 J^*/8$$

With $E=(\sqrt{3}/8)M^{*1/2}Re_i$

$$G\int_0^\infty 1/(1+\xi^2/4)^{2+2Sc}\{\xi\} d\xi = (3/64)M^* Re_i^2 J^*/\{8(3/32)M^*(Re_i)\}$$

$$G[1/(1+\xi^2/4)]^{2+2Sc} = (2Sc+1)(1/32)Re_i J^*$$

Thus G can be estimated as

$$G=Re_i(2Sc+1)(J^*/32)$$

$$\phi=(G/x^*)/\{1+\xi^2/4\}^{2Sc}$$

$$\phi = (2Sc+1)(J^*/32)(Re_i/x^*)/\{1+\xi^2/4\}^{2Sc} \quad \text{(A.48)}$$

$$\phi_0=\{(2Sc+1)J^*/32\}(Re_i/x^*) \quad \text{(A.49)}$$

$$\phi_0/\phi_0(\text{Sc=1})=\{(2\text{Sc+1})/3\} \tag{A.50}$$

If Sc<1, then $\phi_0 < \phi_0(\text{Sc=1})$. Thus, the center line fuel mass fraction for Sc<1 is less than the centerline fuel mass fraction with Sc=1. Hence, the stiochiometric contour will be pulled inward while the reverse happens for Sc>1.

$$\phi_v = v_x/v_{x,i}=(3/32)M^*(Re_i/x^*)/(1+\xi^2/4)^2 \tag{A.26}$$

Let

$$\phi' = \phi(r,x)/\phi_0(r=0,x). \text{ Then} \tag{A.51}$$

$$\phi' = 1/\{1+\xi^2/4\}^{2Sc}$$

Then

$$\phi' = \phi_v'^{Sc} \tag{A.52}$$

If Sc<1, then $\phi' > \phi_v'$ since ϕ'<1

A.4. Mixing and Flame Structure

As before the stoichiometric contour for mixing is the same as the flame contour for the case of combustion.

$$\phi_f=f_\infty/\{1-f_i+f_\infty\}=\{(2\text{Sc+1})/32\}(Re_iJ^*)/(x^*)1/\{1+\xi_f^2/4\}^{2Sc} \tag{A.53}$$

Maximum height is obtained by setting $\xi_f = 0$. Then

$$H^*_{cir}=\{(2\text{Sc+1})/(32\phi_f)\}Re_iJ^* \tag{A.54}$$

Recall that H^* for the 2D jet is proportional to $1/\phi_f^3$ while H^* for the circular jet is proportional to $1/\phi_f$. ϕ_f is typically 0.06 for pure methane flames burning in air. Thus at the same Re_i, the flame height will be much larger for 2D burners compared to circular burners. The reason is that at any given x, the O_2 is accessible from all sides of the jet for the circular jet while for the 2D jet is accessible only from the two lateral sides. For e.g. the mixing layer grows as x^* and hence surface area through which oxygen diffuses increases as x^{*2} while for the 2D jet, the mixing layer grows as $x^{*2/3}$ while surface area grows as $x^{*2/3}$ and as such reduced surface area causes the flame to grow to a large height.

Rewriting (A.53)

$$\{1+\xi_f^2/4\}^{2Sc} = H^*_{cir}/x^*$$

Solve for ξ_f

$$1+\xi_f^2/4 = [(H^*_{cir}/x^*)]^{1/(2Sc)}$$

Where

$$\xi = \sqrt{3}/8\,Re\,M^{*1/2}r^*/x^*$$

$$\xi_f^2 = 4[H^*_{circ}/x^*]^{1/(2Sc)} - 4 \qquad (A.55)$$

Expanding

$$3/64\,Re_i^2\,M^*r^{*2} = 4x^{*(2-1/2Sc)}[H^*_{circ}]^{1/(2Sc)} - 4x^{*2}$$

$$r^{*2}/H^{*2}_{circ} = 256/(3Re_i^2M^*)[\{x^*/H^*_{circ}\}^{(2-1/(2Sc))} - \{x^*/H^*_{circ}\}^2] \qquad (A.56)$$

Gas and Air entrained within flame height

With x=H in (A.35)

$$\dot{m}/\dot{m}_i = 32H^*_{circ}/Re_i$$

Using (A.54)

$$\dot{m}/\dot{m}_i = 32H^*_{circ}/Re_i = J^*\{(2Sc+1)/\phi_f\}$$

Air flow is given as

$$\dot{m}_A/\dot{m}_i = J^*\{(2Sc+1)/\phi_f\text{-}1\}$$

Since $1/\phi_f = \{A{:}F\}_{Stoich} + 1$,

$$\dot{m}_A/\dot{m}_i = J^*\{(2Sc+1)\{A{:}F\}_{Stoich} + 1\}\text{-}1$$

Where (A: I) is air to injected gas ratio .Writing in terms of excess air

$$\dot{m}_A(H^*_{stoich},\infty)/\dot{m}_i - \dot{m}_{A,stoich}/\dot{m}_i = J^*\{(2Sc+1)\{A{:}F\}_{Stoich} + 1\}\text{-}1\text{-}\{A{:}I\}_{stoich}$$

And as fraction or %

$$[\dot{m}_A(H^*_{stoich},\infty) - \dot{m}_{A,stoich}]/\dot{m}_{A,stoich} = [J^*\{(2Sc+1)\{A{:}F\}_{Stoich} + 1\}\text{-}1\text{-}\{A{:}I\}_{stoich}]/[A{:}I]_{stoich}$$

$$[\dot{m}_A(H^*_{stoich},\infty) - \dot{m}_{A,stoich}]/\dot{m}_{A,stoich} = [\{(2Sc+1)J^*_F - 1\}\text{-}1/[A{:}I]_{stoich}[(2Sc+1)J^*_F - 1]$$

With $J_F^* = 1$,

$$\dot{m}_A / \dot{m}_i = \{(2Sc+1)\{A:F\}_{Stoich} + 1\} - 1$$

And excess air fraction

$$\dot{m}_A(H^*_{stoich}, \infty) / \dot{m}_i - \dot{m}_{A,stoich} / \dot{m}_i = \{(2Sc+1)\{A:F\}_{Stoich} + 1\} - 1 - \{A:I\}_{stoich}$$

When Sc = 0,

$$\dot{m}_A / \dot{m}_i = \{A:F\}_{Stoich}$$

And excess air fraction is zero

If $Y_{F,I} = 1$, then

$$\dot{m}_A / \dot{m}_{F,i} = \{A:F\}_{Stoich}$$

At Sc = 1, C = 1; hence

$$\dot{m}_A(H^*_{stoich}, \infty) / \dot{m}_i = [3\{A:F\}_{Stoich} + 1\} - 1] = 3*\{A:F\}_{Stoich} + 2$$

The excess air fraction

$$\dot{m}_A(H^*_{stoich}, \infty) / \dot{m}_i - \dot{m}_{A,stoich} / \dot{m}_i = 2 - [2/\{A:I\}_{stoich}]$$

$$\dot{m}_A(H^*_{stoich}, \infty) / \dot{m}_i - \dot{m}_{A,stoich} / \dot{m}_i = 2 - [2/\{A:I\}_{stoich}] \approx 2 \text{ or } 200\% \text{ excess air}$$

(independent of fuel for all fuels having $Sc \approx 1$)

For any Sc

$$\dot{m}_A(H^*_{stoich},\infty)/\dot{m}_i - \dot{m}_{A,stoich}/\dot{m}_i = J^*\{(2Sc+1)\{A:F\}_{Stoich}+1\}\text{-}1\text{-}\{A:I\}_{stoich}$$

And excess air fraction is given as

$$[\dot{m}_A(H^*_{stoich},\infty)-\dot{m}_{A,stoich}]/\dot{m}_{A,stoich} = [\{(2Sc+1)J^*_F-1\}\text{-}1/[A:I]_{stoich}[(2Sc+1)J^*_F-1]$$

$$[\dot{m}_A(H^*_{stoich},\infty)-\dot{m}_{A,stoich}]/\dot{m}_{A,stoich} \approx [(2Sc+1)J^*_F-1] \approx 2Sc$$

The maximum flame width for circular Jet:

In order to find the maximum width of the flame, r^*_{max}, differentiate Eq. (A.56), to obtain dr^*/dx^* and set the differential to zero:

Thus

$$(2\text{-}1/(2Sc))x^{*(1\text{-}1/(2Sc))}[H^*_{circ}]^{1/(2Sc)}\text{-}2x^* = 0$$

Solving for x^* at which the max width occurs,

$$x^{*(1/(2Sc))}=(1\text{-}1/4Sc)[H^*_{circ}]^{1/(2Sc)}$$

$$x^*/[H^*_{circ}]=[1\text{-}1/4Sc]^{2Sc} \qquad \text{(A.57)}$$

Using (A.57) in (A.56),

$$r_{max}^2/H_{circ}^2=\{256/(3Re_i^2M^*)\}\{1\text{-}1/4Sc\}^{(4Sc\text{-}1)}\text{-}\{1\text{-}1/4Sc\}^{4Sc} \quad (A.58)$$

$$r_{max}^2/H_{circ}^2=\{256/(3Re_i^2M^*)\}\{1\text{-}1/4Sc\}^{(4Sc\text{-}1)}\text{-}\{4Sc/(4Sc\text{-}1)\}$$
$$=\{256/(3Re_i^2M^*)\}\{1\text{-}1/4Sc\}^{(4Sc\text{-}1)}\text{-}\{1/(4Sc\text{-}1)\}$$

$$r_{max}/H_{circ}=\{16/(\sqrt{3}Re_i M^{*1/2})\}\{4Sc\text{-}1\}^{(2Sc\text{-}1/2)}\text{-}\{4Sc\}^{2Sc} \quad (A.59)$$

As Re_i decreases, r_{max}^*/H_{cir}^* increases or the angular effect on blow off becomes important. Particularly for low BTU gases, blow off occurs at lower velocities where angular effect is important.

Substituting for H_{cir}^*,

$$r_{max}^*=\{(2Sc+1)J^*/2\sqrt{3}M^{*1/2}\phi_f\}\{4Sc\text{-}1\}^{(2Sc\text{-}1/2)}/\{4Sc\}^{2Sc} \quad (A.60)$$

The maximum flame width may be unaffected by the variable properties. Since H_{cir}^* is inversely proportional to the oxygen mass fraction, the half width of the flame is inversely proportional $\{Y_{O_2,\infty}/\upsilon Y_{F,i}\}$.

$r_{max}^{*2}\ \phi_f^2$ is only a function of Sc

Again the half width of the flame is inversely proportional to ϕ_f or approximately inversely proportional to $\{Y_{O_2,\infty}/\upsilon Y_{F,i}\}$. Such dependence is independent of Re_i.

$$r_{max}^{*2}\ \phi_f^2 \approx r_{max}^{*2}\{Y_{O_2,\infty}/\upsilon Y_{F,i}\}^2 = f(Sc)$$
$$=(256/(M*3))\{(2Sc+1)/32\}^2\{[(1/2)(2\text{-}1/2Sc)]^{4Sc\text{-}1}\text{-}[(1/2)(2\text{-}1/2Sc)]^{4Sc}\}$$
$$=(256/(M*3))\{(2Sc+1)/32\}^2\{[(1/2)(2\text{-}1/2Sc)]^{4Sc\text{-}1}\{(1\text{-}(1\text{-}1/4Sc)]\}$$

$$r_{max}^{*2}\ \phi_f^2 \approx r_{max}^{*2}\{Y_{O_2,\infty}/\upsilon Y_{F,i}\}^2$$
$$=(256/(M*3))\{(2Sc+1)/32\}^2\{[(1/2)(2-1/2Sc)]^{4Sc-1}$$

$\{1/4Sc\}$, Sc>0.25 for max. width

$$r_{max}^{*} \propto \{Y_{O_2,\infty}/\upsilon Y_{F,i}\} = 1/f \qquad (A.61)$$

For low BTU gases, $Y_{F,i}$ decreases; thus y_{max}^{*} decreases; thus the interaction distance will be reduced.

$$\text{Flame volume} \propto r_{max}^{*2}\ H_f^2 \propto \{Y_{O_2,\infty}/\upsilon Y_{F,i}\}^3 \qquad (A.62)$$

Which is similar to drop flame volume relations. Note that the flame volume for low BTU gases is reduced which will reduce the soot concentration.

Flame Curvature

Differentiating Eq. (A.55) with respect to x^*

$$2\xi_f d\xi_f/dx^* = 4H_{cir}^{*1/(2Sc)}(-1/2Sc)x^{*(-1/(2Sc)-1)}$$

Using definition of $\xi_f = \sqrt{3}/8\,Re_i\,M^{*1/2}r_f^*/x^*$

$$2\{\sqrt{3}/8\,Re_i\,M^{*1/2}r_f^*/x^*\}\sqrt{3}/8\,Re_i\,M^{*1/2}\{(1/x^*)dr_f^*/dx^* - r_f^*/x^{*2}\} =$$
$$4H_{cir}^{*1/(2Sc)}(-1/2Sc)x^{*(-1/(2Sc)-1)}$$

Solving for dr_f^*/dx^*

$$dr_f^*/dx^* = -\{64x^*/(3Scr_f^* Re_i M^*)\}[x^*/H_{cir}^*] + r_f^*/x^*$$

At the flame tip $x^* = H_{cir}^*$, then

$$\{dr_f^*/dx^*\}_{tip} = -\{64/(3ScH_{cir}^* Re_i^2 M^*)\}$$

Thus

$$\tan\theta = dr_f^*/dx^* = \{dr_f^*/dx^*\}[x^*/H_{cir}]^{(-1/2Sc-1)} + r_f^*/x^*$$

A.5. Lift Off and Blow Off Criteria

Lift Off

The velocity on the stoichiometric contour can be determined

$$\phi_v = \{3/32\}\{Re_i M^*/x^*\}/(1+\xi^2/4)^2 \qquad (A.26)$$

Using (A.54),

$$\phi = \{\beta - \beta_\infty\}/\{\beta_i - \beta_\infty\} = \phi_v = \{(2Sc+1)/32\}\{Re_i J^*/x^*\}/(1+\xi^2/4)^{2Sc}$$

$$\phi_f = \{H_{cir}^*/x^*\}/(1+\xi^2/4)^2$$

$$\phi_f = \{\beta - \beta_\infty\}/\{\beta_i - \beta_\infty\} = \phi_v = \{(2Sc+1)/32\}\{Re_i J^*/x^*\}/(1+\xi^2/4)^{2Sc} \qquad (A.48)$$

Recall that along the stoichiometric contour,

$$1+\xi_f^2/4 = [H_{cir}^*/x^*]^{(1/2Sc)}$$

$$\xi_f^2 = 4[H_{cir}^*/x^*]^{(1/2Sc)} - 4 \tag{A.55}$$

Hence, along the stoichiometric contour,

$$\{v_x/v_{x,i}\} = \{3/32\}\{Re_i\, M^*/x^*\}/[H_{cir}^*/x^*]^{1/Sc} \tag{A.63}$$

With $v_x = S$,

$$\{S/v_i\} = \{3/32\}\{Re_i\, M^*/L^*\}/[H_{cir}^*/L^*]^{1/Sc} \tag{A.64}$$

$$L^{*1-1/Sc} = \{3/32\}\{(v_{x,i}/S)\}\{Re_i M^*\}/[H_{cir}^*/L^*]^{1/Sc} \tag{A.65}$$

$$\{L^*/H_{cir}^*\}^{1-1/Sc} = \{3/32\}\{(v_{x,i}/S)\}\{Re_i M^*\}/[H_{cir}^*]$$

$$\{L^*/H_{cir}^*\}^{1-1/Sc} = [\{3/32\}\{(v_{x,i}/S)\}\{Re_i M^*\}/(H_{cir}^*)]^{Sc/Sc-1}$$

Where

$$H_{cir}^* = \{(2Sc+1)/(32\phi_f)\}Re_i J^* \tag{A.54}$$

$$\{L^*/H_{cir}^*\}^{1-1/Sc} = [\{3/32\}\{(v_{x,i}/S)\}\{Re_i M^*\}/((2Sc+1)/(32\phi_f)\}Re_i J^*)]^{Sc/Sc-1}$$
$$= \{3/(2Sc+1)\}\{(v_{x,i}/S)\phi_f\{M^*/J^*\}^{Sc/Sc-1}$$

$$\{L^*/H_{cir}^*\}^{1-1/Sc} = \{3/(2Sc+1)\}\{(v_{x,i}/S)\phi_f\{M^*/J^*\}^{Sc/Sc-1} \tag{A.66}$$

Blow Off

Blow Off occurs if the velocity on the stoichiometric surface exceeds the laminar burn velocity, S, or when $L^* > H^*$. Thus, blow off occurs if

$$\phi_v = \{(v_x - v_{x,\infty})/(v_{x,i} - v_{x,\infty})\}_{\xi_f} > (S - v_{x,\infty})/(v_{x,i} - v_{x,\infty}) \tag{A.67}$$

Using (A.66) and setting $L^* = H^*$,

$$1 = [\{3/(2Sc+1)\}\{v_{x,i}/S\}\phi_f\{M^*/J^*\}]^{Sc/(Sc-1)}$$

$$\{3/(2Sc+1)\}\{v_{x,i}/S\}\phi_f\{M^*/J^*\}]^{Sc/(Sc-1)} = 1$$

$$\{v_{x,i,blow}\} = S\{(2Sc+1)/3\}\{1/\phi_f\}\{J^*/M^*\} \tag{A.68}$$

APPENDIX B

PROCEDURE FOR CALCULATION OF NO_x IN A CIRCULAR LAMINAR JET FLAME

A typical calculation step performed in the above procedure is shown (for the case in which both CO_2 and H_2O is considered simultaneously.

A value of x* is selected for the calculation to begin. This should be chosen in order to be comfortably out of the potential core region. In this work a value of x* = 10 is taken as the starting point for the calculations.

Now at each value of x*, the following variables are calculated:

The value of ξ is varied from 0 to 20 in step intervals of 0.05. At each ξ, the value of r^* is calculated by the formula:

$$r^* = \frac{\xi}{\frac{\sqrt{3}}{8} * \mathrm{M}^{*\frac{1}{2}} * \frac{\mathrm{Re}_i}{\mathrm{x}^*}} \tag{B.1}$$

The following are also calculated at each ξ in that order:

$$\frac{\mathrm{v_x}}{\mathrm{v_{x,max}}} = \frac{1}{[1+\frac{\xi^2}{4}]^2} \tag{B.2}$$

$$\frac{\phi}{\phi_{x,\max}} = \frac{1}{[1+\frac{\xi^2}{4}]^{2Sc}} \tag{B.3}$$

$$v_x = \frac{v_x}{v_{x,max}} * v_{x,max} \tag{B.4}$$

$$\phi = \frac{\phi}{\phi_{x,max}} * \phi_{x,max} \tag{B.5}$$

Mixture fraction $f = \phi * Y_{F,i}$

$$\beta_{F\text{-}O_2} = \phi * (\beta_{F\text{-}O_2,i} - \beta_{F\text{-}O_2,\infty}) + \beta_{F\text{-}O_2,\infty} \tag{B.6}$$

$$Y_F = \beta_{F\text{-}O_2} * Y_{F,i} \tag{B.7}$$

$$Y_{O_2} = \beta_{F\text{-}O_2} * \upsilon_{O_2} + Y_{O_2}(CO_2) + Y_{O_2}(H_2O) \tag{B.8}$$

$$\beta_{h_T\text{-}F} = \phi * (\beta_{h_T\text{-}F,i} - \beta_{h_T\text{-}F,\infty}) + \beta_{h_T\text{-}F,\infty} \tag{B.9}$$

$$T = (\beta_{h_T - F} - Y_F) * \frac{h_c}{C_p} + T_\infty \tag{B.10}$$

$$Y_{N_2} = \phi * (Y_{N_2,i} - Y_{N_2,\infty}) + Y_{N_2,\infty} \tag{B.11}$$

$$\eta = \frac{\xi}{\frac{\sqrt{3}}{8} * M^{*\frac{1}{2}} * Re_i} \tag{B.11a}$$

$$\rho_{mix} = \frac{PM_{mix}}{RT} \tag{B.11b}$$

Exp (Equiv) = (-69000/T)

$$\frac{d[NO]}{dt} = \frac{A_{NO} M_{NO} (\rho_{mix})^{1.5}}{(M_{N_2})(M_{O_2})^{0.5}} \exp\left(\frac{-E}{RT}\right) \frac{(Y_{N_2})(Y_{O_2})^{0.5}}{T^{0.5}} \quad \text{(B.12)}$$

Eq. B.13 has been derived from the extended Zeldovich Mechanism [2].

$$\text{Integral calculated} = \eta * \frac{d[NO]}{dt} \quad \text{(B.13)}$$

The integral is calculated by using the trapezoidal rule.

For calculating the values of Y_{O_2} (from CO_2 equilibrium) and Y_{O_2} (from H_2O equilibrium) the equilibrium constant is ascertained for a given T in the form of:

$K = C_1 - \frac{C_2}{T}$ Where C_1, C_2 are constants.

For solving the simultaneous equilibrium of CO_2 and H_2O, we assume for the reactions $CO_2 \Leftrightarrow CO + 1/2\ O_2$ and the reaction $H_2O \Leftrightarrow H_2 + 1/2\ O_2$ that 'a' moles of H_2O and 'b' moles of CO_2 react in the reaction. Hence the total moles of O_2 will be $\frac{(a+b)}{2}$.

Conducting atom balance for C, H and O in both the reactions and solving, we obtain a quartic equation at each point.

This quartic equation is first converted into a cubic equation and then the cubic equation is solved at each point.

After we obtain both 'a' and 'b', we find X_{O_2} and hence Y_{O_2} at each point.

Hence net Y_{O_2} can be calculated and the above procedure is then followed to find

$$\eta * \frac{d[NO]}{dt}.$$

The method used to calculate the Quartic equation is illustrated as follows [16]:
The equation is of the form:

$$a_1 x^4 + a_2 x^3 + a_3 x^2 + a_4 x^1 + a_5 = 0 \qquad \text{(B.14)}$$

It is normalized by dividing throughout by a_1 and hence we get a new equation of the form:

$$x^4 + bx^3 + cx^2 + dx \ + e = 0 \qquad \text{(B.14 a)}$$

Where b, c, d and e are the coefficients of the equation.
The following values are then calculated:

$$f = \frac{(c - 3b^2)}{8} \qquad \text{(B.15)}$$

$$g = d + \frac{b^3}{8} - \frac{bc}{2} \qquad \text{(B.16)}$$

$$h = e - \frac{3b^4}{256} + \frac{b^2 c}{16} - \frac{bd}{4} \qquad \text{(B.17)}$$

Then for converting into a cubic equation, the following coefficients are calculated:

$$b_1 = \frac{f}{2} \qquad \text{(B.18)}$$

$$c_1 = f^2 - \frac{4h}{16} \tag{B.19}$$

$$d_1 = \frac{-g^2}{64} \tag{B.20}$$

These are the coefficients of the equation:

$$y^3 + b_1 y^2 + c_1 y + d_1 = 0 \tag{B.21}$$

Now for solving the cubic equation, we calculate:

$$f_1 = \frac{3c_1 - b_1^2}{3} \tag{B.22}$$

$$g_1 = \frac{2b_1^3 - 9b_1 c_1 + 27d_1}{27} \tag{B.23}$$

$$h_1 = \frac{g_1^2}{4} + \frac{f_1^3}{27} \tag{B.24}$$

Now based on these coefficients:

$$R = \frac{-g_1}{2} + \sqrt{h_1} \tag{B.25}$$

$$S = (R)^{\frac{1}{3}} \tag{B.25 b}$$

$$T = \frac{-g_1}{2} - \sqrt{h_1} \tag{B.25 c}$$

$$U = (T)^{\frac{1}{3}} \tag{B.25 d}$$

Now the roots can wither be all real or one real and 2 imaginary roots. In our analysis, in all cases the latter is true.

Hence to calculate the roots:-

$$\text{Real root } (y_1) = (S+U) - \frac{b_1}{3} \tag{B.26 a}$$

Imaginary roots y_2 and y_3 are calculated as follows:

$$y_2 = [(S+U) - \frac{b_1}{3}] + i[\frac{\sqrt{3}}{2}(S-U)] \tag{B.26 b}$$

$$y_2 = [(S+U) - \frac{b_1}{3}] - i[\frac{\sqrt{3}}{2}(S-U)] \tag{B.26 c}$$

Now the square root of these complex roots is found as follows:

$$r = \sqrt{[(S+U) - \frac{b_1}{3}]^2 + [\frac{\sqrt{3}}{2}(S-U)]^2} \tag{B.27 a}$$

$$p = \sqrt{y_2} = \sqrt{\frac{\{r - [(S+U) - \frac{b_1}{3}]\}}{2}} + i\left[\frac{[\frac{\sqrt{3}}{2}(S-U)]}{\sqrt{\frac{\{r - [(S+U) - \frac{b_1}{3}]\}}{2}}}\right] \tag{B.27b}$$

$$q = \sqrt{y_2} = \sqrt{\frac{\{r - [(S+U) - \frac{b_1}{3}]\}}{2}} - i\left[\frac{[\frac{\sqrt{3}}{2}(S-U)]}{\sqrt{\frac{\{r - [(S+U) - \frac{b_1}{3}]\}}{2}}}\right] \quad \text{(B.27c)}$$

$$R_1 = \frac{-g}{8r} \quad \text{(B.27d)}$$

$$S_1 = \frac{-b}{4} \quad \text{(B.27e)}$$

Final solution of the quartic equation is:

$$X = R_1 - S_1 + p + q \quad \text{(B.28)}$$

This entire procedure is followed for determining the value of $\eta * \frac{d[NO]}{dt}$ at a particular x*. Now the same process is followed for various values of x* till a point beyond the flame height where T<1400K.

At this point all the values of the integral

$\eta * \frac{d[NO]}{dt}$ at various x* are tabulated and the final integral of

$2\pi x^{*2} \eta * \frac{d[NO]}{dt}$

is calculated at each x*. Then the final answer is tabulated by again applying the trapezoidal rule.

The final integral gives the net production of NO_x in moles/s.

Also total air flow is calculated by calculating $m'(x^*)$ at each x* and integrating over the entire x* values by the trapezoidal rule once more. This is converted into moles of air and hence of various species like N_2 and O_2. From the injected mass of fuel and using stiochiometry, the values of Y_{CO_2} and Y_{H_2O} are also calculated. Y_{O_2} is found by subtracting the total oxygen mass fraction in the entrained air minus the amount of O_2 used up during the combustion of fuel.

The mole fraction of NO_x is found by dividing the net production of NO_x by the net sum of entire species namely $Y_{N_2}, Y_{O_2}, Y_{CO_2}, Y_{H_2O}$ and Y_{NO}. This is multiplied by 10^6 to convert into ppm.

For finding the solution in g/GJ, the following relation is used:

$$\frac{\text{Kmoles of NO}}{m'_{i,F} * h_c}.$$

A similar procedure is followed in the cases when $CO_2 \Leftrightarrow CO + 1/2\ O_2$ equilibrium or $H_2O \Leftrightarrow H_2 + 1/2\ O_2$ equilibrium is assumed apart from the exception that in both these cases, a cubic equation is obtained and not a quartic equation. Similarly in the case of complete combustion reaction being considered, $Y_{O_2} = \beta_{F\text{-}O_2} * \upsilon_{O_2}$ simply as Y_{O_2} from the above reactions is absent.

During the calculation of $EINO_x$

The following formula is used as given by Rokke and workers

$$EINO_x = 22\ Fr^{3/5}\ Y_f^{-1/5}\ \left(\frac{d_0}{\rho_0 u_0}\right) x\ (0.35^{-0.45} + 0.7\ d_0^{0.2}) \qquad \text{(B.29)}$$

Also used for the conversion and confirmation of values of are the following relations:

$EINO_x$ (g/Kg of fuel)= $C * X_{NO} * M_{NO_2} * \frac{1000}{M_F}$ Where C is the number of carbon atoms in one mole of fuel.

For emissions in g/GJ the following relation is used

$$NO_x(\text{in g/GJ}) = \frac{c\, X_{NO}}{(X_{CO_2} + X_{CO})} \frac{M_{NO_2} * 1000}{12.01 * HHV_F} \tag{B.30}$$

This relation can be used to check in the values of ppm and g/GJ interchangeably by setting X_{CO} equal to zero.

For prompt NO_x, an empirical rate relation is used [15] and is given as follows:-

$$\dot{\omega}'''_{\text{prompt NOx}} = A \frac{M^{1+b}}{\rho^{1+b}} C_{O_2}^{b} C_{N_2} C_{CH_4} \exp\left(\frac{-E_a}{RT}\right) \tag{B.31}$$

Where pre-exponential factor A = 9.2 x10^6, b= 0.5 and $\frac{E_a}{R}$ = 30000 (K) respectively.

Using a method similar to thermal NO_x as given above, the total prompt NO_x is calculated

The net NO_x is equal to the sum of thermal NO_x and prompt NO_x.

APPENDIX C

FORTRAN CODE USED TO MODEL THE FORMATION OF NO_x IN A CIRCULAR LAMINAR JET FLAME

Following this is the FORTRAN CODE written to follow the above procedure is given below for the fourth case or when both CO_2 and H_2O dissociation is assumed. The other cases are a subset of this main model and follow the same procedure:

```
C       Program to find the production of NO in a circular laminar jet with H2O and
C       CO2 dissociation also assumed
        PROGRAM MAIN
        DOUBLE PRECISION EQUV,DNODTO,DNODT,EDNODTC,EDNODTB
        DOUBLE PRECISION FFA,FFB,FFC,FFD,FFE,FFF,EDNODTA,GGA CC
        DOUBLE PRECISION BQ,CQ,DQ,EQ,FQ,GQ,HQ,BOQ,COQ,DOQ,FOQ
        DOUBLE PRECISION ROQ,SOQ,TOQ,UOQ, AKK,AK,AANSWO,AANSWT
        DOUBLE PRECISION RONE,SONE,DAAQ,DAQ,CAQ,CAAQ,ETA

C       THE FOLLOWING ARE THE PROPERTIES OF FUELS AND CAN BE
C       VARIED FOR DIFFERENT CONDITIONS

        C=3
        H=8
        N=0
        S=0
        O=0
        HC=46357
        CC=0.410822E04
        CP=1.175
        TINF=300
        YFI=1
        YOINF=0.23
        SC=1
        MSTAR=1
        JSTAR=1
        VI=0.2
        DI=0.002
        AKINVISC=0.1E-04
        VLAM=0.35E0
        ALAMBDA=0.763E-06
```

```
      TI=300
      AMOLESO=(0.5)*((2*C)+(0.5*H)+(2*S)-(O))

      AMOLFUEL=(12.01*C)+(1.01*H)+(16*O)+(14.01*N)+(32*S)
      ANUO=(32*AMOLESO)/AMOLFUEL
      ANUCOTWO=(44.01*C)/AMOLFUEL
      ANUHTWOO=(9.01*H)/AMOLFUEL
      VFLSTAR=VLAM/VI
      BFOINJ=YFI
      S=YOINF/(ANUO*YFI)
      BFOINF=(-1)*S
      BHTFINJ=1+(CP*(TI-TINF))/HC
      BHTFINF=(CP*(TI-TINF))/HC
      RHOD=ALAMBDA/CP
      PHIFST=(S)/(1+S)
      REYN=(DI*VI)/AKINVISC
C     REYN=40
      FLAMEHT=((2*SC+1)*REYN)/(32*PHIFST)
      ANSS=0
      CONE=(2*SC+1)/32
      ANSSP=0


      XSTAR=10
      CTWO=(1.732*MSTAR**0.5)*REYN/XSTAR
      VXMAX=(CONE*REYN*MSTAR)/(XSTAR)
      PHIMAX=(CONE*REYN*JSTAR)/(XSTAR)

C     ITERATING THE VALUES OF ZI

      ZITH=0
      RSTAR=ZITH/CTWO
      VBMAX=1/((1+(0.25*ZITH**2))**2)
      PHIBMAX=1/((1+(0.25*ZITH**2))**(2*SC))
      VXSTAR=VBMAX*VXMAX
      PHI=PHIBMAX*PHIMAX
      F=PHI*YFI
      BTFO=PHI*(BFOINJ-BFOINF)+BFOINF
      BHTF=PHI*(BHTFINJ-BHTFINF)+BHTFINF
      IF(BTFO)36,36,37
36    YF=0
      YOTWO=(-1)*BTFO*ANUO
      GOTO 38
37    YF=BTFO
```

```
      YOTWO=0
      GOTO 38
38    T=((BHTF-YF)*HC/CP)+TINF
      YHTWOO=(1.63409)*(PHI-YF)
      XH=(YHTWOO*AMOLFUEL)/18.02
      ALOGKK=3.0165-(13078.5/T)
      AK=10**ALOGKK
      YCOTWO=ANUCOTWO*((PHI*0.99954)+0.00046-YF)
      XCO=(YCOTWO*AMOLFUEL)/44.01
      ALOGK=4.327-(14436/T)
      AKK=10**ALOGK
      CC=AK/AKK
C     THE QUARTIC EQUATIONS CONSTANTS ARE SOLVED
      BQ=(XCO+(CC*XH)+(2*CC*(AK)**2-(2*AK)**2))/(1-CC)
      CAAQ=(4*XH*(AK)**2)-(4*CC*(AK)**2*(XH)**2)
      CAQ=(CAAQ)-(2*CC*(AK)**2*(XH))
      CQ=(CAQ)/(1-CC)
      DAAQ=(4*CC*(XH)**2*(AK)**2)+(2*CC*(AK)**2*(XH)**2)
      DAQ=DAAQ-(2*(AK)**2*(XH)**2)
      DQ=DAQ/(1-CC)
      EQ=(2*CC*(AK)**2*(XH)**3)/(CC-1)
      FQ=CQ-(3*(BQ)**2)/8
      GQ=DQ+((BQ)**3/8)-(BQ*CQ/2)
      HQ=EQ-(3*(BQ)**4/256)+((BQ)**2*CQ/16)-(BQ*DQ/4)
C     CONVERTING QUARTIC EQUATION INTO A CUBIC EQUATION
      BOQ=FQ/2
      COQ=((FQ)**2-4*HQ)/16
      DOQ=(-1)*(GQ)**2/64
      FOQ=(3*COQ-(BOQ)**2)/3
      GOQ=((2*(BOQ)**3)-(9*BOQ*COQ)+(27*DOQ))/27
      HOQ=((GOQ)**2/4)+((FOQ)**3)/27
      IF(HOQ)39,40,40
39    ROQ=0
      TOQ=0
      SOQ=0
      UOQ=0
      GOTO 47
40    ROQ=((-1)*GOQ/2)+(HOQ)**0.5
      TOQ=((-1)*GOQ/2)-(HOQ)**0.5
      IF(ROQ)42,43,43
42    SOQ=((-1)*ROQ)**(0.333)
      GOTO 44
43    SOQ=ROQ**(0.333)
44    TOQ=((-0.5)*GOQ)-(HOQ**0.5)
```

```
      IF(TOQ)45,46,46
45    UOQ=((-1)*TOQ)**(0.333)
      GOTO 47
46    UOQ=TOQ**(0.333)

      RRO=(SOQ+UOQ)-(BOQ/3)
      RCO=(-1)*(SOQ+UOQ)-(BOQ/3)
      RCOI=(SOQ-UOQ)*0.86607
      GOTO 48
47    RRO=(SOQ-UOQ)-(BOQ/3)
      RCO=(-1)*(SOQ-UOQ)-(BOQ/3)
      RCOI=(SOQ+UOQ)*0.86607

48    RCT=(-1)*(RCO)
      RCTI=(-1)*RCOI
      SQOR=((RCO)**2+(RCOI)**2)**(0.5)
      SSQOR=(SQOR-RCO)
      IF(SSQOR)49,49,50
50    SQCO=((SQOR-RCO)/2)**0.5
      IF(SQCO)49,49,51
49    SQORO=0
      GOTO 52
51    SQORO=RCOI/(2*SQCO)
52    RONE=(-1)*(GQ)/(8*SQOR)
      SONE=BQ/4
      AANSWO=(2*SQORO)+(RONE-SONE)
      AANSWT=(AANSWO*XCO)/(AANSWO-(AANSWO*CC)+(CC*XH))
      AXOTWO=(AANSWO+AANSWT)/2
      IF(FOQ)53,53,54
53    AYOTWO=0
      GOTO 55
54    AYOTWO=AXOTWO*0.6955
      IF(AYOTWO)55,55,56
55    AAYOTWO=0
      GOTO 57
56    AAYOTWO=AYOTWO
57    IF(YOTWO)58,58,59
58    YOTWO=AAYOTWO
59    YOTWO=0+YOTWO
      YNTWO=(PHI*(-0.77))+0.77
      ETA=(8*ZITH)/(1.732*(MSTAR**0.5)*REYN)
      RH=(100*46.01)/(8.314*T)
      EQUV=EXP(-69000/T)
      DNODTO=(1892700*EQUV*YNTWO*(YOTWO**0.5))/(T**0.5)
```

```
      DNODT=(7220*DNODTO*(RH**1.5)*5.39361)
      EDNODTC=DNODT*ETA
      EQUVP=EXP(-30000/T)
      DNODTP=(CC*YNTWO*(YOTWO**0.5)*YF*(RH)*EQUVP)
      EDNODTP=DNODTP*ETA

      ANS=0
      ZI=0.0
      ZIT=-0.05
      FFA=0
      FFB=0
      FFQ=0
      FFR=0
60    ZI=ZI+0.1
      RSTAR=ZI/CTWO
      VBMAX=1/((1+(0.25*ZI**2))**2)
      PHIBMAX=1/((1+(0.25*ZI**2))**(2*SC))
      VXSTAR=VBMAX*VXMAX
      PHI=PHIBMAX*PHIMAX
      F=PHI*YFI
      BTFO=PHI*(BFOINJ-BFOINF)+BFOINF
      BHTF=PHI*(BHTFINJ-BHTFINF)+BHTFINF
      IF(BTFO)61,61,65
61    YF=0
      YOTWO=(-1)*BTFO*ANUO
      GOTO 66
65    YF=BTFO
      YOTWO=0
      GOTO 66
66    T=((BHTF-YF)*HC/CP)+TINF
      YHTWOO=(1.63409)*(PHI-YF)
      XH=(YHTWOO*AMOLFUEL)/18.02
      ALOGKK=3.0165-(13078.5/T)
      AK=10**ALOGKK
      YCOTWO=ANUCOTWO*((PHI*0.99954)+0.00046-YF)
      XCO=(YCOTWO*AMOLFUEL)/44.01
      ALOGK=4.327-(14436/T)
      AKK=10**ALOGK
      CC=AK/AKK
C     NOW THE QUARTIC EQUATIONS CONSTANTS ARE SOLVED
      BQ=(XCO+(CC*XH)+(2*CC*(AK)**2-(2*AK)**2))/(1-CC)
      CAAQ=(4*XH*(AK)**2)-(4*CC*(AK)**2*(XH)**2)
      CAQ=(CAAQ)-(2*CC*(AK)**2*(XH))
      CQ=(CAQ)/(1-CC)
```

```
      DAAQ=(4*CC*(XH)**2*(AK)**2)+(2*CC*(AK)**2*(XH)**2)
      DAQ=DAAQ-(2*(AK)**2*(XH)**2)
      DQ=DAQ/(1-CC)
      EQ=(2*CC*(AK)**2*(XH)**3)/(CC-1)
      FQ=CQ-(3*(BQ)**2)/8
      GQ=DQ+((BQ)**3/8)-(BQ*CQ/2)
      HQ=EQ-(3*(BQ)**4/256)+((BQ)**2*CQ/16)-(BQ*DQ/4)
C     CONVERTING QUARTIC EQUATION INTO A CUBIC EQUATION
      BOQ=FQ/2
      COQ=((FQ)**2-4*HQ)/16
      DOQ=(-1)*(GQ)**2/64
      FOQ=(3*COQ-(BOQ)**2)/3
      GOQ=((2*(BOQ)**3)-(9*BOQ*COQ)+(27*DOQ))/27
      HOQ=((GOQ)**2/4)+((FOQ)**3)/27
      IF(HOQ)67,68,68
67    ROQ=0
      TOQ=0
      SOQ=0
      UOQ=0
      GOTO 75
68    ROQ=((-1)*GOQ/2)+(HOQ)**0.5
      TOQ=((-1)*GOQ/2)-(HOQ)**0.5
      IF(ROQ)70,71,71
70    SOQ=((-1)*ROQ)**(0.333)
      GOTO 72
71    SOQ=ROQ**(0.333)
72    TOQ=((-0.5)*GOQ)-(HOQ**0.5)
      IF(TOQ)73,74,74
73    UOQ=((-1)*TOQ)**(0.333)
      GOTO 75
74    UOQ=TOQ**(0.333)

      RRO=(SOQ+UOQ)-(BOQ/3)
      RCO=(-1)*(SOQ+UOQ)-(BOQ/3)
      RCOI=(SOQ-UOQ)*0.86607
      GOTO 76
75    RRO=(SOQ-UOQ)-(BOQ/3)
      RCO=(-1)*(SOQ-UOQ)-(BOQ/3)
      RCOI=(SOQ+UOQ)*0.86607

76    RCT=(-1)*(RCO)
      RCTI=(-1)*RCOI
      SQOR=((RCO)**2+(RCOI)**2)**(0.5)
      SSQOR=(SQOR-RCO)
```

```
      IF(SSQOR)77,77,78
78    SQCO=((SQOR-RCO)/2)**0.5
      IF(SQCO)77,77,79
77    SQORO=0
      GOTO 80
79    SQORO=RCOI/(2*SQCO)
80    RONE=(-1)*(GQ)/(8*SQOR)
      SONE=BQ/4
      AANSWO=(2*SQORO)+(RONE-SONE)
      AANSWT=(AANSWO*XCO)/(AANSWO-(AANSWO*CC)+(CC*XH))
      AXOTWO=(AANSWO+AANSWT)/2
      IF(FOQ)81,81,82
81    AYOTWO=0
      GOTO 83
82    AYOTWO=AXOTWO*0.6955
      IF(AYOTWO)84,84,85
83    AAYOTWO=0
      GOTO 85
84    AAYOTWO=AYOTWO
85    IF(YOTWO)86,86,87
86    YOTWO=AAYOTWO
87    YOTWO=0+YOTWO
      YNTWO=(PHI*(-0.77))+0.77
      ETA=(8*ZI)/(1.732*(MSTAR**0.5)*REYN)
      RH=(100*46.01)/(8.314*T)
      EQUV=EXP(-69000/T)
      DNODTO=(1892700*EQUV*YNTWO*(YOTWO**0.5))/(T**0.5)
      DNODT=(7220*DNODTO*(RH**1.5)*5.39361)
      EDNODTA=DNODT*ETA
C     WRITE(*,*)EDNODTA
      EQUVP=EXP(-30000/T)
      DNODTP=(CC*YNTWO*(YOTWO**0.5)*YF*(RH)*EQUVP)
      EDNODTP=DNODTP*ETA
      FFQ=FFQ+EDNODTP
      FFA=FFA+EDNODTA
      IF(ZI-20)60,60,88

88    ZIT=ZIT+0.1
      RSTAR=ZIT/CTWO
      VBMAX=1/((1+(0.25*ZIT**2))**2)
      PHIBMAX=1/((1+(0.25*ZIT**2))**(2*SC))
      VXSTAR=VBMAX*VXMAX
      PHI=PHIBMAX*PHIMAX
      F=PHI*YFI
```

```
      BTFO=PHI*(BFOINJ-BFOINF)+BFOINF
      BHTF=PHI*(BHTFINJ-BHTFINF)+BHTFINF
      IF(BTFO)89,89,90
89    YF=0
      YOTWO=(-1)*BTFO*ANUO
      GOTO 91
90    YF=BTFO
      YOTWO=0
      GOTO 91
91    T=((BHTF-YF)*HC/CP)+TINF
      YHTWOO=(1.63409)*(PHI-YF)
      XH=(YHTWOO*AMOLFUEL)/18.02
      ALOGKK=3.0165-(13078.5/T)
      AK=10**ALOGKK
      YCOTWO=ANUCOTWO*((PHI*0.99954)+0.00046-YF)
      XCO=(YCOTWO*AMOLFUEL)/44.01
      ALOGK=4.327-(14436/T)
      AKK=10**ALOGK
      CC=AK/AKK
C     NOW THE QUARTIC EQUATIONS CONSTANTS ARE SOLVED
      BQ=(XCO+(CC*XH)+(2*CC*(AK)**2-(2*AK)**2))/(1-CC)
      CAAQ=(4*XH*(AK)**2)-(4*CC*(AK)**2*(XH)**2)
      CAQ=(CAAQ)-(2*CC*(AK)**2*(XH))
      CQ=(CAQ)/(1-CC)
      DAAQ=(4*CC*(XH)**2*(AK)**2)+(2*CC*(AK)**2*(XH)**2)
      DAQ=DAAQ-(2*(AK)**2*(XH)**2)
      DQ=DAQ/(1-CC)
      EQ=(2*CC*(AK)**2*(XH)**3)/(CC-1)
      FQ=CQ-(3*(BQ)**2)/8
      GQ=DQ+((BQ)**3/8)-(BQ*CQ/2)
      HQ=EQ-(3*(BQ)**4/256)+((BQ)**2*CQ/16)-(BQ*DQ/4)
C     CONVERTING QUARTIC EQUATION INTO A CUBIC EQUATION
      BOQ=FQ/2
      COQ=((FQ)**2-4*HQ)/16
      DOQ=(-1)*(GQ)**2/64
      FOQ=(3*COQ-(BOQ)**2)/3
      GOQ=((2*(BOQ)**3)-(9*BOQ*COQ)+(27*DOQ))/27
      HOQ=((GOQ)**2/4)+((FOQ)**3)/27
      IF(HOQ)92,93,93
92    ROQ=0
      TOQ=0
      SOQ=0
      UOQ=0
      GOTO 99
```

```
93      ROQ=((-1)*GOQ/2)+(HOQ)**0.5
        TOQ=((-1)*GOQ/2)-(HOQ)**0.5
        IF(ROQ)94,95,95
94      SOQ=((-1)*ROQ)**(0.333)
        GOTO 96
95      SOQ=ROQ**(0.333)
96      TOQ=((-0.5)*GOQ)-(HOQ**0.5)
        IF(TOQ)97,98,98
97      UOQ=((-1)*TOQ)**(0.333)
        GOTO 99
98      UOQ=TOQ**(0.333)

        RRO=(SOQ+UOQ)-(BOQ/3)
        RCO=(-1)*(SOQ+UOQ)-(BOQ/3)
        RCOI=(SOQ-UOQ)*0.86607
        GOTO 100
99      RRO=(SOQ-UOQ)-(BOQ/3)
        RCO=(-1)*(SOQ-UOQ)-(BOQ/3)
        RCOI=(SOQ+UOQ)*0.86607

100     RCT=(-1)*(RCO)
        RCTI=(-1)*RCOI
        SQOR=((RCO)**2+(RCOI)**2)**(0.5)
        SSQOR=(SQOR-RCO)
        IF(SSQOR)101,101,102
102     SQCO=((SQOR-RCO)/2)**0.5
        IF(SQCO)101,101,103
101     SQORO=0
        GOTO 104
103     SQORO=RCOI/(2*SQCO)
104     RONE=(-1)*(GQ)/(8*SQOR)
        SONE=BQ/4
        AANSWO=(2*SQORO)+(RONE-SONE)
        AANSWT=(AANSWO*XCO)/(AANSWO-(AANSWO*CC)+(CC*XH))
        AXOTWO=(AANSWO+AANSWT)/2
        IF(FOQ)105,105,106
105     AYOTWO=0
        GOTO 107
106     AYOTWO=AXOTWO*0.6955
        IF(AYOTWO)107,107,108
107     AAYOTWO=0
        GOTO 109
108     AAYOTWO=AYOTWO
109     IF(YOTWO)110,110,111
```

```
110     YOTWO=AAYOTWO
111     YOTWO=0+YOTWO
C       WRITE(*,*)YOTWO
        YNTWO=(PHI*(-0.77))+0.77
        ETA=(8*ZIT)/(1.732*(MSTAR**0.5)*REYN)
        RH=(100*46.01)/(8.314*T)
        EQUV=EXP(-69000/T)
        DNODTO=(1892700*EQUV*YNTWO*(YOTWO**0.5))/(T**0.5)
        DNODT=(7220*DNODTO*(RH**1.5)*5.39361)
        EDNODTB=DNODT*ETA
        FFB=FFB+EDNODTB
        EQUVP=EXP(-30000/T)
        DNODTP=(CC*YNTWO*(YOTWO**0.5)*YF*(RH)*EQUVP)
        EDNODTP=DNODTP*ETA
        FFR=FFR+EDNODTP

        IF(ZIT-20)88,88,112
C       USING THE TRAPEZOIDAL RULE FOR INTEGRATION
112     FIIN=(4*FFA)+(2*FFB)
        ANS=FIIN

        ANSO=ANS+EDNODTC
        VANSO=(0.005773)*(ANSO)/3
        WRITE (*,*) XSTAR,VANSO
        FIINP=((2*FFQ)+(4*FFR))*1.251
        ANSP=FIINP
C       WRITE(*,*)FIIN
        ANSOP=ANSP+EDNODTP
        VANSOP=(0.005773503)*(ANSOP)/3
        WRITE (*,*) XSTAR,VANSOP
        ZONP=((XSTAR*0.002)**2)*VANSOP*6.282
        ZON=((XSTAR*0.002)**2)*VANSO*6.282

C       ITERATING THE VALUES OF AXIAL POINTS OR X*

        GGA=0
        GGQ=0
        XSTARR=9
235     XSTARR=XSTARR+2
        CTWO=(1.732*MSTAR**0.5)*REYN/XSTARR
        VXMAX=(CONE*REYN*MSTAR)/(XSTARR)
        PHIMAX=(CONE*REYN*JSTAR)/(XSTARR)

        ZITH=0
```

```
      RSTAR=ZITH/CTWO
      VBMAX=1/((1+(0.25*ZITH**2))**2)
      PHIBMAX=1/((1+(0.25*ZITH**2))**(2*SC))
      VXSTAR=VBMAX*VXMAX
      PHI=PHIBMAX*PHIMAX
      F=PHI*YFI
      BTFO=PHI*(BFOINJ-BFOINF)+BFOINF
      BHTF=PHI*(BHTFINJ-BHTFINF)+BHTFINF
      IF(BTFO)236,236,237
236   YF=0
      YOTWO=(-1)*BTFO*ANUO
      GOTO 238
237   YF=BTFO
      YOTWO=0
      GOTO 238
238   T=((BHTF-YF)*HC/CP)+TINF
      YHTWOO=(1.63409)*(PHI-YF)
      XH=(YHTWOO*AMOLFUEL)/18.02
      ALOGKK=3.0165-(13078.5/T)
      AK=10**ALOGKK
      YCOTWO=ANUCOTWO*((PHI*0.99954)+0.00046-YF)
      XCO=(YCOTWO*AMOLFUEL)/44.01
      ALOGK=4.327-(14436/T)
      AKK=10**ALOGK
      CC=AK/AKK
C     NOW THE QUARTIC EQUATIONS CONSTANTS ARE SOLVED
      BQ=(XCO+(CC*XH)+(2*CC*(AK)**2-(2*AK)**2))/(1-CC)
      CAAQ=(4*XH*(AK)**2)-(4*CC*(AK)**2*(XH)**2)
      CAQ=(CAAQ)-(2*CC*(AK)**2*(XH))
      CQ=(CAQ)/(1-CC)
      DAAQ=(4*CC*(XH)**2*(AK)**2)+(2*CC*(AK)**2*(XH)**2)
      DAQ=DAAQ-(2*(AK)**2*(XH)**2)
      DQ=DAQ/(1-CC)
      EQ=(2*CC*(AK)**2*(XH)**3)/(CC-1)
      FQ=CQ-(3*(BQ)**2)/8
      GQ=DQ+((BQ)**3/8)-(BQ*CQ/2)
      HQ=EQ-(3*(BQ)**4/256)+((BQ)**2*CQ/16)-(BQ*DQ/4)
C     CONVERTING QUARTIC EQUATION INTO A CUBIC EQUATION
      BOQ=FQ/2
      COQ=((FQ)**2-4*HQ)/16
      DOQ=(-1)*(GQ)**2/64
      FOQ=(3*COQ-(BOQ)**2)/3
      GOQ=((2*(BOQ)**3)-(9*BOQ*COQ)+(27*DOQ))/27
      HOQ=((GOQ)**2/4)+((FOQ)**3)/27
```

```
      IF(HOQ)239,240,240
239   ROQ=0
      TOQ=0
      SOQ=0
      UOQ=0
      GOTO 247
240   ROQ=((-1)*GOQ/2)+(HOQ)**0.5
      TOQ=((-1)*GOQ/2)-(HOQ)**0.5
      IF(ROQ)242,243,243
242   SOQ=((-1)*ROQ)**(0.333)
      GOTO 244
243   SOQ=ROQ**(0.333)
244   TOQ=((-0.5)*GOQ)-(HOQ**0.5)
      IF(TOQ)245,246,246
245   UOQ=((-1)*TOQ)**(0.333)
      GOTO 247
246   UOQ=TOQ**(0.333)

      RRO=(SOQ+UOQ)-(BOQ/3)
      RCO=(-1)*(SOQ+UOQ)-(BOQ/3)
      RCOI=(SOQ-UOQ)*0.86607
      GOTO 248
247   RRO=(SOQ-UOQ)-(BOQ/3)
      RCO=(-1)*(SOQ-UOQ)-(BOQ/3)
      RCOI=(SOQ+UOQ)*0.86607

248   RCT=(-1)*(RCO)
      RCTI=(-1)*RCOI
      SQOR=((RCO)**2+(RCOI)**2)**(0.5)
      SSQOR=(SQOR-RCO)
      IF(SSQOR)249,249,250
250   SQCO=((SQOR-RCO)/2)**0.5
      IF(SQCO)249,249,251
249   SQORO=0
      GOTO 252
251   SQORO=RCOI/(2*SQCO)
252   RONE=(-1)*(GQ)/(8*SQOR)
      SONE=BQ/4
      AANSWO=(2*SQORO)+(RONE-SONE)
      AANSWT=(AANSWO*XCO)/(AANSWO-(AANSWO*CC)+(CC*XH))
      AXOTWO=(AANSWO+AANSWT)/2
      IF(FOQ)253,253,254
253   AYOTWO=0
      GOTO 255
```

```
254     AYOTWO=AXOTWO*0.6955
        IF(AYOTWO)255,255,256
255     AAYOTWO=0
        GOTO 257
256     AAYOTWO=AYOTWO
257     IF(YOTWO)258,258,259
258     YOTWO=AAYOTWO
259     YOTWO=0+YOTWO
C       WRITE(*,*)YOTWO
        YNTWO=(PHI*(-0.77))+0.77
        ETA=(8*ZITH)/(1.732*(MSTAR**0.5)*REYN)
        RH=(100*46.01)/(8.314*T)
        EQUV=EXP(-69000/T)
        DNODTO=(1892700*EQUV*YNTWO*(YOTWO**0.5))/(T**0.5)
        DNODT=(7220*DNODTO*(RH**1.5)*5.39361)
        EDNODTC=DNODT*ETA
        EQUVP=EXP(-30000/T)
        DNODTP=(CC*YNTWO*(YOTWO**0.5)*YF*(RH)*EQUVP)
        EDNODTP=DNODTP*ETA

        ANS=0
        ZI=0.0
        ZIT=-0.05
        FFC=0
        FFD=0
        FFS=0
        FFT=0
260     ZI=ZI+0.1
        RSTAR=ZI/CTWO
        VBMAX=1/((1+(0.25*ZI**2))**2)
        PHIBMAX=1/((1+(0.25*ZI**2))**(2*SC))
        VXSTAR=VBMAX*VXMAX
        PHI=PHIBMAX*PHIMAX
        F=PHI*YFI
        BTFO=PHI*(BFOINJ-BFOINF)+BFOINF
        BHTF=PHI*(BHTFINJ-BHTFINF)+BHTFINF
        IF(BTFO)261,261,262
261     YF=0
        YOTWO=(-1)*BTFO*ANUO
        GOTO 263
262     YF=BTFO
        YOTWO=0
        GOTO 263
263     T=((BHTF-YF)*HC/CP)+TINF
```

```
      YHTWOO=(1.63409)*(PHI-YF)
      XH=(YHTWOO*AMOLFUEL)/18.02
      ALOGKK=3.0165-(13078.5/T)
      AK=10**ALOGKK
      YCOTWO=ANUCOTWO*((PHI*0.99954)+0.00046-YF)
      XCO=(YCOTWO*AMOLFUEL)/44.01
      ALOGK=4.327-(14436/T)
      AKK=10**ALOGK
      CC=AK/AKK
C     NOW THE QUARTIC EQUATIONS CONSTANTS ARE SOLVED
      BQ=(XCO+(CC*XH)+(2*CC*(AK)**2-(2*AK)**2))/(1-CC)
      CAAQ=(4*XH*(AK)**2)-(4*CC*(AK)**2*(XH)**2)
      CAQ=(CAAQ)-(2*CC*(AK)**2*(XH))
      CQ=(CAQ)/(1-CC)
      DAAQ=(4*CC*(XH)**2*(AK)**2)+(2*CC*(AK)**2*(XH)**2)
      DAQ=DAAQ-(2*(AK)**2*(XH)**2)
      DQ=DAQ/(1-CC)
      EQ=(2*CC*(AK)**2*(XH)**3)/(CC-1)
      FQ=CQ-(3*(BQ)**2)/8
      GQ=DQ+((BQ)**3/8)-(BQ*CQ/2)
      HQ=EQ-(3*(BQ)**4/256)+((BQ)**2*CQ/16)-(BQ*DQ/4)
C     CONVERTING QUARTIC EQUATION INTO A CUBIC EQUATION
      BOQ=FQ/2
      COQ=((FQ)**2-4*HQ)/16
      DOQ=(-1)*(GQ)**2/64
      FOQ=(3*COQ-(BOQ)**2)/3
      GOQ=((2*(BOQ)**3)-(9*BOQ*COQ)+(27*DOQ))/27
      HOQ=((GOQ)**2/4)+((FOQ)**3)/27
      IF(HOQ)267,268,268
267   ROQ=0
      TOQ=0
      SOQ=0
      UOQ=0
      GOTO 275
268   ROQ=((-1)*GOQ/2)+(HOQ)**0.5
      TOQ=((-1)*GOQ/2)-(HOQ)**0.5
      IF(ROQ)270,271,271
270   SOQ=((-1)*ROQ)**(0.333)
      GOTO 272
271   SOQ=ROQ**(0.333)
272   TOQ=((-0.5)*GOQ)-(HOQ**0.5)
      IF(TOQ)273,274,274
273   UOQ=((-1)*TOQ)**(0.333)
      GOTO 275
```

```
274     UOQ=TOQ**(0.333)

        RRO=(SOQ+UOQ)-(BOQ/3)
        RCO=(-1)*(SOQ+UOQ)-(BOQ/3)
        RCOI=(SOQ-UOQ)*0.86607
        GOTO 276
275     RRO=(SOQ-UOQ)-(BOQ/3)
        RCO=(-1)*(SOQ-UOQ)-(BOQ/3)
        RCOI=(SOQ+UOQ)*0.86607

276     RCT=(-1)*(RCO)
        RCTI=(-1)*RCOI
        SQOR=((RCO)**2+(RCOI)**2)**(0.5)
        SSQOR=(SQOR-RCO)
        IF(SSQOR)277,277,278
278     SQCO=((SQOR-RCO)/2)**0.5
        IF(SQCO)277,277,279
277     SQORO=0
        GOTO 280
279     SQORO=RCOI/(2*SQCO)
280     RONE=(-1)*(GQ)/(8*SQOR)
        SONE=BQ/4
        AANSWO=(2*SQORO)+(RONE-SONE)
        AANSWT=(AANSWO*XCO)/(AANSWO-(AANSWO*CC)+(CC*XH))
        AXOTWO=(AANSWO+AANSWT)/2
        IF(FOQ)281,281,282
281     AYOTWO=0
        GOTO 283
282     AYOTWO=AXOTWO*0.6955
        IF(AYOTWO)284,284,285
283     AAYOTWO=0
        GOTO 285
284     AAYOTWO=AYOTWO
285     IF(YOTWO)286,286,287
286     YOTWO=AAYOTWO
287     YOTWO=0+YOTWO
C       WRITE(*,*)YOTWO
        YNTWO=(PHI*(-0.77))+0.77
        ETA=(8*ZI)/(1.732*(MSTAR**0.5)*REYN)
        RH=(100*46.01)/(8.314*T)
        EQUV=EXP(-69000/T)
        DNODTO=(1892700*EQUV*YNTWO*(YOTWO**0.5))/(T**0.5)
        DNODT=(7220*DNODTO*(RH**1.5)*5.39361)
        EDNODTA=DNODT*ETA
```

```
      EQUVP=EXP(-30000/T)
      DNODTP=(CC*YNTWO*(YOTWO**0.5)*YF*(RH)*EQUVP)
      EDNODTP=DNODTP*ETA
      FFQ=FFQ+EDNODTP
      FFC=FFC+EDNODTA
      IF(ZI-20)260,260,288

288   ZIT=ZIT+0.1
      RSTAR=ZIT/CTWO
      VBMAX=1/((1+(0.25*ZIT**2))**2)
      PHIBMAX=1/((1+(0.25*ZIT**2))**(2*SC))
      VXSTAR=VBMAX*VXMAX
      PHI=PHIBMAX*PHIMAX
      F=PHI*YFI
      BTFO=PHI*(BFOINJ-BFOINF)+BFOINF
      BHTF=PHI*(BHTFINJ-BHTFINF)+BHTFINF
      IF(BTFO)289,289,290
289   YF=0
      YOTWO=(-1)*BTFO*ANUO
      GOTO 291
290   YF=BTFO
      YOTWO=0
      GOTO 291
291   T=((BHTF-YF)*HC/CP)+TINF
C     WRITE(*,*)T
C      THESE STATEMENTS ARE JUST TO CHECK VALUES IN BETWEEN
C     SOLUTIONS IN THE PROGRAM
C     REMOVING THE "C" IN BETWEEN WILL LEAD TO PRINT THESE
C     VALUES FOR CHECKS IN BETWEEN
      YHTWOO=(1.63409)*(PHI-YF)
      XH=(YHTWOO*AMOLFUEL)/18.02
      ALOGKK=3.0165-(13078.5/T)
      AK=10**ALOGKK
      YCOTWO=ANUCOTWO*((PHI*0.99954)+0.00046-YF)
      XCO=(YCOTWO*AMOLFUEL)/44.01
      ALOGK=4.327-(14436/T)
      AKK=10**ALOGK
      CC=AK/AKK
C     NOW THE QUARTIC EQUATIONS CONSTANTS ARE SOLVED
      BQ=(XCO+(CC*XH)+(2*CC*(AK)**2-(2*AK)**2))/(1-CC)
      CAAQ=(4*XH*(AK)**2)-(4*CC*(AK)**2*(XH)**2)
      CAQ=(CAAQ)-(2*CC*(AK)**2*(XH))
      CQ=(CAQ)/(1-CC)
      DAAQ=(4*CC*(XH)**2*(AK)**2)+(2*CC*(AK)**2*(XH)**2)
```

```
      DAQ=DAAQ-(2*(AK)**2*(XH)**2)
      DQ=DAQ/(1-CC)
      EQ=(2*CC*(AK)**2*(XH)**3)/(CC-1)
      FQ=CQ-(3*(BQ)**2)/8
      GQ=DQ+((BQ)**3/8)-(BQ*CQ/2)
      HQ=EQ-(3*(BQ)**4/256)+((BQ)**2*CQ/16)-(BQ*DQ/4)
C     CONVERTING QUARTIC EQUATION INTO A CUBIC EQUATION
      BOQ=FQ/2
      COQ=((FQ)**2-4*HQ)/16
      DOQ=(-1)*(GQ)**2/64
      FOQ=(3*COQ-(BOQ)**2)/3
      GOQ=((2*(BOQ)**3)-(9*BOQ*COQ)+(27*DOQ))/27
      HOQ=((GOQ)**2/4)+((FOQ)**3)/27
      IF(HOQ)292,293,293
292   ROQ=0
      TOQ=0
      SOQ=0
      UOQ=0
      GOTO 299
293   ROQ=((-1)*GOQ/2)+(HOQ)**0.5
      TOQ=((-1)*GOQ/2)-(HOQ)**0.5
      IF(ROQ)294,295,295
294   SOQ=((-1)*ROQ)**(0.333)
      GOTO 296
295   SOQ=ROQ**(0.333)
296   TOQ=((-0.5)*GOQ)-(HOQ**0.5)
      IF(TOQ)297,298,298
297   UOQ=((-1)*TOQ)**(0.333)
      GOTO 299
298   UOQ=TOQ**(0.333)

      RRO=(SOQ+UOQ)-(BOQ/3)
      RCO=(-1)*(SOQ+UOQ)-(BOQ/3)
      RCOI=(SOQ-UOQ)*0.86607
      GOTO 300
299   RRO=(SOQ-UOQ)-(BOQ/3)
      RCO=(-1)*(SOQ-UOQ)-(BOQ/3)
      RCOI=(SOQ+UOQ)*0.86607

300   RCT=(-1)*(RCO)
      RCTI=(-1)*RCOI
      SQOR=((RCO)**2+(RCOI)**2)**(0.5)
      SSQOR=(SQOR-RCO)
      IF(SQCO)301,301,303
```

```
301     SQORO=0
        GOTO 304
303     SQORO=RCOI/(2*SQCO)
304     RONE=(-1)*(GQ)/(8*SQOR)
        SONE=BQ/4
        AANSWO=(2*SQORO)+(RONE-SONE)
        AANSWT=(AANSWO*XCO)/(AANSWO-(AANSWO*CC)+(CC*XH))
        AXOTWO=(AANSWO+AANSWT)/2
        IF(FOQ)305,305,306
305     AYOTWO=0
        GOTO 307
306     AYOTWO=AXOTWO*0.6955
        IF(AYOTWO)307,307,308
307     AAYOTWO=0
        GOTO 309
308     AAYOTWO=AYOTWO
309     IF(YOTWO)310,310,311
310     YOTWO=AAYOTWO
311     YOTWO=0+YOTWO
C       WRITE(*,*)YOTWO
        YNTWO=(PHI*(-0.77))+0.77
        ETA=(8*ZIT)/(1.732*(MSTAR**0.5)*REYN)
        RH=(100*46.01)/(8.314*T)
        EQUV=EXP(-69000/T)
C       WRITE(*,*)EQUV
        DNODTO=(1892700*EQUV*YNTWO*(YOTWO**0.5))/(T**0.5)
        DNODT=(7220*DNODTO*(RH**1.5)*5.39361)
        EDNODTB=DNODT*ETA
C       WRITE(*,*)EDNODTB
        FFD=FFD+EDNODTB
        IF(ZIT-20)288,288,312
C       USING THE TRAPEZOIDAL RULE FOR INTEGRATION
312     FIIN=(4*FFC)+(2*FFD)
        ANS=FIIN

        ANSO=ANS+EDNODTC
        VANSO=(0.005773/3)*(ANSO)
        WRITE (*,*) XSTARR,VANSO
        FIINP=((2*FFQ)+(4*FFR))*1.251
        ANSP=FIINP
C       WRITE(*,*)FIIN
        ANSOP=ANSP+EDNODTP
        VANSOP=(0.005773503)*(ANSOP)/3
        WRITE (*,*) XSTAR,VANSOP
```

```
      ZONPO=((XSTAR*0.002)**2)*VANSOP*6.282
      ZONO=((XSTARR*0.002)**2)*VANSO*6.282
C     WRITE(*,*)ZONO
      GGA=GGA+ZONO
      GGQ=GGQ+ZONPO
      IF (XSTARR-99)235,331,331

331   GGB=0
      GGR=0
      XSTARRR=10
332   XSTARRR=XSTARRR+2
      CTWO=(1.732*MSTAR**0.5)*REYN/XSTARRR
      VXMAX=(CONE*REYN*MSTAR)/(XSTARRR)
      PHIMAX=(CONE*REYN*JSTAR)/(XSTARRR)

      ZITH=0
      RSTAR=ZITH/CTWO
      VBMAX=1/((1+(0.25*ZITH**2))**2)
      PHIBMAX=1/((1+(0.25*ZITH**2))**(2*SC))
      VXSTAR=VBMAX*VXMAX
      PHI=PHIBMAX*PHIMAX
      F=PHI*YFI
      BTFO=PHI*(BFOINJ-BFOINF)+BFOINF
      BHTF=PHI*(BHTFINJ-BHTFINF)+BHTFINF
      IF(BTFO)333,333,334
333   YF=0
      YOTWO=(-1)*BTFO*ANUO
      GOTO 335
334   YF=BTFO
      YOTWO=0
      GOTO 335
335   T=((BHTF-YF)*HC/CP)+TINF
      YHTWOO=(1.63409)*(PHI-YF)
      XH=(YHTWOO*AMOLFUEL)/18.02
      ALOGKK=3.0165-(13078.5/T)
      AK=10**ALOGKK
      YCOTWO=ANUCOTWO*((PHI*0.99954)+0.00046-YF)
      XCO=(YCOTWO*AMOLFUEL)/44.01
      ALOGK=4.327-(14436/T)
      AKK=10**ALOGK
      CC=AK/AKK
      IF(CC-1)336,337,336
337   CC=CC+0.01
      GOTO336
```

```
C       NOW THE QUARTIC EQUATIONS CONSTANTS ARE SOLVED
336     BQ=(XCO+(CC*XH)+(2*CC*(AK)**2-(2*AK)**2))/(1-CC)
        CAAQ=(4*XH*(AK)**2)-(4*CC*(AK)**2*(XH)**2)
        CAQ=(CAAQ)-(2*CC*(AK)**2*(XH))
        CQ=(CAQ)/(1-CC)
        DAAQ=(4*CC*(XH)**2*(AK)**2)+(2*CC*(AK)**2*(XH)**2)
        DAQ=DAAQ-(2*(AK)**2*(XH)**2)
        DQ=DAQ/(1-CC)
        EQ=(2*CC*(AK)**2*(XH)**3)/(CC-1)
        FQ=CQ-(3*(BQ)**2)/8
        GQ=DQ+((BQ)**3/8)-(BQ*CQ/2)
        HQ=EQ-(3*(BQ)**4/256)+((BQ)**2*CQ/16)-(BQ*DQ/4)
C       CONVERTING QUARTIC EQUATION INTO A CUBIC EQUATION
        BOQ=FQ/2
        COQ=((FQ)**2-4*HQ)/16
        DOQ=(-1)*(GQ)**2/64
        FOQ=(3*COQ-(BOQ)**2)/3
        GOQ=((2*(BOQ)**3)-(9*BOQ*COQ)+(27*DOQ))/27
        HOQ=((GOQ)**2/4)+((FOQ)**3)/27
        IF(HOQ)339,340,340
339     ROQ=0
        TOQ=0
        SOQ=0
        UOQ=0
        GOTO 347
340     ROQ=((-1)*GOQ/2)+(HOQ)**0.5
        TOQ=((-1)*GOQ/2)-(HOQ)**0.5
        IF(ROQ)342,343,343
342     SOQ=((-1)*ROQ)**(0.333)
        GOTO 344
343     SOQ=ROQ**(0.333)
344     TOQ=((-0.5)*GOQ)-(HOQ**0.5)
        IF(TOQ)345,346,346
345     UOQ=((-1)*TOQ)**(0.333)
        GOTO 347
346     UOQ=TOQ**(0.333)

        RRO=(SOQ+UOQ)-(BOQ/3)
        RCO=(-1)*(SOQ+UOQ)-(BOQ/3)
        RCOI=(SOQ-UOQ)*0.86607
        GOTO 348
347     RRO=(SOQ-UOQ)-(BOQ/3)
        RCO=(-1)*(SOQ-UOQ)-(BOQ/3)
        RCOI=(SOQ+UOQ)*0.86607
```

```
348     RCT=(-1)*(RCO)
        RCTI=(-1)*RCOI
        SQOR=((RCO)**2+(RCOI)**2)**(0.5)
        SSQOR=(SQOR-RCO)
        IF(SSQOR)349,349,350
350     SQCO=((SQOR-RCO)/2)**0.5
        IF(SQCO)349,349,351
349     SQORO=0
        GOTO 352
351     SQORO=RCOI/(2*SQCO)
352     RONE=(-1)*(GQ)/(8*SQOR)
        SONE=BQ/4
        AANSWO=(2*SQORO)+(RONE-SONE)
        AANSWT=(AANSWO*XCO)/(AANSWO-(AANSWO*CC)+(CC*XH))
        AXOTWO=(AANSWO+AANSWT)/2
        IF(FOQ)353,353,354
353     AYOTWO=0
        GOTO 355
354     AYOTWO=AXOTWO*0.6955
        IF(AYOTWO)355,355,356
355     AAYOTWO=0
        GOTO 357
356     AAYOTWO=AYOTWO
357     IF(YOTWO)358,358,359
358     YOTWO=AAYOTWO
359     YOTWO=0+YOTWO
        YNTWO=(PHI*(-0.77))+0.77
        ETA=(8*ZITH)/(1.732*(MSTAR**0.5)*REYN)
        RH=(100*46.01)/(8.314*T)
        EQUV=EXP(-69000/T)
        DNODTO=(1892700*EQUV*YNTWO*(YOTWO**0.5))/(T**0.5)
        DNODT=(7220*DNODTO*(RH**1.5)*5.39361)
        EDNODTC=DNODT*ETA
        EQUVP=EXP(-30000/T)
        DNODTP=(CC*YNTWO*(YOTWO**0.5)*YF*(RH)*EQUVP)
        EDNODTP=DNODTP*ETA

        ANS=0
        ZI=0.0
        ZIT=-0.05
        FFE=0
        FFF=0
        FFU=0
```

```
      FFV=0
360   ZI=ZI+0.1
      RSTAR=ZI/CTWO
      VBMAX=1/((1+(0.25*ZI**2))**2)
      PHIBMAX=1/((1+(0.25*ZI**2))**(2*SC))
      VXSTAR=VBMAX*VXMAX
      PHI=PHIBMAX*PHIMAX
      F=PHI*YFI
      BTFO=PHI*(BFOINJ-BFOINF)+BFOINF
      BHTF=PHI*(BHTFINJ-BHTFINF)+BHTFINF
      IF(BTFO)361,361,362
361   YF=0
      YOTWO=(-1)*BTFO*ANUO
      GOTO 363
362   YF=BTFO
      YOTWO=0
      GOTO 363
363   T=((BHTF-YF)*HC/CP)+TINF
      YCOTWO=ANUCOTWO*((PHI*0.99954)+0.00046-YF)
      XCO=(YCOTWO*AMOLFUEL)/44.01
      ALOGK=4.327-(14436/T)
      AKK=10**ALOGK
      CC=AK/AKK
      IF(CC-1)364,365,364
365   CC=CC+0.01
      GOTO364
C     NOW THE QUARTIC EQUATIONS CONSTANTS ARE SOLVED
364   BQ=(XCO+(CC*XH)+(2*CC*(AK)**2-(2*AK)**2))/(1-CC)
      CAAQ=(4*XH*(AK)**2)-(4*CC*(AK)**2*(XH)**2)
      CAQ=(CAAQ)-(2*CC*(AK)**2*(XH))
      CQ=(CAQ)/(1-CC)
      DAAQ=(4*CC*(XH)**2*(AK)**2)+(2*CC*(AK)**2*(XH)**2)
      DAQ=DAAQ-(2*(AK)**2*(XH)**2)
      DQ=DAQ/(1-CC)
      EQ=(2*CC*(AK)**2*(XH)**3)/(CC-1)
      FQ=CQ-(3*(BQ)**2)/8
      GQ=DQ+((BQ)**3/8)-(BQ*CQ/2)
      HQ=EQ-(3*(BQ)**4/256)+((BQ)**2*CQ/16)-(BQ*DQ/4)
C     CONVERTING QUARTIC EQUATION INTO A CUBIC EQUATION
      BOQ=FQ/2
      COQ=((FQ)**2-4*HQ)/16
      DOQ=(-1)*(GQ)**2/64
      FOQ=(3*COQ-(BOQ)**2)/3
      GOQ=((2*(BOQ)**3)-(9*BOQ*COQ)+(27*DOQ))/27
```

```
      HOQ=((GOQ)**2/4)+((FOQ)**3)/27
      IF(HOQ)367,368,368
367   ROQ=0
      TOQ=0
      SOQ=0
      UOQ=0
      GOTO 375
368   ROQ=((-1)*GOQ/2)+(HOQ)**0.5
      TOQ=((-1)*GOQ/2)-(HOQ)**0.5
      IF(ROQ)370,371,371
370   SOQ=((-1)*ROQ)**(0.333)
      GOTO 372
371   SOQ=ROQ**(0.333)
372   TOQ=((-0.5)*GOQ)-(HOQ**0.5)
      IF(TOQ)373,374,374
373   UOQ=((-1)*TOQ)**(0.333)
      GOTO 375
374   UOQ=TOQ**(0.333)

      RRO=(SOQ+UOQ)-(BOQ/3)
      RCO=(-1)*(SOQ+UOQ)-(BOQ/3)
      RCOI=(SOQ-UOQ)*0.86607
      GOTO 376
375   RRO=(SOQ-UOQ)-(BOQ/3)
      RCO=(-1)*(SOQ-UOQ)-(BOQ/3)
      RCOI=(SOQ+UOQ)*0.86607

376   RCT=(-1)*(RCO)
      RCTI=(-1)*RCOI
      SQOR=((RCO)**2+(RCOI)**2)**(0.5)
      SSQOR=(SQOR-RCO)
      IF(SSQOR)377,377,378
378   SQCO=((SQOR-RCO)/2)**0.5
      IF(SQCO)377,377,379
377   SQORO=0
      GOTO 380
379   SQORO=RCOI/(2*SQCO)
380   RONE=(-1)*(GQ)/(8*SQOR)
      SONE=BQ/4
      AANSWO=(2*SQORO)+(RONE-SONE)
      AANSWT=(AANSWO*XCO)/(AANSWO-(AANSWO*CC)+(CC*XH))
      AXOTWO=(AANSWO+AANSWT)/2
      IF(FOQ)381,381,382
381   AYOTWO=0
```

```
      GOTO 383
382   AYOTWO=AXOTWO*0.6955
      IF(AYOTWO)384,384,385
383   AAYOTWO=0
      GOTO 385
384   AAYOTWO=AYOTWO
385   IF(YOTWO)386,386,387
386   YOTWO=AAYOTWO
387   YOTWO=0+YOTWO
      YNTWO=(PHI*(-0.77))+0.77
      ETA=(8*ZI)/(1.732*(MSTAR**0.5)*REYN)
      RH=(100*46.01)/(8.314*T)
      EQUV=EXP(-69000/T)
      DNODTO=(1892700*EQUV*YNTWO*(YOTWO**0.5))/(T**0.5)
      DNODT=(7220*DNODTO*(RH**1.5)*5.39361)
      EDNODTA=DNODT*ETA
      EQUVP=EXP(-30000/T)
      DNODTP=(CC*YNTWO*(YOTWO**0.5)*YF*(RH)*EQUVP)
      EDNODTP=DNODTP*ETA
      FFQ=FFQ+EDNODTP
      FFE=FFE+EDNODTA
      IF(ZI-20)360,360,388

388   ZIT=ZIT+0.1
      RSTAR=ZIT/CTWO
      VBMAX=1/((1+(0.25*ZIT**2))**2)
      PHIBMAX=1/((1+(0.25*ZIT**2))**(2*SC))
      VXSTAR=VBMAX*VXMAX
      PHI=PHIBMAX*PHIMAX
      F=PHI*YFI
      BTFO=PHI*(BFOINJ-BFOINF)+BFOINF
      BHTF=PHI*(BHTFINJ-BHTFINF)+BHTFINF
      IF(BTFO)389,389,390
389   YF=0
      YOTWO=(-1)*BTFO*ANUO
      GOTO 391
390   YF=BTFO
      YOTWO=0
      GOTO 391
391   T=((BHTF-YF)*HC/CP)+TINF
      YHTWOO=(1.63409)*(PHI-YF)
      XH=(YHTWOO*AMOLFUEL)/18.02
      ALOGKK=3.0165-(13078.5/T)
      AK=10**ALOGKK
```

```
      YCOTWO=ANUCOTWO*((PHI*0.99954)+0.00046-YF)
      XCO=(YCOTWO*AMOLFUEL)/44.01
      ALOGK=4.327-(14436/T)
      AKK=10**ALOGK
      CC=AK/AKK
      IF(CC-1)392,393,392
393   CC=CC+0.01
      GOTO392
C     NOW THE QUARTIC EQUATIONS CONSTANTS ARE SOLVED
392   BQ=(XCO+(CC*XH)+(2*CC*(AK)**2-(2*AK)**2))/(1-CC)
      CAAQ=(4*XH*(AK)**2)-(4*CC*(AK)**2*(XH)**2)
      CAQ=(CAAQ)-(2*CC*(AK)**2*(XH))
      CQ=(CAQ)/(1-CC)
      DAAQ=(4*CC*(XH)**2*(AK)**2)+(2*CC*(AK)**2*(XH)**2)
      DAQ=DAAQ-(2*(AK)**2*(XH)**2)
      DQ=DAQ/(1-CC)
      EQ=(2*CC*(AK)**2*(XH)**3)/(CC-1)
      FQ=CQ-(3*(BQ)**2)/8
      GQ=DQ+((BQ)**3/8)-(BQ*CQ/2)
      HQ=EQ-(3*(BQ)**4/256)+((BQ)**2*CQ/16)-(BQ*DQ/4)
C     CONVERTING QUARTIC EQUATION INTO A CUBIC EQUATION
      BOQ=FQ/2
      COQ=((FQ)**2-4*HQ)/16
      DOQ=(-1)*(GQ)**2/64
      FOQ=(3*COQ-(BOQ)**2)/3
      GOQ=((2*(BOQ)**3)-(9*BOQ*COQ)+(27*DOQ))/27
      HOQ=((GOQ)**2/4)+((FOQ)**3)/27
      IF(HOQ)396,397,397
396   ROQ=0
      TOQ=0
      SOQ=0
      UOQ=0
      GOTO 403
397   ROQ=((-1)*GOQ/2)+(HOQ)**0.5
      TOQ=((-1)*GOQ/2)-(HOQ)**0.5
      IF(ROQ)398,399,399
398   SOQ=((-1)*ROQ)**(0.333)
      GOTO 400
399   SOQ=ROQ**(0.333)
400   TOQ=((-0.5)*GOQ)-(HOQ**0.5)
      IF(TOQ)401,402,402
401   UOQ=((-1)*TOQ)**(0.333)
      GOTO 403
402   UOQ=TOQ**(0.333)
```

```
      RRO=(SOQ+UOQ)-(BOQ/3)
      RCO=(-1)*(SOQ+UOQ)-(BOQ/3)
      RCOI=(SOQ-UOQ)*0.86607
      GOTO 404
403   RRO=(SOQ-UOQ)-(BOQ/3)
      RCO=(-1)*(SOQ-UOQ)-(BOQ/3)
      RCOI=(SOQ+UOQ)*0.86607

404   RCT=(-1)*(RCO)
      RCTI=(-1)*RCOI
      SQOR=((RCO)**2+(RCOI)**2)**(0.5)
      SSQOR=(SQOR-RCO)
      IF(SSQOR)405,405,406
406   SQCO=((SQOR-RCO)/2)**0.5
      IF(SQCO)405,405,407
405   SQORO=0
      GOTO 408
407   SQORO=RCOI/(2*SQCO)
408   RONE=(-1)*(GQ)/(8*SQOR)
      SONE=BQ/4
      AANSWO=(2*SQORO)+(RONE-SONE)
      AANSWT=(AANSWO*XCO)/(AANSWO-(AANSWO*CC)+(CC*XH))
      AXOTWO=(AANSWO+AANSWT)/2
      IF(FOQ)409,409,410
409   AYOTWO=0
      GOTO 411
410   AYOTWO=AXOTWO*0.6955
      IF(AYOTWO)411,411,412
411   AAYOTWO=0
      GOTO 413
412   AAYOTWO=AYOTWO
413   IF(YOTWO)414,414,415
414   YOTWO=AAYOTWO
415   YOTWO=0+YOTWO
      YNTWO=(PHI*(-0.77))+0.77
      ETA=(8*ZIT)/(1.732*(MSTAR**0.5)*REYN)
      RH=(100*46.01)/(8.314*T)
      EQUV=EXP(-69000/T)
      DNODTO=(1892700*EQUV*YNTWO*(YOTWO**0.5))/(T**0.5)
      DNODT=(7220*DNODTO*(RH**1.5)*5.39361)
      EDNODTB=DNODT*ETA
      FFF=FFF+EDNODTB
      IF(ZIT-20)388,388,416
```

```
C       USING THE TRAPEZOIDAL RULE FOR INTEGRATION
416     FIIN=(4*FFE)+(2*FFF)
        ANS=FIIN

        ANSO=ANS+EDNODTC
        VANSO=(0.005773/3)*(ANSO)
C       THE AXIAL VALUES AND THE VALUE OF INTEGRAL D[NO]/DX IS
        REPORTED AT ALL AXIAL POINTS
        WRITE (*,*) XSTARRR,VANSO
        FIINP=((2*FFQ)+(4*FFR))*1.251
        ANSP=FIINP
C       WRITE(*,*)FIIN
        ANSOP=ANSP+EDNODTP
        VANSOP=(0.005773503)*(ANSOP)/3
        WRITE (*,*) XSTAR,VANSOP
        ZONPOO=((XSTAR*0.002)**2)*VANSOP*6.282
        ZONOO=((XSTARRR*0.002)**2)*VANSO*6.282
        GGB=GGB+ZONOO
        GGR=GGR+ZONPOO

        IF (XSTARRR-100) 332,332,3300
3300    FABC=(4*GGA)+(2*GGB)
        ANSS=FABC

        FABCP=(4*GGQ)+(2*GGR)
        ANSSP=FABCP

        ANSSO=ANSS+ZON
        ANSSOP=ANSSP+ZONP

        VZON=(ANSSO*0.002)/3
        VZONP=(ANSSOP*0.002)/3

        WRITE (*,*) VZON
        WRITE (*,*) VZONP

        VMOLES=VZON/30.01
        VMOLESP=VZONP/30.01

        WRITE(*,*) VMOLES
        WRITE(*,*) VMOLESP

        RHOOI=(100*AMOLFUEL)/(8.314*TI)
        AMII=(RHOOI*VI*(DI**2)*3.141)/4
```

```
WRITE(*,*)AMII

GGJ=(VMOLES*1000*46.01*1000000)/(AMII*HC)
WRITE(*,*) GGJ

GGJP=(VMOLESP*1000*46.01*1000000)/(AMII*HC)
WRITE(*,*) GGJP

PPM=(VMOLES*10000)/(0.13658E-07)
WRITE(*,*)PPM

PPMP=(VMOLESP*10000)/(0.13658E-07)
WRITE(*,*)PPMP

EINOX=(VZON*1000)/AMII
WRITE(*,*)EINOX

TOTALNOX=PPM+PPMP
WRITE(*,*)TOTALNOX

TOTALNOXGJ=GGJ+GGJP
WRITE(*,*)TOTALNOXGJ

STOP
END
```

APPENDIX D

A TABLE OF EXPERIMENTAL VALUES USED FOR VALIDATION OF MODEL

Table D.1: Experimetnal Data Values used for Validation of Model. Referenced from [13].

d_o **(mm)**	u_o **(m/s)**	Y_f	$EINO_x$ **(g/Kg fuel)**
10	5	1	2.766
10	20	1	2.561
20.5	1	1	1.6649
20.5	5	1	1.7728
20.5	10	1	1.9442
29.5	1	1	1.8161
29.5	3	1	1.8748
29.5	5	1	1.9971

APPENDIX E

METHODS FOR REPORTING NO_x IN VARIOUS UNITS

Emission levels for utilities are reported as g per GJ (or lb per mmBTU) of heat released while for automobiles it is reported in g per mile. A few are reported as ppm and as ratio of emission in g per kg of fuel burned called Emission Index (EI NO_x). One could convert from one form to other.

1. Reporting as ppm:

Many of the analyzers yield gas composition in mole % (or volume %) on dry basis. Since pollutants are in trace amounts, they are reported in parts per million (ppm). For the pollutant species k,

$$\text{Species k in ppm} = X_k * 10^6, \qquad \text{(E.1)}$$

(interpreted as molecules per million dry molecules).

Where X_k is in mole fraction. For Hg content in solid fuel like coal, the ppm indicates the mass of species in g per million g of solid fuel.

2. Emission Index (g/kg of fuel)

Alternately, the emission index EINO expressed as g/kg of fuel can be used

EI of species k = mass of pollutant species k /mass of fuel = $\{ m_k/m_F \}$

$$= X_k \, N_{p,\,dry} * M_k/m_F \qquad \text{(E.2)}$$

Where $N_{p,\,dry}$, number of product dry moles

$$C_cH_hO_oN_nS_s + aO_2 + 3.76\,aN_2 + b\,H_2O(g) \rightarrow x\,CO_2 + (c\text{-}x)\,CO + (h/2+b)H_2O + (a\text{-}a_{st})O_2 + 3.76\,aN_2 + c\,NO + sSO_2$$

If X_{CO} and X_{CO_2} are measured, then

$$X_{CO_2} = x/\ N_{p,\,dry}\ ,\ X_{CO} = (c\text{-}x)/\ N_{p,\,dry} \qquad \text{(E.3a,b)}$$

Adding eqs. (E.3a) and (E.3b), product dry moles is solved as,

$$N_{p,\,dry} = c/\ \{X_{CO} + X_{CO_2}\} \qquad \text{(E.4)}$$

and using the result in eq. (E.2) with k=NO,

$$EINO\ (g/kg\ of\ Fuel) = \{c^*\ X_{NO}/\ (X_{CO_2} + X_{CO})\}\ M_{NO_2}\ 1000/M_F \qquad \text{(E.5)}$$

Where M_F =c* 12.01+ h*1.01+n*14.01+0*16+s*32 (kg/ kmole of fuel) (E.6)

For reporting k= NO emission, the EPA stipulates that M_k for NO should be that of NO_2 (M_{NO_2} = 46.01) instead of 30 since NO is eventually converted into NO_2 in atmosphere which plays a major role in destruction of O_3 .

EI of any pollutant species k in g/kg of fuel is given as

$$\{c^*X_kM_k\}\ *\ (1000\ g/kg)/\ [\{X_{CO} + X_{CO_2}\}M_F] \qquad \text{(E.7)}$$

3. Emissions in Mass Units Per Unit Heat Value (g /GJ)

Pollutant species k can be reported as,

$$\text{NO in } \frac{g}{GJ} = \frac{c\ X_{NO}}{(X_{CO_2} + X_{CO})} \frac{M_{NO_2} * 1000}{M_F\ HHV_F\ (GJ/kg)} \text{ , fuel on atom basis} \quad \text{(E.8)}$$

$$\text{NO in } \frac{g}{GJ} = \frac{Y_c\ X_{NO}}{(X_{CO_2} + X_{CO})} \frac{M_{NO_2} * 1000}{12.01 \text{ x } M_F\ HHV_F\ (GJ/kg)} \text{ , fuel on elemental basis} \quad \text{(E.9)}$$

For gaseous fuels, heating values are available in GJ/m^3. Thus standard temperature and pressure are used to calculate the volume in m^3. 1 kmole occupies $\overline{v}_{STP}$ = 22.4 m^3 at STP of 0°C, 101 kPa and 24.5 m^3/kmole at STP of 25° C and 101 kpa. Since HHV (GJ/kg) * M_F = HHV' (GJ/m^3) $\overline{v}_{STP}$, then for gaseous fuels, Eq. (24) is written as,

$$\text{"k" in } \frac{g}{GJ} = \frac{c\ X_k}{(X_{CO_2} + X_{CO})} \frac{M_k * 1000}{HHV_F'(GJ/m^3) * \overline{v}_{STP}} \text{ , gaseous fuels on atom basis} \quad \text{(E.10)}$$

For k=NO

$$\text{NO in } \frac{g}{GJ} = \frac{c\ X_{NO}}{(X_{CO_2} + X_{CO})} \frac{M_{NO_2} * 1000}{M_F\ HHV_F\ (GJ/kg)} \quad \text{(E.11)}$$

$$\text{NO in } \frac{g}{GJ} = \frac{Y_c\ X_{NO}}{(X_{CO_2} + X_{CO})} \frac{M_{NO_2} * 1000}{12.01 \text{ x } M_F\ HHV_F\ (GJ/kg)} \quad \text{(E.12)}$$

In automobiles instead of GJ, kW hr or HP hr is used; Thus

NO in g per kWhr = NO in g per GJ x 0.0036 (E.13)

NO in g per HP = NO in g per GJ x 0.00268 (E.14)

VITA

Vivek Siwatch was born September 18, 1981 in Chandigarh, India and currently resides at 207 – C, Spruce Avenue in College Station; TX. He graduated with first class distinction and departmental honors from Delhi College of Engineering with a Bachelor of Engineering in Mechanical Engineering degree in May 2003. He enrolled in the graduate school at Texas A&M University in the Fall of 2003 and received his Master of Science in Mechanical Engineering in December 2005.

He can be reached through the Department mailbox addressed for Vivek Siwatch, Department of Mechanical Engineering, Texas A&M University, College Station, TX-77843.